The Neogene development of the Zagros Foreland Basin in the Lurestan-Arc, Iran. A new integrated model using geochemistry, clay mineralogy and micropalaeontology

Dissertation

der Mathematisch-Naturwissenschaftlichen Fakultät

der Eberhard Karls Universität Tübingen

zur Erlangung des Grades eines

Doktors der Naturwissenschaften

(Dr. rer. nat.)

vorgelegt von

Christian Artur Friedrich Dietzel

aus Heppenheim

Tübingen

2024

Gedruckt mit Genehmigung der Mathematisch-Naturwissenschaftlichen Fakultät der Eberhard Karls Universität Tübingen.

Tag der mündlichen Qualifikation:	13.12.2024
Dekan:	Prof. Dr. Thilo Stehle
1. Berichterstatterin:	Prof. Dr. Madelaine Böhme
2. Berichterstatter:	Dr. Christoph Berthold
3. Berichterstatter:	Prof. Dr. Thomas Aigner

Acknowledgements

Firstly, I would like to thank my supervisors Prof. Madelaine Böhme and Dr. Christoph Berthold for supervising my dissertation. This thesis was enabled by the results of Prof. Madelaine Böhme's field campaign to the Changuleh and Zarrinabad syncline-anticline structures in November 2018, which lead to new insights into Neogene hyper-aridity in Northern Arabia and provided the necessary sediment samples and geological field observations for this thesis. This dissertation would also not have been possible without the generous funding and scientific support provided by her. The analytical part of this dissertation would not have been feasible without the supervision of Dr. Christoph Berthold whose experience and skill in the identification and quantification of clay minerals using X-ray diffraction enabled the lab work for this dissertation. Both Prof. Madelaine Böhme and Dr. Christoph Berthold are thanked for the fruitful discussions and support during the making of this dissertation. I am grateful for the help provided by Dr. Uwe Kirscher in preparing and interpreting and discussing the large new data sets. I also want to thank PD Dr. Haytham El Atfy for his continued support throughout this thesis and the sharing of his invaluable knowledge on micropalaeontological topics. I furthermore would like to acknowledge the great lab supervision provided in the SEM labs by Dr. Hartmut Schulz as well as Dr. Tatiana Miranda as well as the supervision by Annette Flicker during sample preparation as well as in the XRD-lab. Agnes Fatz provided a great support in the photographic documentation of samples. Prof. Dr. Mahmoud Majidifard provided valuable insight into the geology of Iran in the revision of the published manuscripts. This work would also not have been possible without Dr. Heiner Taubald, who provided the XRF analysis for the geochemistry. In addition to my supervisors several other people have supported me during the making of my PhD and helped me keep track during my publication. Hereby I am especially grateful to Dr. Martin Ebner and PD Dr. Andreas Matzke. Over the years I have enjoyed the support by various people in the Institute who are in alphabetical order Prof. Thomas Aigner, Dr. Felix Augustin, Dr. Anna Ayvazyan, Thomas Binder, Dr. Gabriel Ferreira, Dr. Ahmed Gooma, Josephina Hartung, Pannagiotis Kampouridis, Christina Kyriakouli, Dr. Frieder

Lauxmann, Thomas Lechner, Florian Ludwig, Tobias Massonne, Dr. Christian Sommer and Adrian Tröscher.

I want to also thank my partner Robin Hagenbach for his support and would also to like to thank my family especially my parents Dr. Hans Dietzel and Christa Dietzel who have constantly supported me in life and by nurturing my interest in science and enabled me to pursue as career as a geologist.

Table of Contents

Abbreviations

Fm. : Formation

Mb. : Member

Ma : Million years ago

My : Million years

NADX : Neogene Arabian Desert climaX

Sp. : Species

XRD : X-ray diffraction

XRF : X-ray fluorescence

Summary

The Mesopotamian Foreland Basin represents an important sedimentary archive for the Neogene evolution of the Zagros Mountain Belt and the adjacent Arabian Shield. In this dissertation a combined sedimentary profile from the Zarrinabad and Changuleh syncline anticline structures was analysed using whole rock geochemistry, clay mineralogy and micropalaeontological data of 84 samples and compared to previously published data of soluble salt geochemistry and magnetic susceptibility from Böhme et al. (2021). The combined profile has previously been dated by magnetostratigraphy and encompasses Sediments from the Serravallian (12.6 Ma) to the earliest Pleistocene (2.4 Ma) (Homke et al., 2004). It comprises the uppermost parts of the evaporative Gachsaran Formation, fluvial sediments of the lower Aghajari Member, alluvio-fluvial-aeolian sediments of the Lahbari Member and alluvial conglomerates of the Bakthiary Formation.

Increased transformation of illite and chlorite to smectite by chemical weathering indicates a change from arid to semi-arid climate conditions from the Serravallian towards the mid Tortonian. Geochemical analysis of the sediments using whole rock XRF data also demonstrates a significant provenance shift during the early-mid Tortonian. An increase in mafic and ultramafic elements such as Mg, Cr and Ni as well as radiolarians indicates enhanced uplift and erosion of ophiolites, mafic magmatites as well as radiolarites from the Imbricate Zagros zone. The additional magnesium availability gives then rise to the formation of palygorskite in soils along the floodplain. A reduction in chemical weathering and a transition towards arid climate conditions is indicated in clay mineralogy in the early Messinian. Clay mineralogy and geochemistry are reflective of significant change at the onset of the hyper-arid Lahbari Member at 5.6 Ma. A strong increase in soluble salts is encompassed by an increase in palygorskite, which is not coupled to local magnesium availability as demonstrated in the Lower Aghajari Member. The Lahbari Member is interpreted to comprise fine-grained distal alluvial fans in a bajada environment originating from older Gachsaran and Aghajari sediments

of the uplifting along the Zagros Mountain Front Flexure due to tectonic basin convergence. These fine-grained alluvial fans are interbedded with thick silts with aeolian contribution which are geochemically indicated to have largely been recycled from the local alluvial material. Additional atmospheric nitrate and chloride, which is distributed throughout these silts was likely sourced externally from atmospheric deposition during a penecontemporaneous hyper-arid period (NADX). Clay mineralogy indicates an increase in humidity towards arid conditions the upper part of the Lahbari Member in the Zanclean. The Lahbari Member is superseded by coarse grained conglomerates of the Bakthyari Formation at 2.5 Ma reflecting the deepening of erosion into older well consolidated strata of the neighboring uplifting Anaran Anticline. Several samples througout the profile contained small charophyte gyrogonites of *Chara vulgaris*, *Chara globularis*, *Nitellopsis obtusa* and *Chara* sp. giving information on freshwater availibility on the floodplain such as in temporary ponds after seasonal flooding. Furthermore, XRD analysis revealed the presence of the zeolite mineral erionite in many samples throughout the whole sedimentary profile, which can form from weathering of volcanic glass in alkaline conditions.

Zusammenfassung

Das Mesopotamische Vorlandbecken repräsentiert ein wichtiges Sedimentarchiv über die neogene Entwicklung des Zagrosgebirges sowie des benachbarten arabischen Schildes. Für diese Dissertation wurde ein zusammengesetztes Sedimentprofil aus den Zarrinabad- sowie Changuleh Synklinal-Antiklinalstrukturen analysiert. Hierzu wurden neue Röntgendiffraktionsmessungen an Tonmineralen, Gesamtgesteinsgeochemie-RFA Analysen sowie mikropaläontologische Untersuchungen an 84 Proben durchgeführt. Diese wurden mit bereits bekannten Daten von Böhme et al. (2021) zur Geochemie und Verteilung von leicht löslichen Salzen, magnetischen Suszeptiblität und Korngröße gemeinsam neu interpretiert. Nach einer früheren magnetostratigraphischen Untersuchung umfasst das Sedimentprofil eine Altersspanne vom Serravallium (12,6 Ma) bis ins älteste Pleistozän (2,4 Ma) (Homke et al., 2004). Der älteste Teil des Profils besteht aus dem obersten Teil der evaporitischen Gachsaran Formation. Darauf folgen fluviatile Sedimente des unteren Aghajari Members, sowie darüber die alluvialen, äolischen und in geringen Maßen fluviatilen Ablagerung des Lahbari Members. Den jüngsten und obersten Teil des Profils bilden die alluvialen Konglomerate der Bakthiary Formation.

Der Übergang des Serravalliums ins Tortonium im unteren Aghajari Member ist tonmineralogisch durch die verstärkte Verwitterung von Illit und Chlorit zu Smektit gekennzeichnet, bedingt durch einen Übergang von ariden zu semi-ariden Klimaverhältnissen mit höherer Wasserverfügbarkeit. RFA Gesamtgesteinsgeochemiemessungen an Proben aus dem frühen Tortonium zeigen einen starken Anstieg an mafischen Elementen, welcher auf die verstärkte Heraushebung und Erosion von mafischen Gesteinen der Gaveh-Rud Zone sowie ultramafischen Ophioliten in der Zagros-Schuppenzone zurückzuführen ist. Diese tektonischen Veränderungen führten ebenso zu einer verstärkten Erosion von Radiolariten in der der Zagros-Schuppenzone, welche sich in einer erhöhten Anzahl an Radiolarien in den Proben spiegelt. Die erhöhte Magnesiumverfügbarkeit in den semi-ariden bis ariden Paleoböden lässt sich ebenfalls durch die Bildung von Palygorskit nachweisen, welche

quantitativ zum Magnesiumgehalt steigt. Ab dem frühen Messinium weist die Tonmineralzusammensetzung auf einen Übergang von semi-ariden zu ariden Klimaverhältnissen mit einer Reduktion der chemischen Verwitterung hin. Der Übergang zum hyper-ariden Lahbari Member um 5,6 Ma zeigt sich an verschiedenen tonmineralogischen sowie geochemischen Indikatoren: Ein starker Anstieg an Nitrat, Halit und Strontium, sowie ein starker Anstieg des Palygorskitanteils in der Tonfraktion, welcher sich nicht wie im unteren Aghajari Member auf einen Anstieg an der Magnesiumverfügbarkeit zurückführen lässt. Diese Dissertation interprätiert den Lahbari Member als eine Wechsellagerung aus distalen, feinkörnigen Schuttfächern sowie aus selbigen remobilisierten äolischen Siltablagerungen. Tektonische Modellierungen sowie Gesamtgesteinsgeochemie deuten darauf hin, dass die remobilisierten Siltablagerungen größtenteils aus älteren Gachsaran Evaporiten sowie Aghajari-Siliziklastika bestehen, welche bei der tektonischen Heraushebung der benachbarten Anaran Antiklinale erodiert wurden. Da die lokalen Gachsaran Evaporite nach Literaturangaben wenig bis kein Halit enthalten, kann die hohe Konzentration an feinverteiltem Halit sowie Nitrat in den äolischen Schluffsteinen am besten durch einen zusätzlichen, zeitgleichen atmosphärischen Eintrag erklärt werden. Die Erhaltung und Ablagerung der leicht löslichen Salze wurde hierbei durch hyper-aride Klimaverhältnisse bedingt, welche sich auf veränderte regionale Klimasysteme während einer Paratethys Tiefstandphase nach dem Höhepunkt der Messinischen Salinitätskrise zurückführen lassen (NADX). Ab dem Zanclium deutet eine verstärkte Smektitbildung auf einen Übergang von hyperariden zu ariden Verhältnissen hin. Der Übergang des Lahbari Member in die grobkörnigen Konglomerate der Bakthiary Formation zum Beginn des Pleistozäns lässt sich auf die verstärkte Erosion diagenetisch verfestigten älteren Gesteinen aus dem Inneren der sich weiter heraushebenden, benachbarten Anaran Antiklinale zurückführen. In verschiedenen Proben des gesamten Profils wurden kleine Gyrogonite von *Chara vulgaris*, *Chara globularis*, *Nitellopsis obtusa* sowie *Chara* sp. gefunden. Aus dem Auftreten dieser Arten von Armleuchteralgen konnten zusätzliche Informationen über die Verfügbarkeit von Süßwasser in saisonalen Teichen auf der Überflutungsebene gewonnen werden. In zahlreichen Proben aus dem gesamten Profil

wurde das Zeolithmineral Erionit nachgewiesen, welches typischerweise durch die Verwitterung von vulkanischem Glas unter alkalischen Bedingungen entsteht.

List of publications

Erklärung nach § 5 Abs. 2 Nr. 8 der Promotionsordnung der Math.-Nat. Fakultät

-Anteil an gemeinschaftlichen Veröffentlichungen-

Nur bei kumulativer Dissertation erforderlich!

Declaration according to § 5 Abs. 2 No. 8 of the PhD regulations of the Faculty of Science

-Collaborative Publications-

For Cumulative Theses Only!

Last Name, First Name: Dietzel, Christian Artur Friedrich

List of Publications

1. Dietzel, C., Berthold, C. Kirscher, U., Majidifard, M., Böhme, M. 2023. Using clay mineralogy and micropalaeontological observations to unravel Neogene climate variations in Northern Arabia. Arabian Journal of Geosciences 16 (5) 343

2. Dietzel, C., Berthold, El-Atfy, H., Majidifard, M., Böhme, M. 2024. Reworked Mesozoic radiolarians in Miocene-Pliocene foreland sediments in the Zagros Belt, Iran. Rivista Italiana di Palaeontologia e Stratigrafia 130 (1) 35-46

3. Dietzel, C., Berthold, C. Kirscher, U., Majidifard, M., Böhme, M. 2024. A revised model for Neogene Zagros foreland sedimentation in the Lurestan Arc based on new geochemical data. Basin Research 36 (2)

Nr.	**Accepted publication yes/no**	**List of authors**	Position of candidate in list of authors	Scientific ideas by the candidate (%)	Data generation by the candidate (%)	Analysis and Interpretation by the candidate (%)	Paper writing done by the candidate (%)
1	yes	5	1	80	70	80	90
2	yes	5	1	80	80	80	80
3	yes	5	1	80	70	90	90

I confirm that the above-stated is correct.

Date, Signature of the candidate

I/We certify that the above-stated is correct.

Date, Signature of the doctoral committee or at least of one of the supervisors

Further Publications not included in this thesis but written during the PhD

The following publications have been published by peer reviewed international journals and are listed here in chronological order.

4) Böhme, M., Spassov, N., Majidifard, M., Gärtner, A., Kirscher, U., Marks, Dietzel, C., Uhlig, G., El Atfy, H., Begun, D. Winklhofer, M. 2021. Neogene hyperaridity in Arabia drove the directions of mammalian dispersal between Africa and Eurasia. 2(85) communications earth & environment

Introduction

The Zagros Mountain Belt and the adjacent Mesopotamian Foreland Basin represent an important archive to study the Neogene tectonic and paleoclimatic evolution of the Eurasian-Arabian realm. It represents a crossroad for Neogene mammalian dispersal patterns between Africa and Eurasia which were likely impacted by shifting climate patterns (Böhme et al., 2021). A prime location is to study the sedimentological and tectonic evolution as well as paleoclimate patterns is found in the Zarrinabad and Changuleh syncline-anticline structures at the margin of the Simply Folded Zagros belt 10 km E of Mehran at the Iran-Iraq border. The sediments in the syncline-anticline structures have previously been dated by magnetostratigraphy (Homke et al., 2004). The terrestrial sediments, which are easily accessible along the Zarrinabad and Changuleh syncline-anticline structures have been dated from the mid Tortonian to the early Pleistocene and comprise the Gachsaran Formation, Aghajari Formation (Lower Aghajari Member + Lahbari Member) and the Bakthiari Formation. A first provenance investigation along the profile using Apatite Fission Track Thermochronology of 5 sediment samples was undertaken (Homke et al., 2010). This study gave the first information about changing erosional patterns in the adjacent Zagros Fold and Thrust belt. The evolution of fold and fault structures adjacent to the sampling area has furthermore been investigated by Emami et al. (2010). This study provided important information about the rheological behaviour of the different competent and incompetent strata of the Mesopotamian Foreland basin during convergence of the Arabian and Eurasian plates as well as a first model for explaining the unique sedimentation patterns of the Lahbari Member. A paleoclimatic study using the geochemistry and presence of highly soluble salts such as chlorides, nitrates and bromides but also grainsize modelling and heavy mineral analysis of select samples gave insight into the evolution of paleoclimate and aridity trends between 12.6 Ma and 2.4 Ma and recognised the importance of aeolian processes during the deposition of the Lahbari Member (Böhme et al., 2021).

1.1 Geological setting

From the northeast to the southwest the Zagros mountain belt comprises five sub-parallel structural domains which are divided by major thrust faults (fig 1.) : (1) the Urumia–Dokhtar Magmatic Arc, (2) the magmatic and metamorphic Sanandaj–Sirjan Zone, (3) the Imbricate Zone (also called High Zagros Thrust Belt or Crush Zone in Iran or Thrust Zone and Nappe Zone in Iraq), (4) the Simply Folded Belt (High Folded Zone in Iraq), and (5) the) Foothill Zone which is partially covered by the Mesopotamian–Persian Gulf foreland basin (Low Folded Zone in Iraq). (Vergés et al., 2011b). The Sanandaj-Sirjan Zone and the Imbricate Zone are separated by the Main Zagros Fault, which has been interpreted to represent the Neo-Tethys suture in Iran (Blanc et al., 2003; Homke et al., 2010; Le Garzic et al., 2019). The Main Zagros Fold has been overprinted by the active dextral Main Recent Fold during the last 3-5 My (Mohajjel and Fergusson, 2013).

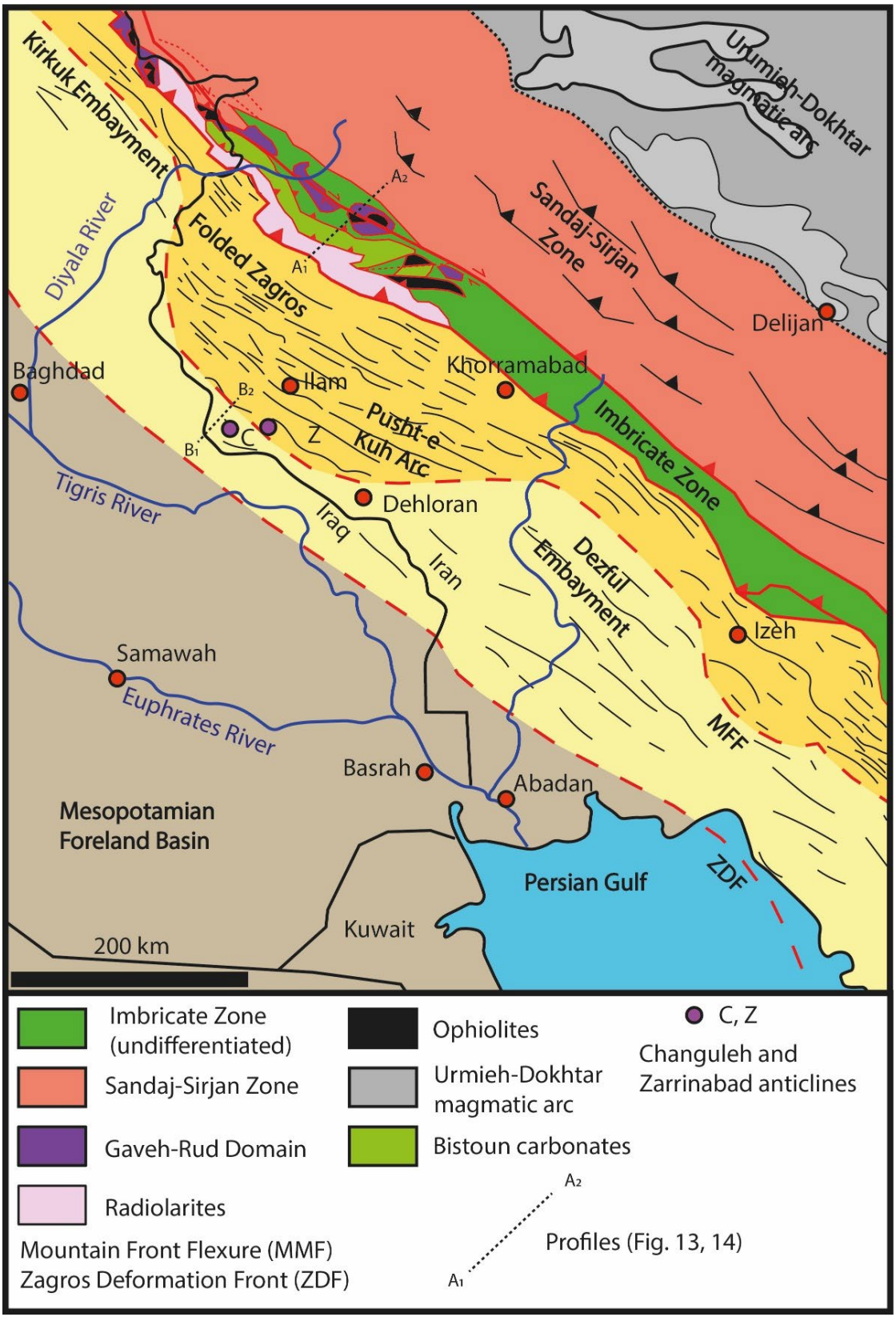

Figure 1. Geotectonic overview map of the northeastern Mesopotamian Foreland Basin. Map modified from Verges et al. (2011) with imbricate Zagros modified from (Ali et al., 2014) (Dietzel et al. 2024b)

(1) The Urumia–Dokhtar Magmatic Belt (UDMB) represents the active margin of the Iranian plate with Andean-type tholeiitic, calc–alkaline, and K-rich alkaline extrusive and intrusive rocks. It forms a linear structure of 150 km width. The oldest lithologies in this magmatic belt are formed by pre-Jurassic calc-alkaline intrusive rocks, exposed in the southeastern part of the UDMB. Volcanism in the UDMB began and peaked in the Eocene, whilst the youngest pyroclastic rocks and lava flows are of Pliocene age and alkaline and calc-alkaline composition. (Berberian et al., 1982; Berberian and King, 1981; Honarmand et al., 2013)

(2) The Sanandaj-Sirjan Zone (SSZ) has a length of over 1300 km and width of 150 – 200 km separating the central Iran block originating from Gondwana, from the Arabian plate. It comprises Paleozoic–Cretaceous sedimentary and metamorphic rocks which have been intruded by Jurassic–Oligocene plutons (Alavi, 1994; Stoecklin, 1968). The metamorphic assemblages of the SSZ mainly record greenschist to amphibolite facies metamorphism. The SSZ has been affected by at least two major episodes of deformation. The second episode of deformation has been linked to the collision of the Arabian and Iranian plate during the late Cretaceous. (Mohajjel and Fergusson, 2000). The calc-alkaline plutons show variable magmatic differentiation with a compositional range from gabbro to granite (Alavi, 1994; Baharifar et al., 2004; Berberian and King, 1981).

(3) The Imbricate Zone is characterized by a tectonic melange of highly deformed accreted lithologies. It comprises distal parts of the Arabian margin, mesozoic ophiolithes and accretionary prisms of island arcs (Blanc et al., 2003; Le Garzic et al., 2019; Vergés et al., 2011b). In the Lurestan Zone in Iran the following succession can be found from the Northeast to the Southwest, which is divided by four thrust faults: I Gaveh-Rud domain (known as Walash-Naopurdan intra oceanic island arc in Iraq), II Cretaceous mafic and ultramafic ophiolites, III Late Triassic to middle Cretaceous Bistun-Avroman limestones, IV Jurassic-Cretaceous Qulqula-Kermanshah radiolarites. The Imbricate Zone lies discordantly on top of the Simply Folded Belt along a major thrust fault called the High Zagros Fault, which partially

accommodates intense basin shortening within the Iranian-Arabian collision zone (Ali et al., 2014).

(4) The Simply Folded Belt represents the Cambrian-Holocene sedimentary cover of the subducting Arabian Plate margin. The sedimentary cover is affected by a fold and thrust system which accommodates the shortening of the Mesopotamian foreland basin in the collision zone. In the Lurestan Arc of Iran, the whole sedimentary succession of ~ 10 km thickness above the lower Ediacaran-Cambrian- Hormuz salt is affected by folding, with ductile halite acting as an incompetent detachment plane. A further detachment plane affecting fold geometry is found higher up in the sedimentary succession in the ductile evaporites of the Miocene Gachsaran formation (Alavi, 2007; Blanc et al., 2003; McQuarrie, 2004; Molinaro et al., 2004; Mouthereau et al., 2007; Sepehr et al., 2006; Sherkati and Letouzey, 2004; Vergés et al., 2011a).

(5) The buried foothills comprise the same sedimentary succession as the Simply Folded Belt, but have not yet been strongly affected by crustal shortening. They are separated from the Simply Folded Zagros Belt by the Mountain Front Flexure, which forms a 3 km structural relief in the Pusht-e-Kuh Arc (Berberian, 1995; Emami et al., 2010).

1.1.1 Development of the Zagros Mountain Belt

Since the end of the Precambrian, Zagros Mountain Belt and Mesopotamian Foreland Basin have evolved through various tectonic settings. In the Paleozoic, the Mesopotamian Foreland Basin was part of the stable supercontinent of Gondwana, then a passive continental margin in the Mesozoic, and became a convergent orogen in the Cenozoic (Bahroudi and Koyi, 2004). Since then, the Zagros Mountain Belt and Mesopotamian Foreland Basin have been formed as the result of a complex multi stage orogeny. It was initiated by the obduction of sub-oceanic crust above the Arabian margin during the Campanian to Paleocene. In the Neogene, the collision of the Arabian and central Iranian blocks culminated the Zagros orogeny (Alavi, 1994; Homke et al., 2010; Saura et al., 2015). The obduction event involved emplacement of the Triassic Bisotun-Avroman carbonates, Cretaceous Kermanshah ophiolites and Jurassic-

Cretaceous Qulqula-Kermanshah radiolarites (Ali et al., 2014; Wrobel-Daveau et al., 2010). The obduction of dense ophiolites and radiolarites onto the Arabian continental crust resulted in formation of proto-foreland basins like the Amiran basin due to a flexure of the Arabian lithosphere (Homke et al., 2009). As a result of continued tectonic convergence onto the margin of the Arabian Plate, the mélange of ophiolites and radiolarite terranes are structurally overlain by the volcano-sedimentary rocks of the Gaveh-Rud domain, which developed during the Eocene and Oligocene as an intra-oceanic-island arc within the intervening Neotethys Ocean (Ali et al., 2014). The contemporary Mesopotamian Foreland Basin started to develop after the emplacement of the Sanandaj-Sirjan Zone during the Oligocene in response to crustal thickening in the hinterland. Continued convergence between the Arabian and the Iranian plate resulted in the deformation of the margins of the syntectonically formed Mesopotamian Foreland Basin, initiating the development of the Simply Folded Belt. The deformation front generally propagated towards southwest (Etemad-Saeed et al., 2020; Lawa et al., 2013; Le Garzic et al., 2019; Wrobel-Daveau et al., 2010).

1.1.2 Miocene-Pliocene tectonic development of the Lurestan Arc

The sedimentary infill of the Mesopotamian Foreland Basin provides evidence for the contemporaneous tectonic evolution of the adjacent Zagros orogen. The clastic infill is highly variable along the 1300 km SE to NE strike, as different strata in the Zagros Mountains were subject to erosion at the same time (Etemad-Saeed et al., 2020; Homke et al., 2010; Koshnaw et al., 2017). Furthermore variable aeolian sediment input contributed towards the infill of the Mesopotamian Foreland Basin (Böhme et al., 2021). The following lithologies Tortonian-Pleistocene strata are currently exposed along the Zarrinabad and Changuleh syncline anticline structures, where this thesis is based:

Gachsaran Formation

The evaporitic sediments of the Gachsaran Formation (Fatha Formation in Iraq) have been deposited in several restricted sub-basins with limited sea contact under arid climate conditions within the Mesopotamian Foreland basin. While the Dezful sub-basin as well as the Kirkuk

sub-basin feature thick halite deposits, the occurrence of halite is generally rare in the Pust-e-Kuh sub-basin (Bahroudi and Koyi, 2004). However, some undefined salt extrusions have been mentioned in the Anaran Anticline structure (Emami et al., 2010). At the Zarrinabad Anticline the upper Gachsaran Formation comprises of thick well-bedded evaporites, blue to red silty-clay beds and green to brown sandstones. At the top dm-scale carbonate banks alternate with fine-grained sandstone beds, which feature wave-ripples. Pedogenic gypsum concretions and show redox mottling can be observed in mudstones suggesting fluctuating sea levels with the depositional environment changing between restricted marine shoreface and terrestrial backshore facies. Homke et al. (2004) located the transition towards the Lahbari Mb. at 12.8 Ma, while, based on the observation of a bed rich in marine shells, Böhme et al. (2021) suggested a later transition to the Lower Aghajari Fm. at 12.3 Ma.

Aghajari Formation

The Aghajari Fm. (Upper Fars Fm. in Syria, Injana Fm. in Iraq and Dibdiba Fm. in Kuwait) comprises syntectonic Zagros Molasses sediments and is regionally subdivided into the lower Aghajari Member and the Lahbari Member. In the Lurestan arc it represents a 2.4 km-thick depositional profile of fine-clastic to fluvial sediments, dated by magnetostratigraphy from the late middle Miocene to the base of the Pleistocene (Homke et al. 2004).

The Lower Aghajari Member can be distinguished by the presence of thick sandstone channels often showing cross-bedding structures interbedded with fine grained mudstones. In the Chaguleh Anticline, the well-consolidated sandstone beds towards the middle of the profile section display thicknesses ranging from several meters to tens of meters. Thin layers of conglomerates at the bottom of sandstone layers can be found appearing in the last 130 m underneath the transition to the Lahbari Mb (Homke et al. 2004). Layers of silty mudstone likely representing overbank deposits. These mudstones show pedogenic carbonate and redox mottling and the infrequent presence of Charophyte gyrogonites (Böhme et al. 2021). Apatite Fission Tracks cooling ages of two select sediment samples from the early and late Tortonian of the Lower Aghajari Formation are congruent with a sediment source in the Sanandaj-Sirjan

zone and Gaveh-Rud domain (Homke et al., 2010). An onset of growth strata is observed between 8.1 Ma and 7.2 Ma in the Changuleh syncline, indicating the progression of the Mountain Front Flexure (Homke et al., 2004). At 5.6 Ma sandstones in the Lahbari Member become sparser and thinner. The sedimentation is dominated by thick structureless beige silt and mudstones with high chloride and nitride contents. A reappearance of sandstones in small channels is observed at ~3.5 Ma.(Böhme et al., 2021). The Lahari Member at the Lurestan Arc has been suggested to comprise reworked material from the Gachsaran Formation and Lower Aghajari Formation, regionaly uplifted at the Mountain Front Flexure based on tectonic modelling (Emami et al., 2010). Contrastingly Böhme et al. (2021) suggested a primary deposition of aeolian silts originating from the west during a period of hyper-arid climate (NADX). At 2.4 Ma the Lahbari Formation is succeeded by coarse grained conglomerates sourced from the uplifting Anaran Anticline towards the East (Emami et al., 2010).

1.2 Paleoclimatic development of Northern Arabia

Khormali et al. (2005) reconstructed a long-term warm and arid climate from the Eocene to Pliocene in southern Iran, by using clay mineralogy. A sub-arid climate has furthermore been suggested for the Mesopotamian Foreland Basin by Al-Juboury (2009) based on the formation of palygorskite and evaporite deposits in elongated lagoonal basins of the Fatha Formation in a fluvial-tidal environment during the middle Miocene. Arid conditions from the middle Miocene towards late Miocene were also reconstructed by geochemical weathering in indices (Etemad-Saeed et al., 2020). Using empirical thresholds of soluble nitrate, chlorite and bromide in soils, Böhme et al. (2021) suggested transient periods of Arabian hyperaridity at 8.75 Ma, 7.78 Ma, 7.5 Ma and 6.25 Ma corresponding to Paratethys low-stands. Furthermore Böhme et al. (2021) inferred a sustained hyper-arid period between 5.6 Ma and 3.3 Ma (Neogene Arabian Desert Climax, NADX) from soluble salt geochemistry and the deposition of aeolian silts. These aridity variations are interpreted to be linked to paleo sea-level variations. While transient periods of hyperaridity and NADX match with significant Ponto Caspian low-stands, periods of Ponto Caspian high-stands corresponded well to a more humid (semi-arid) climate in Mesopotamia.

NADX correlates with the >2 My long separation of the Caspian Sea from the Black Sea basin after at peak of desiccation of the Mediterranean during the Messinian Salinity Crisis at 5.59 Ma (Manzi et al., 2013). Paratethys shrinkage strengthened the Siberian Pressure High and therefore blocked the moisture-carrying westerlies from reaching Western Asia and Northern Arabia leading to increased aridity in that region (Böhme et al., 2021; Perşoiu et al., 2019).

1.3 Objectives

The Miocene-Pliocene sediments sampled by Böhme et al. (2021) at the Zarrinabad and Changuleh syncline-anticline structures provide an important reference archive for climate development in the Mesopotamian basin. While geochemical thresholds of soluble salt can provide good indications for paleoclimate development, many question regarding paleoenvironmental conditions require further data. The aim of this thesis is to gain a comprehensive understanding of palaeosedimentology, -climatology and -environment from the Lurestan arc from the middle Tortonian towards the lower Pleistocene. Therefore, multiple proxies such as XRF-whole rock geochemistry, clay mineralogy and micropalaeontology were utilized. These additional proxies can help constrain the influence of detrital salt or post diagenetic leaching of soluble salts from sediments. Furthermore, these additional proxies should help paint a better picture of the sedimentary environment and corresponding development of the provenance areas in the Zagros Mountain Belt. Comparison with published data from other sedimentary profiles in the Zagros mountain belt should help constrain obduction, erosion and subsequent sedimentation throughout space and time. This dissertation will be a first attempt in comparing high resolution clay mineralogy with soluble salt geochemistry and whole-rock geochemistry and thereby enhance the understanding of clay mineralogy in a dynamic semi-arid to hyper arid environment. Applying these methods requires careful planning, as the 84 sediment samples to be analysed consist of only 50 g of mudstone each, which necessitates a conservative use of the limited sample material, to extract as much information as possible.

Methods

2.1 Clay minerals as indicator of paleoclimate and provenance

Clay minerals are an important component of soils and sediments. They are formed by the wethering and breakdown of alumosilicate minerals such as feldspars or micas (Allen and Hajek, 1989). Common cay minerals in soils are illite, chlorite, smectite, kaolinite and palygorskite. The clay mineral assemblage in soils is influenced by a variety of different factors: 1: primary mineral assemblage of the parent rock, 2: input of detrital clay minerals, 3: weathering conditions such as temperature, precipitation and evaporation, 4: geomorphological conditions such as relief of landscape and drainage of soils (Allen and Hajek, 1989; Chamley, 1989; Singer, 1980). Subsequent erosion of soils can lead to a transport of clay minerals towards sedimentary basins, where clay mineral assemblages will integrate geological and climate impact over a larger region (Singer, 1984). Subsequent diagenesis of sedimentary rocks can furthermore influence a clay mineral assemblage (Chamley, 1989). When using clay minerals as a paleoclimate proxy they should always be employed alongside other proxies such as palynology, geochemistry or stable isotopes to differentiate the impact of climate and parent rock mineralogy or detrital clay minerals (Chamley, 1989; Singer, 1984).

Illite $(K, H_3O)(Al,Mg,Fe)_2(Si,Al)_4O_{10}[(OH)_2 \cdot (H_2O)]$ is a non swellable phyllosilicate with a 2:1 structure comprising of a silica tetrahedron (T) aluminium octahedron (O) and another silica tetrahedron (T) layer. The space in-between the T-O-T layers is occupied by a potassium cation but also H_3O (in contrast to muscovite). Illite is common in relatively unweathered soils and often inherited from parent rocks such as aluminium rich granites, shales, siltstones, and a variety of alluvial sediments and may result from alteration of coarser muscovite particles during pedogenesis (Allen and Hajek, 1989)

Chlorite $(Mg,Fe)_3(Si,Al)_4O_{10}(OH)_2 \cdot (Mg,Fe)_3(OH)_6$ are non swellable phyllosilicates with a T-O-T O structure where the negatively charged T-O-T layer is neutralized by an additional

positively charged O layer instead of an interlayer cation. Chlorite is commonly derived from the erosion of low-grade metamorphic rocks and is often inherited in soils, being relatively stable to weathering in pedogenic environments (Allen and Hajek, 1989).

Smectite group minerals have a similar 2:1 T-O-T structure as Illite minerals, however the space in-between the T-O-T layers is occupied by different cations but also water molecules and other polar liquids, giving smectite minerals swelling properties. Smectites are common in well-developed soils in temperate-arid regions were leaching of cations is restricted. In Iran most smectite in semi-arid and arid soils to have originated from transformation of palygorskite and illite. The transformation from palygorskite generally occurred at P/ET (ratio of mean annual precipitation to evapotranspiration) > 0.4 (Khormali and Abtahi, 2003)

Kaolinite $Al_2Si_2O_5(OH)_4$ is a non swellable 1:1 silicate mineral with a T-O structure without any interlayer cation. It originates from intense weathering in near-surface environments from the transformation of other clay minerals, where all large cations such as potassium have been leached. Its formation is most pronounced in humid tropical climate zones, with alternate wet and dry seasons, where drainage is unimpeded (Allen and Hajek, 1989; Tardy et al., 1973)

Palygorskite $(Mg,Al)_2Si_4O_{10}(OH)\cdot 4(H_2O)$ is a fibrous sheet silicate, commonly found in semi-arid or arid climate conditions requiring alkaline fluids with high Mg and Si activities (Singer, 1980, 1989). The authigenic formation of palygorskite by chemical precipitation has been reported from evaporative basins such as lakes and shallow saline lagoons, soils and in open oceans by hydrothermal alteration of basaltic glass or volcanic sediments (Al-Juboury, 2009; Callen, 1984; Chamley, 1989; Millot, 1970; Singer, 1979) palygorskite is often associated with pedogenic carbonates in semi-arid regions (Al-Juboury, 2009). Precipitation of gypsum in arid soils can also lead to favourable conditions of for palygorskite genesis by a relative increase in Mg activity in pore water by the preferential uptake of Ca (Khademi and Mermut, 1998). Palygorskite can form from illite and smectite at a loss of K and Al and a relative increase in Si and Mg (Suárez et al., 1994).

The distribution of clay minerals can be analysed using oriented (textured) samples of the clay fraction < 2µm using XRD. Generally, soft sediment samples can be dispersed by carefully submerging the bottom of the sample in a porcelain crucible in de-ionized water to gently disaggregate the mineral particles using the swelling properties of the smectitic clay minerals the clay fraction. Afterwards the sample can be separated by sieving of the sand fraction with a fine sieve and subsequent separation of the fraction < 2 µm in Atterberg columns after de-ionisation of the suspension. Then, a concentrated suspension of clay minerals is dried on glass slides (e.g. Brindley and Brown, 1980; Lehmann et al., 2004). Oftentimes several mineral phases are present in the clay-sized fraction with overlapping intensities of the reflexes, different orientation effects of the individual phases, swelling effects of smectites and the background in the pattern is difficult to define which leads to significant errors and uncertainties in exact clay mineral quantification (Brindley and Brown, 1980). Therefore, a comparison of the integrated reflex intensities might not be suitable for the task of clay mineral quantification. For this reason, it makes more sense to use a semi-quantitative analysis by comparing the height only of the main reflex of glycolated oriented samples (001 chlorite; 002 smectite, illite; 110 palygorskite; 100 erionite) (Johns et al., 1954).

2.2 Bulk XRF-geochemisty

Bulk rock geochemistry can be useful in determining sediment composition and changes in sediment provenance. As petrographic classification of mudstones and sandstones is sometimes hampered by a small grain size or weathering, different geochemical schemes have been developed in the past using bulk geochemistry. The most common classification is hereby the Pettijohn diagram based on the ratio of log ($Na_2O/K2O$) vs. log (SiO_2/Al_2O_3) (Pettijohn et al., 1972). In order to overcome limitations in the Pettijohn classification of shales and wackestones, the Sandclass diagram was subsequently proposed by Herron (1988) which has been shown to provide more robust classification using log ($Fe_2O_3/K2O$) vs. log (SiO_2/Al_2O_3). This classification should furthermore be more suitable for samples containing high amounts of soluble halite. In order to put the information on the relative abundance of

elements in sediments in a sedimentary basin into a geological framework, it can be helpful to normalize them to the composition of upper continental crust (McLennan, 2001). Bulk geochemistry can give further evidence about the tectonic provenance setting of clastic sediments, such as an oceanic island arc, continental island arc, active continental arc or passive margin setting using ratios of K_2O/Na_2O vs SiO_2, Al_2O_3/SiO vs. Fe_2O3 + MgO or TiO_2 vs. Fe_2O3 + MgO due to magmatic differentiation and sediment sorting characteristics (Bhatia, 1983; Roser and Korsch, 1986). Changes in bulk magmatic differentiation trends in a source area comprising igneous rocks can furthermore be determined using a ternary diagram of Zr–$15Al_2O_3$-$300TiO_2$. These elements are relatively conservative to the influence weathering, additionally they can show sorting effects between the sand fraction (zircons) and clay fraction (micas) (Garcia et al., 1994). Additional information about the input from ultramafic sources can be indicated by the mixing curves in the Y/Ni vs. Cr/V diagram (Hiscott, 1984). Bulk geochemistry can also indicate paleo weathering and climate trends, such as by the SiO_2/Al_2O_3 ratio (Etemad-Saeed et al., 2020).

2.3 Micropalaeontology

Microfossils in continental sediments can present an important archive for environmental and climatological conditions. While analysis of palynomorphs is an important tool to monitor environmental change over time, high barriers exist can exist for sample preparation due to the necessity of utilizing a HF lab (eg. El Atfy et al., 2021). Other microfossils are readily found in Neogene continental lake or floodplain sediments have a lower barrier for analysis. charophyte gyrogonites are formed by calcification of oospores of certain extant and extinct charophytes (Soulié-Märsche and García, 2015). Charophytes have been documented from various lake, pond, riverine and brackish environments (Blindow and van de Weyer, 2015). As different taxa of charophytes can have unique preferences for water salinity or water depth identification of gyrogonites can give helpful information about water availivility in arid environments (Kröpelin and Soulié-Märsche, 1991; Soulié-Märsche, 1993). The mass occurrence of certain fossil charophyte taxa in floodplain sediments may furthermore

document environmental stress (Vicente et al., 2016). Taxonomic identification of ostracod shells in continental sediments can give further information on water depth or water salinity in continental archives (Mezquita et al., 1999).

The erosion of biogenic sediments can furthermore lead to the redeposition of allochthonous microfossils, which can give information about the provenance of sediments. For example Upper Cretaceous planktic foraminifera assemblages have been reported to have been transported with little disturbance by fluvial suspensions for 1200-2400 km and were redeposited in Quaternary shallow nearshore sediments (Otvos and Bock, 1976). Similarly, fluvial reworking of radiolarians has also been reported in literature, however detailed studies on the impact of redeposition onto the assemblage are scarce (Al-Sayigh, 2013; Li and Li, 2019).

Results and Discussion

3.1 Using clay mineralogy and micropalaeontological observations to unravel Neogene climate variations in Northern Arabia

This is a summary of the results of the above titled publication from Dietzel et al. (2023), which constitutes a part of this cumulative dissertation. The represented results are not further cited as the manuscripts are part of this dissertation and found in the appendix.

The sediment samples used for soluble salt geochemistry by Böhme et al. (2021) were resampled to test the robustness of the previously employed soluble-salt proxy by comparison with clay mineral data. All 84 mudstone samples taken at the Zarrinabad and Changuleh syncline-anticline structures were prepared for clay mineral analysis. Clay mineral analysis < 2 µm was performed using a Bruker D8 advance diffractometer with a Cu-sealed tube running at 40kV/20mA, a Göbel mirror parallel beam optics, a 0.2-mm divergence slit, a fixed knife edge to suppress air scatter, and a 1D-VÅNTEC 1-detector in scanning mode with a step size of 0.008° 2θ and 360sec/ resulting in a measurement time of approximately 2h for the range from 2°2Theta - 55 °2Theta. The clay minerals along the profile comprised highly variable proportions of smectite, illite, chlorite, palygorskite, as well as the zeolite mineral erionite. The abundance of individual clay mineral was estimated in a semi-quantitative way by comparing the height of the main reflex intensities with appropriate correction factors to account for reflex overlaps. The presence of palygorskite implied both a high Mg activity in the soils during formation and the presence of arid climate conditions (Singer, 1984). Furthermore, during sample preparation charophyte gyrogonites and gypsum rhyzocretes were noted in several samples. Comparison of clay mineral data to soluble salt data indicated a systematic post-diagenic leaching of highly soluble salts at the Zarrinabad profile, which rendered the previous interpretation as unreliable. From the base of the profile at the Gachsaran Formation to the top at the Bakthiari Formation the following observations were made, the results are graphically presented in figure 2:

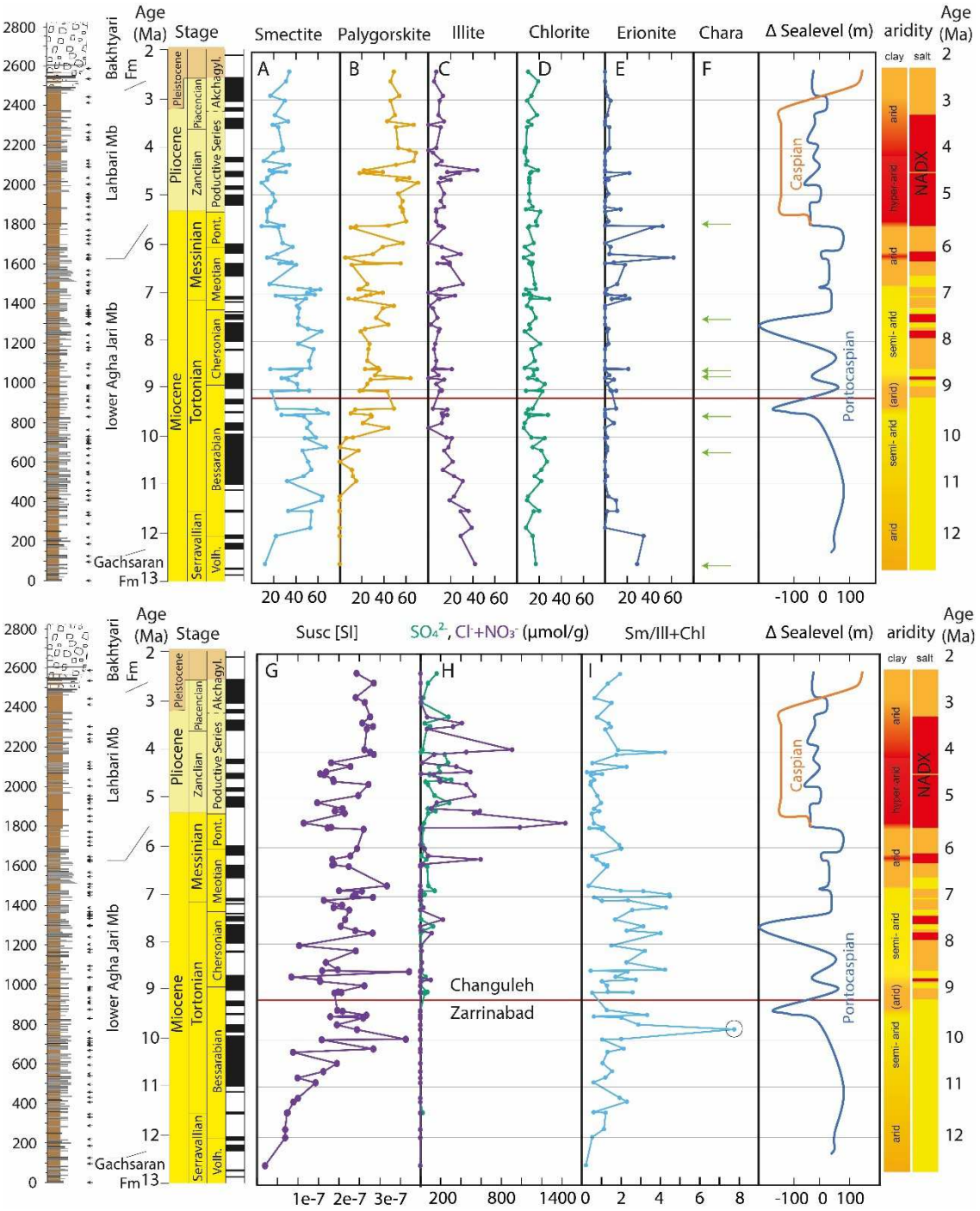

Figure 2. Variability plot of clay minerals % as function of XRD reflex intensity. Occurrence of charophytes marked by green arrows. Stratigraphic profile, sea level variations, magnetic susceptibility, soluble salt and sulphate data adapted from Böhme et al. (2021). Smectite / illite + chlorite ratio as indicator for soil moisture availability with higher ratios indicating higher moisture due to transformation of illite and chlorite to smectite. Right columns: long-term aridity interpretation based on clay mineral ratios beside soluble salt-based interpretations of Böhme et al. (2021) (Dietzel et al. 2023)

Gachsaran Formation

Clay mineralogy is indicative of an arid climate during deposition of the Gachsaran Formation. While many sub-basins of the Gachsaran Formation have been interpreted to have been deposited in a hyper saline setting the newly described presence of *Chara* sp. is indicative of freshwater-brackish conditions during deposition at the top of Gachsaran Formation.

Lower Aghajari Member

The base of the Lower Aghajari member is characterized by ilite, chlorite and minor smectite, indicating low weathering and arid climate during deposition. At ~ 10 Ma palygorskite increases sub-parallel to magnetic susceptibility. This is interpreted to be potentially indicative of additional mafic-ultramafic input due to increased erosion of obducted ophiolites in the Imbricated Zagros leading to an increased input in magnetite and magnesium (Etemad-Saeed et al., 2020). The ratio of smectite/illite + chlorite increases from the late Serravallian towards the mid Tortonian (~ 9.5 Ma). This ratio has been shown to be sensitive to of water availability in recent palygorskite-rich soils in Iran (Hashemi et al., 2013) and thus likely indicates a gradual transition from arid towards semi-arid climate conditions. A drop in of smectite/(illite + chlorite) ratio between ~9.5 and ~8.8 Ma points towards an intermittent more arid period. Between 8.75 Ma and 6.9 Ma the sediment samples are generally characterized by a high abundance of smectite, a low percentage of iillite and moderate presence of chlorite and palygorskite indicating an increase in soil water availability interpreted as semi-arid climate conditions. A sudden drop of the smectite/(illite + chlorite) ratio is caused by a strong decrease in smectite and increase in illite after 6.9 Ma until the onset of the Lahbari Member, while no major change in mafic input is indicated by magnetic susceptibility measurements. This shift in clay mineralogy is interpreted as a shift towards permanent arid conditions. The occurrence of small gyrogonites of *Chara* sp. *Chara vulgaris*, and *Chara globularis* has been noted is sediment samples throughout the lower Aghajari Mb. at 10.25 Ma, 9.51 Ma, 8.69 Ma, 8.56 Ma. Furthermore, etched gyrogonites of *Nitellopsis obtusa* were found at in a highly saline sample from 7.5 Ma. The occurrence of *Chara* sp. *Chara vulgaris*, and *Chara globularis* has been

interpreted to be related the presence of ephemeral ponds along the paleo-floodplain (Vicente et al., 2016). The occurance of *Nitellopsis obtusa* is usually related to more permanent deeper bodies of freshwater in arid environments (Kröpelin and Soulié-Märsche, 1991; Soulié-Märsche, 1993). Its presence in a sample that was previously interpreted to represent an intermittent hyper-arid period (Böhme et al., 2021) could be explained by redeposition from older lake sediments. A comparison of new clay mineralogical data and soluble salt data by Böhme et al. (2021) indicates systematic post depositional leaching of salts in samples from the Zarrinabad syncline that has not been observed at the Changuleh syncline-anticline structure. This leaching is firstly indicated by the very low soluble salt concentrations in all of the samples from the Zarrinabad sampling site Compared to samples from the Changuleh sampling site. Soluble salts are secondly absent in Zarrinabad samples where a high amount of palygorskite or a low smectite/illite + chlorite ratio is indicative of arid conditions. This post depositional leaching has likely been caused by a comparatively higher recent mean annual precipitation at the Zarrinabad sampling site (150-250 mm/a vs 85-150 mm/a) (Nikpour et al., 2022).

Lahbari Member

The clay mineralogy of the Lahbari Member between 5.59 and 4.6 Ma is generally characterized by the lowest smectite/illite + chlorite ratio throughout the sedimentary profile as well as a predominance of palygorskite. The observed clay mineralogy is compatible with the previous interpretation of hyperaridity during NADX (Böhme et al., 2021). Elevated gypsum, halite and palygorskite content in the samples might also be partially derived from other evaporative sediments due to a strong increase in aeolian dust input from a westerly source (Böhme et al., 2021). Alternatively it could be regionally sourced from tectonically exposed evaporitic sediments of the Gachsaran Formation eroded within the folded Zagros (Emami et al., 2010). The period between 4.44 and 4.33 Ma is marked by a strong decrease in palygorskite an increase in illite and smectite as well as soluble salts. This might be interpreted as unfavourable geochemical conditions for palygorskite formation conditions, a change in

parent material input or possibly short-term cooling leading to a reduction in chemical weathering. From 4.25 Ma until 2.4 Ma the clay mineralogy is generally characterized by an increase in smectite and palygorskite and a reduction in illite and in chlorite. Smectite/(illite + chlorite) points to higher soil water availability and increased chemical weathering compared to the interval between 5.59 Ma and 4.6 Ma under hyper-arid climate conditions.

Erionite

The study furthermore revealed the widespread presence of the zeolite mineral erionite throughout the sedimentary profile. Erionite has not been previously reported from this region. The presence of erionite is most likely related to the decomposition of detrital volcanic glass in the semi-arid to hyper arid flood plain sediments in the presence of alkaline and saline pore water (Hay, 1964; Surdam and Eugster, 1976). It is not clear whether the presence of volcanic glass is related to redeposited volcanoclastic material or syn-depositional ashfall events.

New open questions

In order to better differentiate the influence of climate impact and changing parent material input further detailed geochemical analysis of all the samples used for clay mineral analysis was found to be necessary. Geochemical provenance analysis will help constrain the changing influence of mafic input on palygorskite genesis and furthermore help constrain the origin of soluble salts, gypsum and palygorskite in the hyper arid sediments of the Lahbari Member. Furthermore, a detailed palynological analysis of the sediment profile would help to explain further inconsistencies in the climatological interpretation of soluble salt analysis and clay mineralogy.

3.2 Reworked Mesozoic radiolarians in Miocene-Pliocene foreland sediments in the Zagros Belt, Iran

This is a summary of the results of the above titled publication from Dietzel et al. (2024a), which constitutes a part of this cumulative dissertation. The represented results are not further cited as the manuscripts are part of this dissertation and found in the appendix

The observation of charophyte gyrogonites, that were visible with the naked eye, lead to a detailed micropaleontological investigation of the fraction > 63 µm. Microfossils in sediments can be both of detrital or autochthonous origin. While autochthonous microfossils such as charophyte gyrogonites or ostracods can give important insights into environmental conditions during sediment deposition, allochthonous microfossils can reflect changes in detrital sediment origin. Micropalaeontological analysis using a binocular revealed the widespread presence of Cretaceous marine radiolarians in the Neogene Zagros foreland sediments. This allochthonous radiolarian assemblage showed distinct differences compared to literature reports of autochthonous radiolarian assemblages reported in radiolarites from the imbricated Zagros. While previous studies from the Zagros Foreland Basin have already used the percentage of radiolarite clasts in conglomerates for quantification of clastic input from the Qulqula-Kermanshah radiolarites in the imbricated Zagros, this study is the first attempt to count individual radiolarians within mudstones for provenance purposes.

A total of 359 radiolarian skeletons was recognized and separated in 36 out of 84 samples. An increase in radiolarians per fossiliferous sample was noted in samples younger than ~10 Ma (fig 3.). This contemporaneous with an increase in palygorskite increase and likely associated with an increase in the uplift and erosion of mafic ophiolites as well as radiolarites in the Imbricated Zagros. An increase in radiolarian clasts has also been identified in Zagros Foreland sediments in the Dezful embayment, 200 km SE of this study area, one My later at ~ 9 Ma where it has been linked to tectonic exhumation and erosion of radiolarites (Etemad-

Saeed et al., 2020).

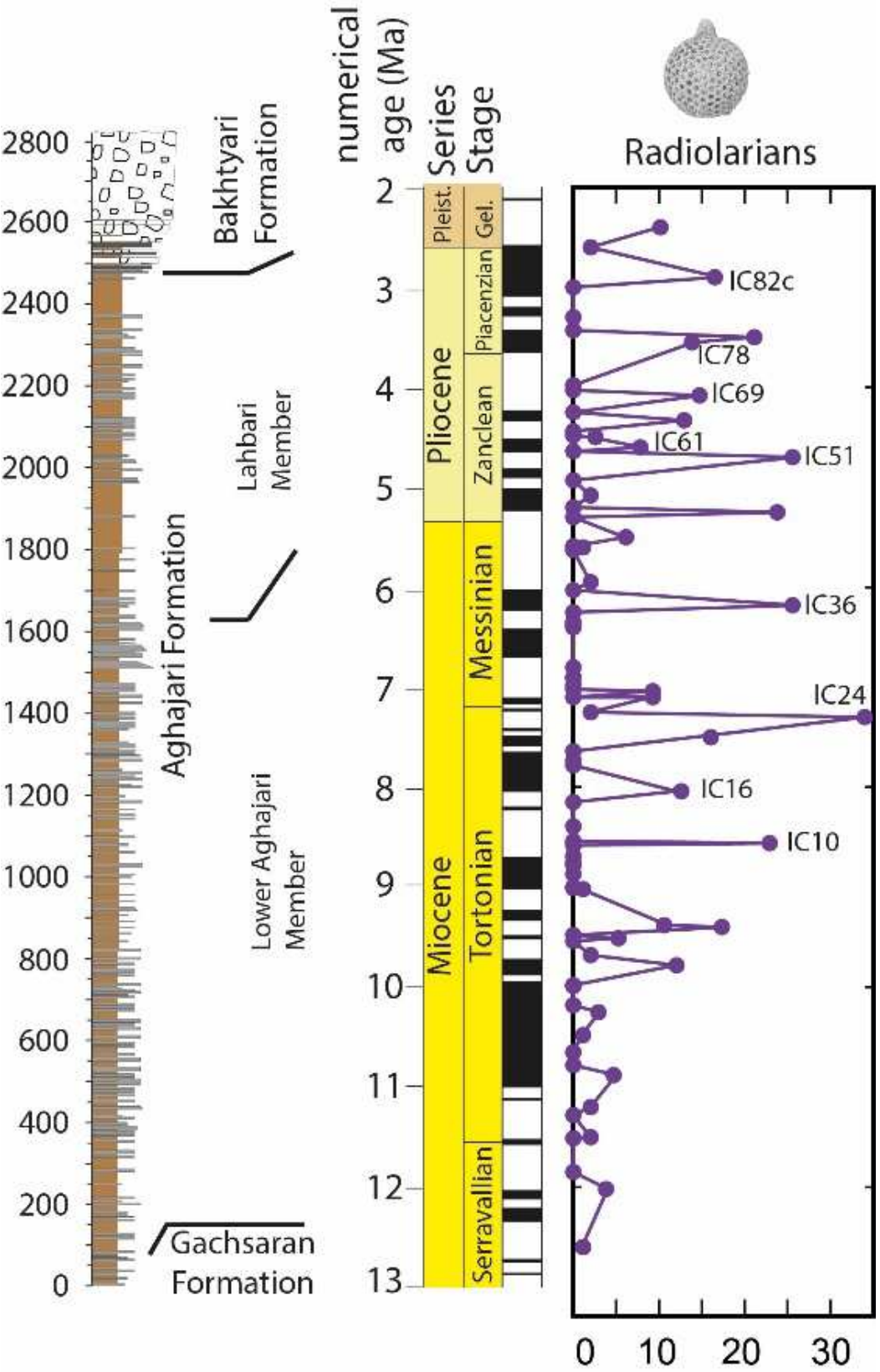

Figure 3. Combined stratigraphic profile of the sampling sites at the Zarrinabad anticline and Changuleh syncline-anticline structure. Sedimentary profile and magnetostratigraphic timescale adapted from Homke et al. (2004) sampling points adapted from Böhme et al. (2021). Line and points represent the

numbers of radiolarians found under the binocular in 5g of sediment sample. Number marks sample ID and position of illustrated radiolaria within the profile (Dietzel et al. 2024a).

The following taxa were identified in samples throughout the profile (fig 4.):

Systematic palaeontology

Class Radiolaria Müller, 1858

Subclass Polycystinea Ehrenberg, 1839, emend. Riedel, 1967

Order Nassellaria Ehrenberg, 1875

Family Archaeodictyomitridae Pessagno, 1976

Genus *Tharnala* Pessagno, 1977

Tharnala sp.

Family Artostrobiidae Riedel, 1967

Genus Rhopalosyringium Campbell and Clark, 1944

Rhopalosyringium sp.

Family Williriedellidae Dumitrica, 1970

Genus *Cryptamphorella* Dumitrica, 1970

Cryptamphorella conara Foreman, 1968

Cryptamphorella sp. cf. *C. conara* Foreman, 1968

Cryptamphorella ? sp.

Genus *Holocryptocanium* Dumitrica, 1970

Holocryptocanium barbui Dumitrica, 1970

Holocryptocanium sp. cf. *H. astiense* Pessagno, 1977

Order Spumellaria Ehrenberg, 1875

Family Dactyliosphaeridae Squinabol, 1904

Genus *Dactyliosphaera* Squinabol 1904

Dactyliosphaera ? sp.

Family Parvivaccidae Pessagno & Yang, 1989, emend. Dumitrica & Caulet, in De Wever et al. (2001)

Genus Praeconosphaera Yang, 1993

Praeconosphaera sp. cf. P. antiqua ? Parona, 1890

Family Praeconocaryommidae Pessagno, 1976

Genus *Praeconocaryomma* Pessagno, 1976

Praeconocaryomma sp. cf. *P californiaensis* Pessagno, 1976

Family *Xiphostylidae* Haeckel, 1881

Genus *Archaeocenosphaera* Pessagno, 1989

Archaeocenosphaera ? sp.

Archaeocenosphaera clathrata Parona, 1890

Archaeocenosphaera ? *mellifera* O'Dogherty, 1994

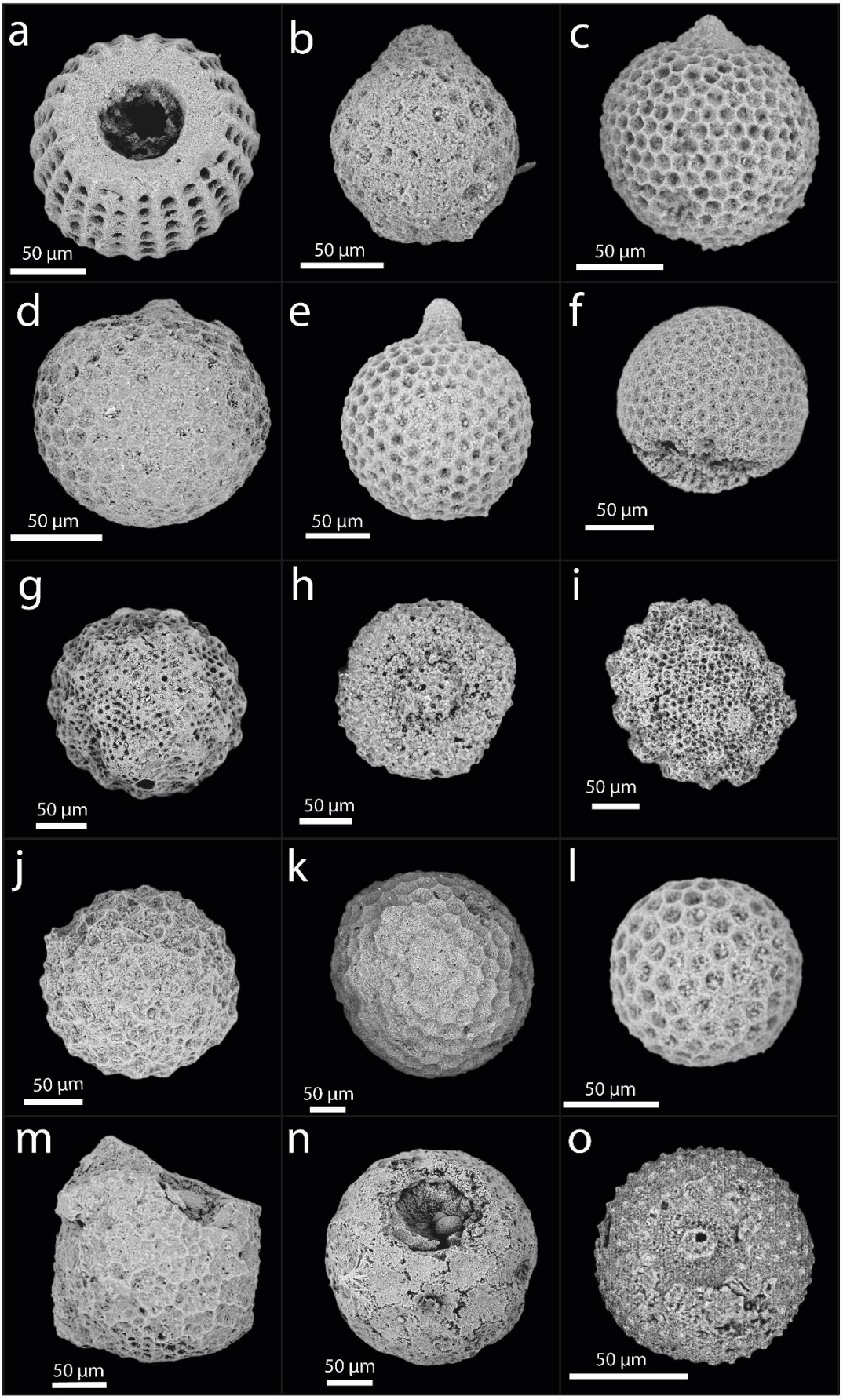
a
50 µm
b
50 µm
c
50 µm
d
50 µm
e
50 µm
f
50 µm
g
50 µm
h
50 µm
i
50 µm
j
50 µm
k
50 µm
l
50 µm
m
50 µm
n
50 µm
o
50 µm

Figure 4. SEM-Illustrations of allochthonous Jurassic and Cretaceous Radiolaria found in Lower Aghajari Formation and Lahbari Member:

a. *Tharnala* sp. sample IC21 7.5 Ma; b. *Rhopalosyringium* sp. sample IC69, 4.08 Ma; c. *Cryptamphorella conara* Foreman, 1968 sample IC51, 4.7 Ma; d. *Cryptamphorella* sp ?, sample IC21, 7.5 Ma; e. *Cryptamphorella* ? sp. 2 sample IC82c, 2.9 Ma; f. *Holocryptocanium barbui* Dumitrica, 1970 sample IC 51, 4.7 Ma; *g. Holocryptocanium* sp. cf. *H. astiense* Pessagno, 1977 sample IC 61, 4.6 Ma; h. *Dactyliosphaera* ? sample IC10, 8.56 Ma; i. *Praeconosphaera* sp. cf. *P. antiqua* Parona, 1890 *sample IC51 4.7 Ma*; j *Praeconocaryomma* sp. cf. *C. californiaensis* Pessagno, 1976, *sample IC 24, 7.3 Ma;* k. *Achaeocenosphaera* ? sp. sample IC26, 7.04 Ma; l. *Archaeocenosphaera clathrata* Parona, 1890 sample IC78, 3.55 Ma; m. *Archaeocenosphaera* ? *mellifera* O'Dogherty 1994 sample IC16, 8.04 Ma; n. Gen. et spec. indet. 1 sample IC 21 7.5 Ma o. Gen. et sp. indet. 2, sample IC61, 4.6 Ma (Dietzel et al. 2024a)

The radiolarian assemblage identified in this study is distinct from autochthonous assemblages as reported by Al-Qayim et al. (2018) and Gharib and De Wever (2010). The allochthonous assemblages of the hard radiolarite cherts of the the Qulqula-Kermanshah radiolarites are characterized both by compact-spherical radiolarians as well as highly branched-fragile taxa. The latter were not found in the allochthonous assemblage described in this study. A prime factor accounting for these differences could be a preferred erosion of interbedded radiolarian claystones. The radiolarian assemblage in claystones possibly represents the "Crypto-Archaeo" Assemblage, characterized by low diversity, ecologically tolerant forms (chiefly cryptocephalic and cryptothoracic Nassellarians and *Archeodictyomitra* spp.). These radiolarians have been interpreted to originate in the Subtropical Gyre (Baumgartner et al. 2023). In the Imbricate Zagros the "Crypto-Archaeo" Assemblage might be found in the Red Radiolarian Claystone Unit (RRCU). While in this study *Holocryptocanium barbui* (Dumitrica) is the most commonly observed taxon, in the RRCU of the Qulqula – Kermanshah radiolarites as a potential source area (Al-Qayim et al. 2018), it has been reported alongside *Archaeodictyomitra mitra* (Dumitrica), *Angulobracchia portmanni* s.l. (Baumgartner) and *Pseudodictyomitra carpatica* (Lozyinak).

The distortion of the primary radiolarian assemblage was possibly augmented by secondary transport sorting of radiolarians. The compact spherical taxa with hexagonal surface structures likely proofed more stable to wear and tear during transport than taxa with protruding fragile spines. According to an experimental study, radiolarian skeletons show a variation in sinking speed in seawater between 13 and 416 m per day (Takahashi and Honjo, 1983). Shell weight

showed highest correlation with sinking speed, while some taxa with a large spine surface demonstrated significantly reduced sinking rates. Compact, spherical radiolarians with silica infill might therefore settle to the ground quicker in a slowly flowing river, than radiolarians of a more complex structure with a higher surface-weight ratio. All factors considered, a combination of these factors likely presents an explanation for the differences between the autochthonous assemblage in the Mesozoic radiolarites in the Imbricate Zagros and the allochthonous assemblage in the Neogene foreland basin.

3.3 A revised model for Neogene Zagros foreland sedimentation in the Lurestan Arc based on new geochemical data

This is a summary of the results of the above titled publication of (Dietzel et al., 2024b), which constitutes a part of this cumulative dissertation. The represented results are not further cited as the manuscripts are part of this dissertation and found in the appendix

This paper reports on the results of a detailed geochemical analysis of samples along the Zarrinabad and Changuleh Syncline-Anticline structures. The results allude to significant change in Provenance of the sediments during the deposition of the Gachsaran Formation, Lower Aghajari Member and Lahbari Member.

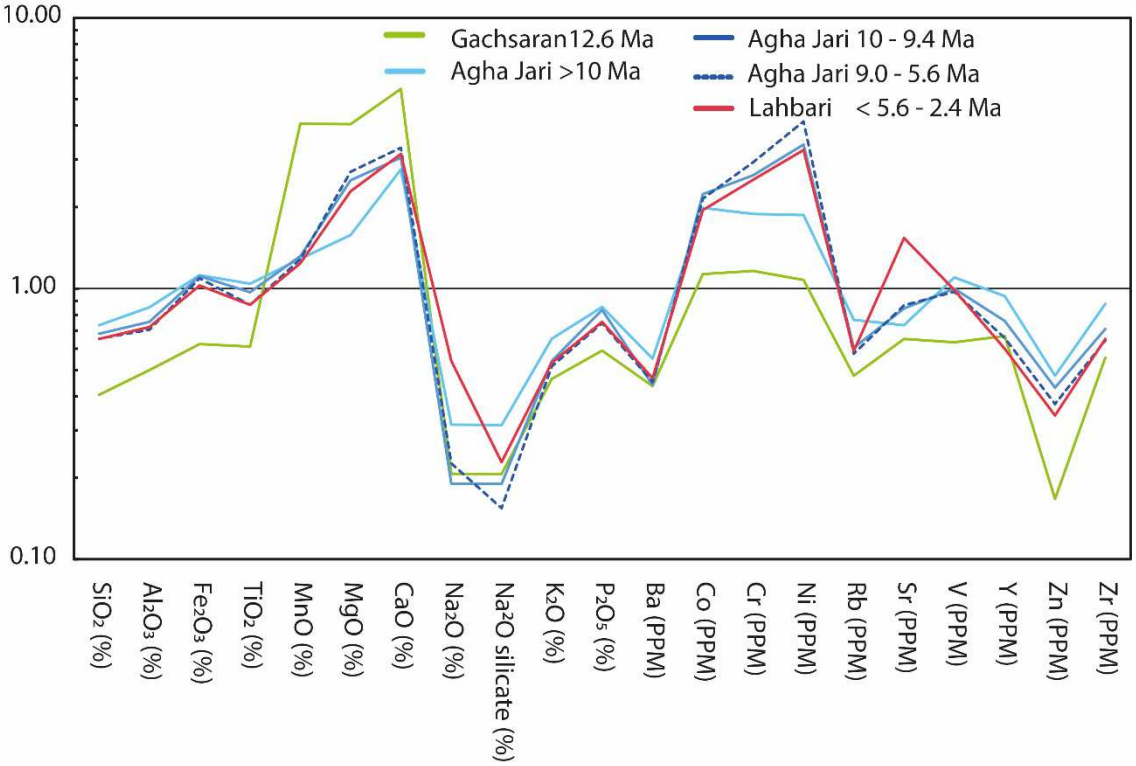

Figure 5. Major, minor and trace elements of geochemically distinct sample groups normalized to Post Archaean Australian Shale after McLennan, (2001) (Dietzel et al. 2024b)

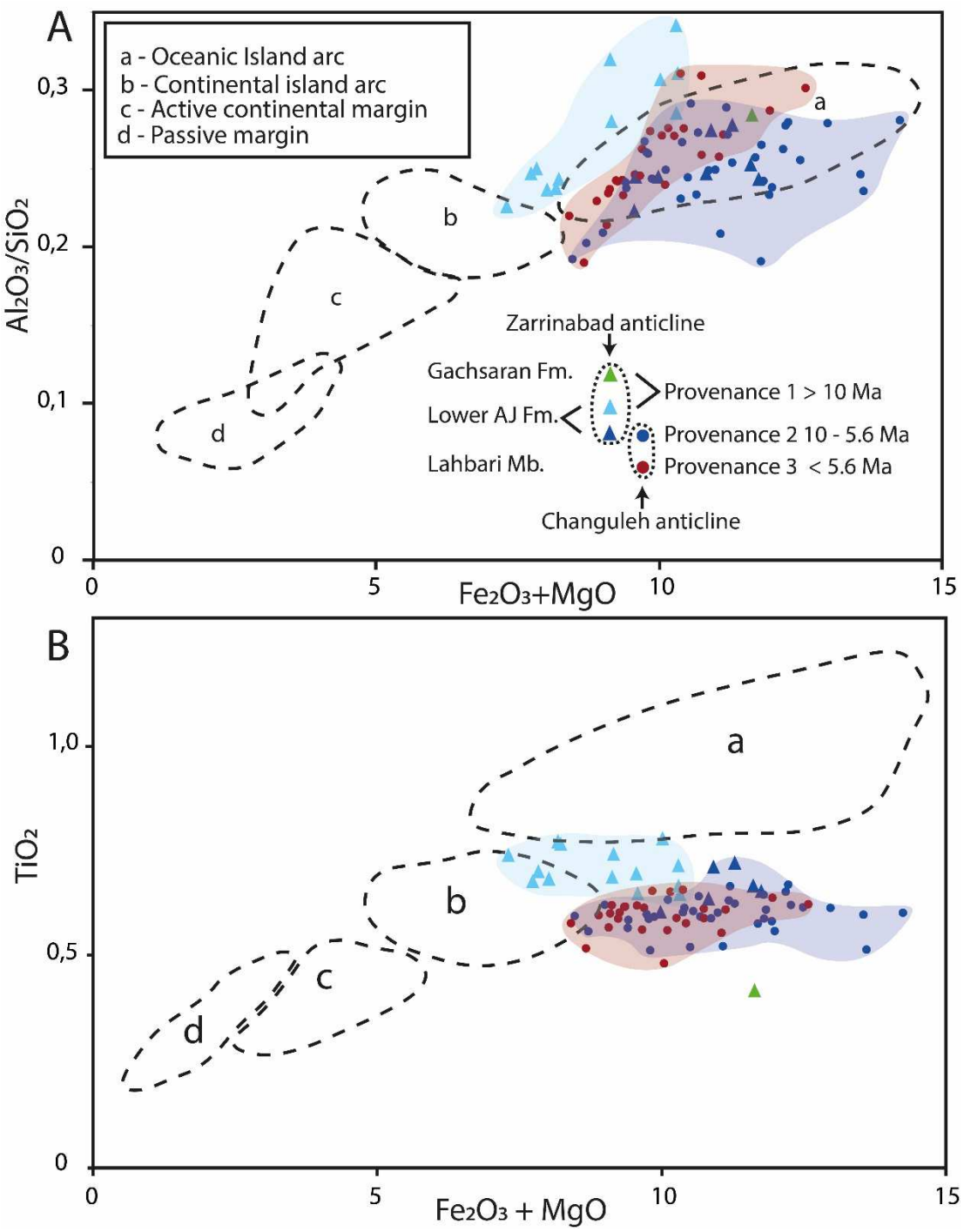

Figure 6. A determination of tectonic provenance of sandstone-mudstone suites using Al_2O_3/SiO_2 ratio content and K_2O/Na_2O ratio modified after Bathia (1983) for samples from the Gachsaran Fm., Lower Aghajari Mb. and Lahbari Mb.; b Determination of tectonic provenance of sandstone-mudstone suites using Al_2O_3/SiO_2 ratio content and TiO_2 content modified after Bathia (1983) for samples from the Gachsaran Fm, the Lower Aghajari Mb. and the Lahbari Mb. (Dietzel et al. 2024b)

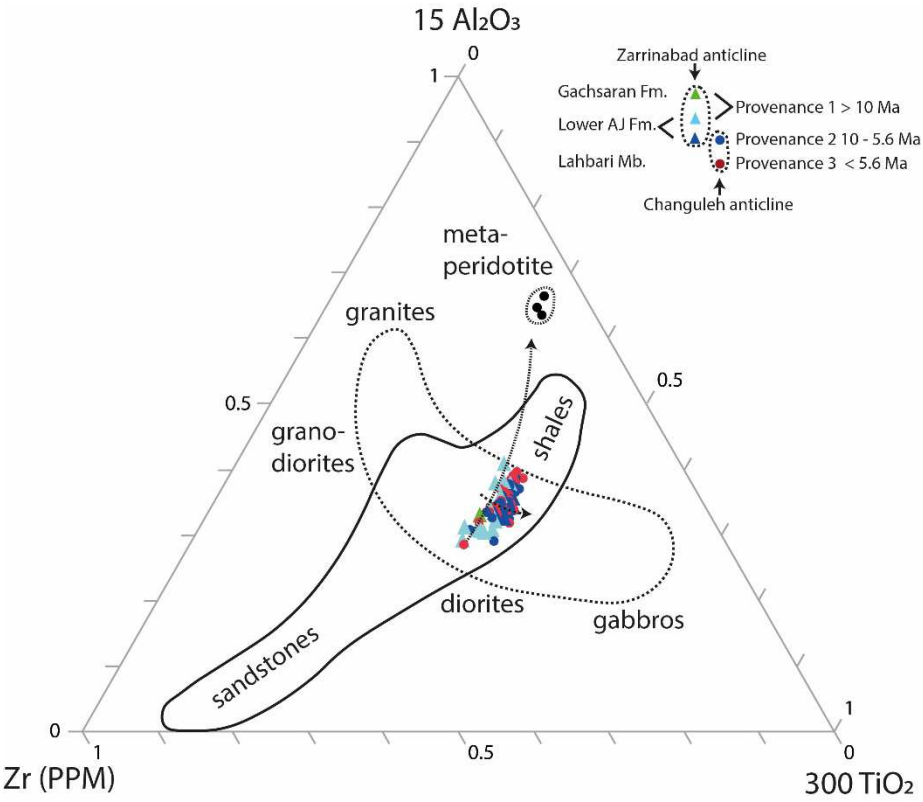

Figure 7. Ternary diagram of Zr–15Al2O3-300TiO2 (Garcia et al. 1994), as an indicator for magmatic differentiation trends in the source area and sediment recycling processes of sandstones and associated shales for samples from the Gachsaran Fm., the Lower Aghajari Mb. and the Lahbari Mb. Meta-peridotite data from the Kermanshah ophiolite is shown as additional reference from Saccani et al. (2013) Coarse dotted arrow represents the increased input of mafic components in provencance 2 compared to provenance 1. Fine dotted arrow indicates potential mixing line of additional ultramafic material which however is limeted due to low total Zr,TiO_2 and Al_2O_3 content in ultramafic rocks (Dietzel et al. 2024b).

Gachsaran Formation

The sediment sample from Gachsaran Formation is characterized by a high Mg content which is related to secondary dolomitization. The samples are geochemically depleted in felsic elements and enriched in mafic elements (fig. 5). The samples are indicated to originate from an arc-setting origin (fig. 6).

Lower Aghajari Member

Samples from the lower Aghajari Member older than ~10 Ma are generally show the lowest enrichment in mafic and lowest depletion in felsic elements of along the sedimentary profile

(fig. 5). The samples are geochemically classified as shale according to the Sandclass diagram (Herron, 1988) and indicate a geochemical provenance setting in-between a continental island arc and a oceanic island arc suite (fig.5). According to the Zr–15Al2O3-300TiO2 diagram by Garcia et al. (1994), which describes magmatic differentiation trends in the source area, their composition is generally dioritic (fig.7). The sediments are most likely primarily derived from material originating from the Sanandaj-Sirjan Zone and deposited in a fluvial environment (fig. 9). Samples younger than 10 Ma are more enriched in ultramafic and mafic elements such as Mg, Ni and Cr and more depleted in felsic elements such as Zr, Na and Si (fig 5). This is probably related to tectonic change in the Imbricate Zagros, which lead to the increased erosion of ultramafic ophiolites and the mafic volcanoclastic sediments of the Gaveh Rud domain (fig. 9). The increase in mafic erosion was already suspected based on the increase in magnetic susceptibility and palygorskite (Dietzel et al. 2023). This is also contemporaneous with the increase in radiolarians per sample, which is related to increased erosion of radiolarites (Dietzel et al., 2024). Between ~10 Ma and 5.6 Ma samples are generally strongly enriched in mafic and ultramafic elements and depleted in felsic elements (fig.5). Geochemically the origin is associated with an oceanic island arc suite albeit the samples are relatively low in Ti (fig.6). A similar geochemical shift towards a more mafic composition in foreland sediments has already been observed in samples from the Kirkuk embayment to the North at ~12 Ma and at the Dezful Embayment to the SE at ~9 Ma (Etemad-Saeed et al., 2020). This new data therefore helps in constraining the deformation across the Imbricate Zagros, which likely migrated from the N towards the SE during the late Serravallian towards the mid Tortonian. No major change in geochemistry is seen at the transition from the Zarrinabad profile towards the Changuleh profile between 9.4 Ma and 9 Ma, which is indicative of a large homogenizing catchment area (figs. 5, 6, 7). The next major shift in sediment geochemistry is indicated at the onset of the Lahbari Member. Overall palygorskite content in the Lower Aghajari Member is closely controlled by the amount of MgO available, which in turn is coupled to input of mafic clastics from the Imbricate Zagros (fig. 8).

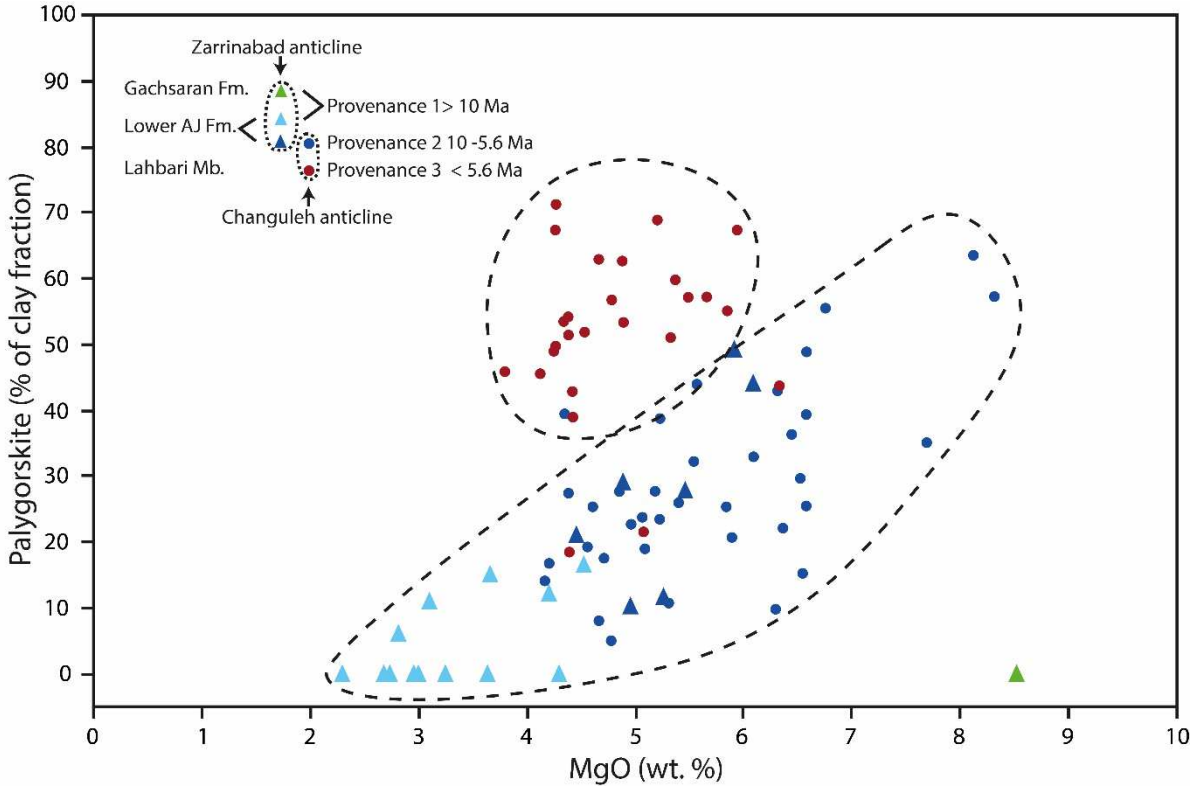

Figure 8. Palygorskite content (Dietzel et al. 2023) vs. MgO (wt.%)

Lahbari Member

The Lahbari Member is geochemically distinct from the lower Aghajari Formation by an increase in Sr and Na_2O (fig. 5). Furthermore, the Lahbari Member is characterized by a marked increase in highly soluble salts as well as sulphate (fig.2) (Böhme et al., 2021). Palygorskite also shows a sharp increase, which, unlike in the Lower Aghajari Formation, is decoupled from MgO. On geochemical tectonic provenance classification diagrams using $K_2O/Na_2O_{silikate}$ vs. SiO_2, Al_2O_3/SiO_2 vs. Fe_2O_3 + MgO, TiO_2 vs. Fe_2O_3 + MgO, Zr vs. $15Al_2O_3$ vs. $300TiO_2$, Y/Ni vs. Cr/V and in the Sandclass diagram all samples of the Lahbari Member plot exactly in-between the samples older than 10 Ma and younger than 10 Ma (figs. 6, 7 and appendix 3). This points to a sedimentary origin largely from a mixture of older Lower Aghajari and Gachsaran sediments, which were regionally uplifted above the proposed low-angle blind thrust, which generated the Pusht-e Kuh Arc rise around 5.5 Ma as suggested by Emami et al. (2010). These sediments are represented by large unconsolidated sandstone sheets, likely deposited by distal alluvial fans of along a bajada environment (fig.10). The sedimentation was

however affected by superimposed contemporaneous hyper-aridification due to a Pontocaspian sea-level drop off (Böhme et al., 2021). The hyper-arid climate was beneficial in the pile-up of thick aeolian siltstones, which were to a large extend recycled from the fine grained alluvial fans in the piedmont of the rising Pusht-e Kuh (Lurestan) Arc. While the additional palygorskite and Sr and sulphate in the Lahbari Member probably originates from the Gachasaran Formation material within these fans (eg. Al-Juboury, 2009), the local Gachsaran evaporites have been reported to be poor in halite (Bahroudi and Koyi, 2004). Furthermore, no salt-pan crusts are discernible throughout the Lahbari Member as typically seen after the evaporation of saline brines. The high amounts of fine-grained nitrides and chlorides therefore likely originates from additional atmospheric deposition. These chloride and nitrate minerals were preserved in the siltstones due to the prevailing hyper-arid climate conditions during NADX. An intermittent interval of fluvial deposition might be present between 4.5 Ma and 4.3 Ma, where clay mineralogy, geochemical trends and soluble sat geochemistry are similar to those found in the Lower Aghajari Mb. A transition towards coarse grained alluvial fans marks the transition towards the conglomeratic Bakthiari Formation at 2.5 Ma. This transition reflects a steepening relief in front of the MFF and the alluvial redeposition of more competent strata from a deeper stratigraphic level in the Anaran Anticline (fig.10).

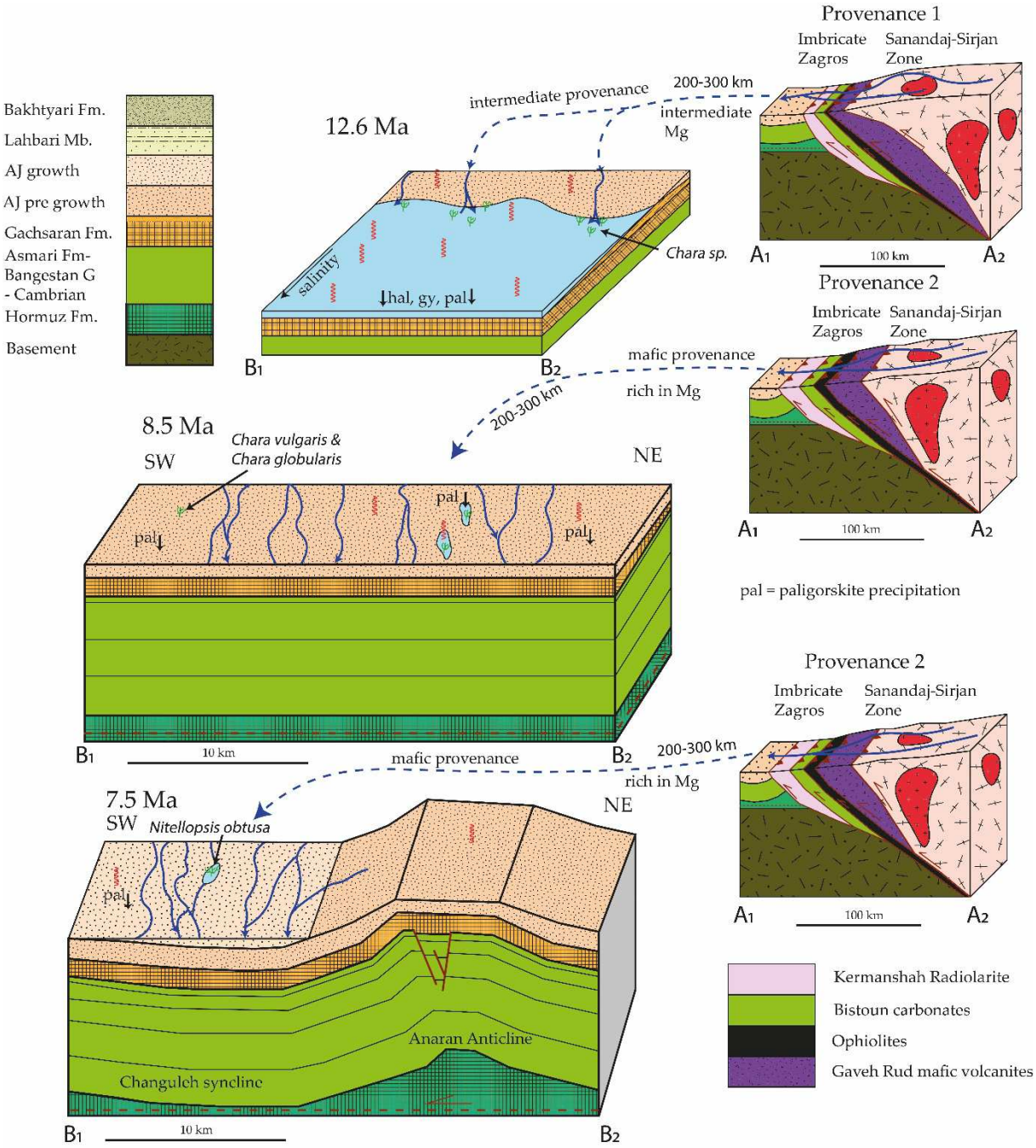

Figure 9. Proposed tectonic and sedimentological evolution of the central Imbricate Zagros NE of the Lurestam arc as source area (right) and the Changuleh-Anaran syncline anticline structure as sink area (left) during the Serravallian and Tortonian. General Changuleh-Anaran syncline-anticline structure evolution modified after Emami et al. (2010), geological cross section of the Imbricate Zagros modified after Ali et al. (2014). pal=palygorskite precipitation, micropalaeontology from Dietzel et al. (2023) (Dietzel et al. 2024b).

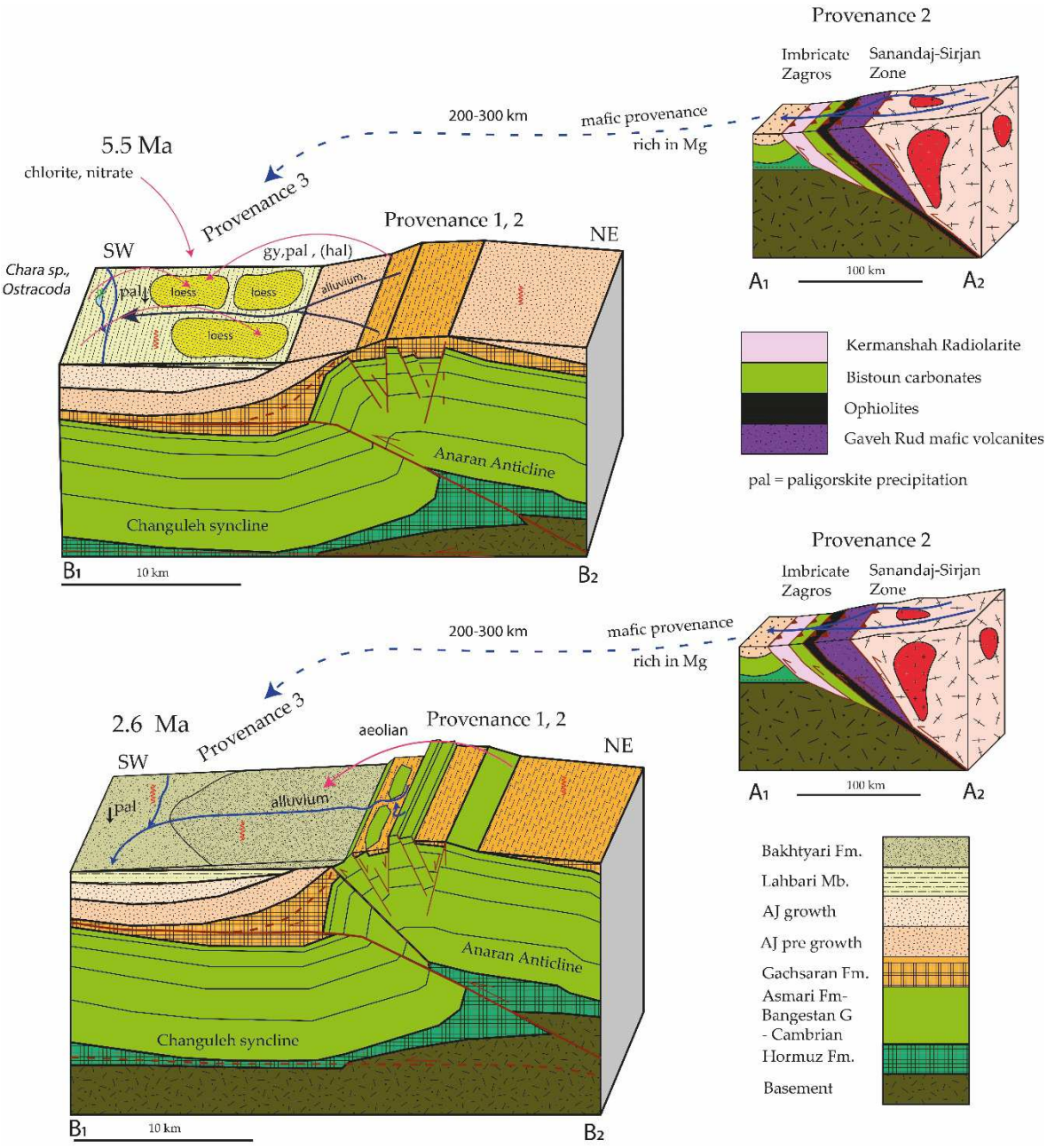

Figure 10. Proposed tectonic and sedimentological evolution of the central Imbricate Zagros NE of the Lurestan arc as source area (right) and the Changuleh-Anaran syncline anticline structure as sink area (left) during the Messinian and Pliocene. General Changuleh-Anaran syncline-anticline structure evolution modified after Emami et al. (2010), geological cross section of the Imbricate Zagros modified after Ali et al. (2014). pal=palygorskite precipitation, micropalaeontology from (Dietzel et al., 2023) (Dietzel et al. 2024b).

4. Conclusion

The three studies shed new light on the Neogene depositional environment of the Mesopotamian Foreland Basin highlighting the complex interactions of tectonics and climate during sediment deposition. While lower parts of the evaporitic Gachsaran Formation often contain palygorskite, gypsum and sometimes halite (Al-Juboury, 2009), no palygorskite gypsum or halite was detected in the dolomitic sample taken from uppermost Gachsaran Formation even though clay mineralogy is indicative of arid climate conditions. The probable explanation is a post depositional magnesium enrichment by dolomite-formation close to the shoreline by aqueous solutions, as low chromium and nickel contents point to a low initial presence of mafic magnesium rich minerals within the sediment. The presence of charophyte gyrogonites is also indicative of non-saline conditions during deposition likely due to ample freshwater supply from rivers in along the shoreline of the shallow evaporative Gachsaran basin. The Lower Aghajari Member until ~ 10 Ma represents an arid floodplain-environment, where the geochemically intermediate material originating from the Sanandaj-Sirjan Zone is only weakly affected by chemical weathering along the floodplain as witnessed by the very low smectite/(illite + chlorite) ratio. Gradual tectonic change in the source region of the imbricated Zagros is indicated by a multitude of proxies: Increase of magnetic susceptibility, MgO, Cr, Ni and chlorite point to the obduction of ultramafic ophiolites and mafic volcanoclastic rocks of the Gaveh-Rud Formation. A contemporaneous obduction of radiolarites is witnessed by an increase in the number of reworked radiolarians per sample. This increase in MgO enabled the formation of palygorskite within the arid soils of the floodplain in an almost linear relationship. At the same time a slow gradual increase in smectite and an increase smectite/illite + chlorite ratio gives evidence to a growing soil moisture availability. This gradual transition towards semi-arid climate conditions from ~12 Ma towards ~ 10 Ma is perhaps a result of changing precipitation patterns along the headwaters due to a rise up of the imbricated Zagros mountain range. This is also augmented by a gradual increase in the sedimentation rate. Between 8.2 and 7.1 the sedimentation starts to be locally affected by westward

progressing deformation in the Simply Folded Belt as documented in the first appearance of growth strata (Homke et al., 2004). A major shift is apparent in clay mineralogy but not in geochemical composition, magnetic susceptibility or number of radiolarians per sample in samples younger 6.9 Ma. A strong decrease of smectite and increase in illite indicate more limited chemical weathering. This might be due to aridification or cooling or due to a sudden regional change in drainage patterns in the headwaters due to the folding up of anticlines in the Simply Folded Belt. No adequate correlation is seen between this long-term change in clay mineralogy and modelled sea level change in the Pontocaspian sea as a proposed driver for regional climate trends (Böhme et al., 2021) and is therefore rather caused by regional tectonic change. Lithologically the onset of the Lahbari Member is marked by the deposition of thin sheets of immature, alluvial sandstones from distal alluvial fans in a bajada environment interbedded with thick structureless aeolian siltstones. Geochemical and clay-mineralogical analysis of siltstones point to a sedimentary origin characterized by a mixture of older Lower Aghajari and Gachsaran sediments with the addition of highly soluble nitrate and chloride salts from atmospheric origin. The deposition of alluvial fans was likely caused by redeposition of older Lower Aghajari and Gachsaran sediments, which were regionally uplifted above the proposed low-angle blind thrust, generating the Pusht-e-Kuh (Lurestan) Arc rise around 5.5 Ma (Emami et al., 2010). Fine grained clastic material from these fans along the floodplain was then remobilized by strong Shamal winds from the west during a superimposed hyper-arid phase of climate (NADX) (e.g. Böhme et al., 2021) leading to the deposition of aeolian silts in the piedmont of the mountain front flexure. Further tectonic obduction of the diagenetically consolidated, older core of the neighbouring Anaran Anticline eventually resulted in the deposition of coarse-grained alluvial conglomerates at 2.5 Ma.

This thesis demonstrates the necessity of employing multiple proxies in order to reach a robust sedimentological and paleoclimatological model. While soluble salt can be useful in delineating short phases of high aridity, it proofed highly sensitive to post depositional leaching and intermittent phases of high aridity sometimes correlated inadequately with interpretations from clay mineralogy. Clay mineralogy is less sensitive to post depositional leaching in the

interpretation of paleoclimatological trends. However extreme care must be taken in clay mineralogical change across a sedimentary profile as it is highly geochemically sensitive to changing parent material input and detrital clay minerals. The sensitivity to changing parent material geochemistry was demonstrated by the sensitivity of palygorskite formation both to local weathering conditions and magnesium availability. However the smectite/(illite + chlorite) ratio as suggested by Hashemi et al. (2013) appeared to be a helpful proxy for water availability in palygorskite rich soils. Detailed micropalaeontological investigation proofed useful in two aspects: The observation of charophyte gyrogonites provided information on paleoenvironmental conditions such as freshwater availability, water salinity and environmental stress at the time of sediment deposition during the Miocene. The investigation of allochthonous radiolarians within the sediments gave additional information on sediment provenance and tectonic change in the Imbricate Zagros, which matched well with the geochemical results. In order to verify or adapt the current palaeoclimatological interpretation a detailed palynological study along this reference profile would be highly warranted for comparative purposes. A second fieldwork campaign would be useful in order to geochemically investigate deeper parts of the Gachsaran formation for traces of palygorskite, and soluble salts within the Anaran anticline and visually trace the distal alluvial fans in the Lahbari Member back to the proposed source region. The Changuleh Anticline is currently the only well-dated outcrop of Miocene-Late Pliocene sediments. It would therefore be advisable to investigate drillcores from the wider Mesopotamian foreland basin in Iraq for contemporaneous sedimentological and geochemical records in order to better delineate local versus regional palaeoclimatological and sedimentological signals.

References

Al-Juboury, A. I., 2009, Palygorskite in Miocene rocks of northern Iraq: environmental and geochemical indicators: Acta Geologica Polonica, v. 59, no. 2, p. 269-282.

Al-Qayim, B. A., Baziany, M. M., and Ameen, B. M., 2018, Mesozoic Tethyan Radiolarite age determination, Zagros suture zone, Kurdistan, NE Iraq: The Iraqi Geological Journal, p. 17-33.

Al-Sayigh, A. R. S., 2013, Neorotalia omanensis and Operculina musawaensis from the Sultanate of Oman: Sultan Qaboos University Journal for Science [SQUJS], v. 18, p. 41-53.

Alavi, M., 1994, Tectonics of the Zagros orogenic belt of Iran: new data and interpretations: Tectonophysics, v. 229, no. 3-4, p. 211-238.

-, 2007, Structures of the Zagros fold-thrust belt in Iran: American Journal of science, v. 307, no. 9, p. 1064-1095.

Ali, S. A., Mohajjel, M., Aswad, K., Ismail, S., Buckman, S., and Jones, B., 2014, Tectono-stratigraphy and structure of the northwestern Zagros collision zone across the Iraq-Iran border: Faculty of Science, Medicine and Health - Papers: part A. 2058.

Allen, B., and Hajek, B., 1989, Mineral occurrence in soil environments: Minerals in soil environments, v. 1, p. 199-278.

Baharifar, A., Moinevaziri, H., Bellon, H., and Piqué, A., 2004, The crystalline complexes of Hamadan (Sanandaj–Sirjan zone, western Iran): metasedimentary Mesozoic sequences affected by Late Cretaceous tectono-metamorphic and plutonic events: Comptes Rendus Geoscience, v. 336, no. 16, p. 1443-1452.

Bahroudi, A., and Koyi, H. A., 2004, Tectono-sedimentary framework of the Gachsaran Formation in the Zagros foreland basin: Marine and Petroleum Geology, v. 21, no. 10, p. 1295-1310.

Berberian, F., Muir, I., Pankhurst, R., and Berberian, M., 1982, Late Cretaceous and early Miocene Andean-type plutonic activity in northern Makran and Central Iran: Journal of the Geological Society, v. 139, no. 5, p. 605-614.

Berberian, M., 1995, Master “blind” thrust faults hidden under the Zagros folds: active basement tectonics and surface morphotectonics: Tectonophysics, v. 241, no. 3-4, p. 193-224.

Berberian, M., and King, G., 1981, Towards a paleogeography and tectonic evolution of Iran: Canadian journal of earth sciences, v. 18, no. 2, p. 210-265.

Bhatia, M. R., 1983, Plate tectonics and geochemical composition of sandstones: The Journal of Geology, v. 91, no. 6, p. 611-627.

Blanc, E.-P., Allen, M. B., Inger, S., and Hassani, H., 2003, Structural styles in the Zagros simple folded zone, Iran: Journal of the Geological Society, v. 160, no. 3, p. 401-412.

Blindow, I., and van de Weyer, K., 2015, Ökologie der Characeen: Armleuchteralgen: Die Characeen Deutschlands, p. 79-95.

Böhme, M., Spassov, N., Majidifard, M. R., Gärtner, A., Kirscher, U., Marks, M., Dietzel, C., Uhlig, G., El Atfy, H., and Begun, D. R., 2021, Neogene hyperaridity in Arabia drove the directions of mammalian dispersal between Africa and Eurasia: Communications Earth & Environment, v. 2, no. 1, p. 1-13.

Brindley, G., and Brown, G., 1980, Quantitative X-ray mineral analysis of clays: Crystal structures of clay minerals and their X-ray identification, v. 5, p. 411-438.

Callen, R. A., 1984, Clays of the palygorskite-sepiolite group: depositional environment, age and distribution, Developments in sedimentology, Volume 37, Elsevier, p. 1-37.

Campbell, A. S., and Clark, B. L., 1944, Radiolaria from upper Cretaceous of middle California, Geological Society of America.

Chamley, H., 1989, Clay Sedimentology, Clay Sedimentology, 623 p.:

De Wever, P., Dumitrica, P., Caulet, J. P., Nigrini, C., and Caridroit, M., 2001, Radiolarians in the sedimentary record, Gordon and Breach Science Publisher.

Dietzel, C., El Atfy, H., Berthold, C., Majidifard, M., and Böhme, M., 2024a, Reworked Mesozoic radiolarians in Miocene-Pliocene foreland sediments in Zagros Belt, Iran: Rivista Italiana di Paleontologia e Stratigrafia, v. 130(1).

Dietzel, C. A., Berthold, C., Kirscher, U., Majidifard, M. R., and Böhme, M., 2023, Using clay mineralogy and micropalaeontological observations to unravel Neogene climate variations in Northern Arabia: Arabian Journal of Geosciences, v. 16, no. 5, p. 343.

Dietzel, C. A., Kirscher, U., Berthold, C., Majidifard, M. R., and Böhme, M., 2024b, A revised model for Neogene Zagros foreland sedimentation in the Lurestan arc based on new geochemical data: Basin Research, v. 36, no. 2, p. e12861.

Dumitrica, P., 1970, Cryptocephalic and cryptothoracic Nassellaria in some Mesozoic deposits of Romania: Rev Roum Geol Geophys Geogr, Serie de Geologie, v. 14, p. 45-124.

El Atfy, H., El Beialy, S. Y., El Khoriby, E. M., and Uhl, D., 2021, Continental palynomorphs from the Dabaa Formation, North-Western Desert, Egypt: a contribution to the reconstruction of the vegetation on the southern shores of the Tethys Ocean during the Early Oligocene: Botanical Journal of the Linnean Society, v. 197, no. 3, p. 291-321.

Emami, H., Vergés, J., Nalpas, T., Gillespie, P., Sharp, I., Karpuz, R., Blanc, E., and Goodarzi, M., 2010, Structure of the Mountain Front Flexure along the Anaran anticline in the Pusht-e Kuh Arc (NW Zagros, Iran): insights from sand box models: Geological Society, London, Special Publications, v. 330, no. 1, p. 155-178.

Etemad-Saeed, N., Najafi, M., and Vergés, J., 2020, Provenance evolution of Oligocene–Pliocene foreland deposits in the Dezful embayment to constrain Central Zagros exhumation history: Journal of the Geological Society, v. 177, no. 4, p. 799-817.

Foreman, H. P., 1968, Upper Maestrichtian Radiolaria of California: Special Papers in Palaeontology, v. 3.0

Garcia, D., Fonteilles, M., and Moutte, J., 1994, Sedimentary fractionations between Al, Ti, and Zr and the genesis of strongly peraluminous granites: The Journal of Geology, v. 102, no. 4, p. 411-422.

Gharib, F., and De Wever, P., 2010, Radiolaires mésozoïques de la formation de Kermanshah (Iran): Comptes Rendus Palevol, v. 9, no. 5, p. 209-219.

Haeckel, E., 1881, Prodromus systematis radiolarium, Entwurf eines Radiolarien-Systems auf Grund von Studien der challenger-radiolarien: Jenaische Zeitschrift für Naturwissenschaft, v. 15, p. 418.

Hashemi, S., Baghernejad, M., and Najafi, G. M., 2013, Clay mineralogy of gypsiferous soils under different soil moisture regimes in Fars Province, Iran: Journal of Agricultural Science and Technology, v. 15, p. 1053-1068.

Hay, R. L., 1964, Phillipsite of saline lakes and soils: American Mineralogist: Journal of Earth and Planetary Materials, v. 49, no. 9-10, p. 1366-1387.

Herron, M. M., 1988, Geochemical classification of terrigenous sands and shales from core or log data: Journal of Sedimentary Research, v. 58, no. 5, p. 820-829.

Hiscott, R. N., 1984, Ophiolitic source rocks for Taconic-age flysch: Trace-element evidence: Geological Society of America Bulletin, v. 95, no. 11, p. 1261-1267.

Homke, S., Vergés, J., Garcés, M., Emami, H., and Karpuz, R., 2004, Magnetostratigraphy of Miocene–Pliocene Zagros foreland deposits in the front of the Push-e Kush arc (Lurestan Province, Iran): Earth and Planetary Science Letters, v. 225, no. 3-4, p. 397-410.

Homke, S., Vergés, J., Serra-Kiel, J., Bernaola, G., Sharp, I., Garcés, M., Montero-Verdú, I., Karpuz, R., and Goodarzi, M. H., 2009, Late Cretaceous–Paleocene formation of the proto–Zagros foreland basin, Lurestan Province, SW Iran: Geological Society of America Bulletin, v. 121, no. 7-8, p. 963-978.

Homke, S., Vergés, J., Van Der Beek, P., Fernandez, M., Saura, E., Barbero, L., Badics, B., and Labrin, E., 2010, Insights in the exhumation history of the NW Zagros from bedrock and detrital apatite fission-track analysis: Evidence for a long-lived orogeny: Basin Research, v. 22, no. 5, p. 659-680.

Honarmand, M., Omran, N. R., Corfu, F., Emami, M. H., and Nabatian, G., 2013, Geochronology and magmatic history of a calc-alkaline plutonic complex in the Urumieh-Dokhtar Magmatic Belt, Central Iran: Zircon ages as evidence for two major plutonic episodes: Neues Jahrbuch für Mineralogie-Abhandlungen, v. 190, no. 1, p. 67-77.
Johns, W. D., Grim, R. E., and Bradley, W. F., 1954, Quantitative estimations of clay minerals by diffraction methods: Journal of Sedimentary Research, v. 24, no. 4, p. 242-251.
Khademi, H., and Mermut, A., 1998, Source of palygorskite in gypsiferous Aridisols and associated sediments from central Iran: Clay minerals, v. 33, no. 4, p. 561-578.
Khormali, F., and Abtahi, A., 2003, Origin and distribution of clay minerals in calcareous arid and semi-arid soils of Fars Province, southern Iran: Clay Minerals, v. 38, no. 4, p. 511-527.
Khormali, F., Abtahi, A., and Owliaie, H., 2005, Late Mesozoic—Cenozoic clay mineral successions of southern Iran and their palaeoclimatic implications: Clay minerals, v. 40, no. 2, p. 191-203.
Koshnaw, R. I., Horton, B. K., Stockli, D. F., Barber, D. E., Tamar-Agha, M. Y., and Kendall, J. J., 2017, Neogene shortening and exhumation of the Zagros fold-thrust belt and foreland basin in the Kurdistan region of northern Iraq: Tectonophysics, v. 694, p. 332-355.
Kröpelin, S., and Soulié-Märsche, I., 1991, Charophyte remains from Wadi Howar as evidence for deep Mid-Holocene freshwater lakes in the Eastern Sahara of Northwest Sudan: Quaternary Research, v. 36, no. 2, p. 210-223.
Lawa, F., Koyi, H., and Ibrahim, A., 2013, Tectono-stratigraphic evolution of the NW segment OF the Zagros fold-thrust belt, Kurdistan, NE Iraq: Journal of Petroleum Geology, v. 36, no. 1, p. 75-96.
Le Garzic, E., Vergés, J., Sapin, F., Saura, E., Meresse, F., and Ringenbach, J., 2019, Evolution of the NW Zagros Fold-and-Thrust Belt in Kurdistan Region of Iraq from balanced and restored crustal-scale sections and forward modeling: Journal of Structural Geology, v. 124, p. 51-69.
Lehmann, M., Berthold, C., Pabst, W., Gregorová, E., and Nickel, K., Particle Size and Shape Characterization of Kaolins-Comparison of Settling Methods and Laser Diffraction, *in* Proceedings Key Engineering Materials2004, Volume 264, Trans Tech Publ, p. 1387-1390.
Li, X., and Li, G., 2019, First Report of Redeposited Cretaceous Radiolarians in the Eocene Sand-Shale Member of Zhepure Formation, Tüna, Yadong, Tibet: Land-Ocean Linkage: Pelagic Cherts in Mesozoic Neritic-Terrestrial Sequences in East Asia, v. 9, p. 568.
Manzi, V., Gennari, R., Hilgen, F., Krijgsman, W., Lugli, S., Roveri, M., and Sierro, F. J., 2013, Age refinement of the Messinian salinity crisis onset in the Mediterranean: Terra Nova, v. 25, no. 4, p. 315-322.
Matsuoka, A., 1984, Late Jurassic four-segmented nassellarians (radiolaria) from Shikoku, Japan: Journal of Geosciences, Osaka City University, v. 27, p. 143-153.
McLennan, S. M., 2001, Relationships between the trace element composition of sedimentary rocks and upper continental crust: Geochemistry, Geophysics, Geosystems, v. 2, no. 4.
McQuarrie, N., 2004, Crustal scale geometry of the Zagros fold–thrust belt, Iran: Journal of structural Geology, v. 26, no. 3, p. 519-535.
Mezquita, F., Tapia, G., and Roca, J., 1999, Ostracoda from springs on the eastern Iberian Peninsula: ecology, biogeography and palaeolimnological implications: Palaeogeography, Palaeoclimatology, Palaeoecology, v. 148, no. 1-3, p. 65-85.
Millot, G., 1970, Geology of clays: weatering, sedimentology, geochemistry, Springer-Verlag.
Mohajjel, M., and Fergusson, C., 2013, Jurassic to Cenozoic tectonics of the Zagros Orogen in northwestern Iran: International Geology Review, v. 56, no. 3, p. 263-287.
Mohajjel, M., and Fergusson, C. L., 2000, Dextral transpression in Late Cretaceous continental collision, Sanandaj–Sirjan zone, western Iran: Journal of Structural geology, v. 22, no. 8, p. 1125-1139.
Molinaro, M., Guezou, J.-C., Leturmy, P., Eshraghi, S., and de Lamotte, D. F., 2004, The origin of changes in structural style across the Bandar Abbas syntaxis, SE Zagros (Iran): Marine and Petroleum Geology, v. 21, no. 6, p. 735-752.

Mouthereau, F., Tensi, J., Bellahsen, N., Lacombe, O., De Boisgrollier, T., and Kargar, S., 2007, Tertiary sequence of deformation in a thin-skinned/thick-skinned collision belt: The Zagros Folded Belt (Fars, Iran): Tectonics, v. 26, no. 5.

Nikpour, N., Fotoohi, S., Hosseini, S. Z., Negaresh, H., and Bahrami, S., 2022, An assessment of land degradation and its effects on geomorphology using LADA model: a case study of Ilam Province, west of Iran: Environmental Earth Sciences, v. 81, no. 10, p. 274.

O'Dogherty, L., 1994, Biochronology and paleontology of mid-Cretaceous radiolarians from northern Apennines (Italy) and Betic Cordillera (Spain), Section des sciences de la terre, Université de Lausanne.

Otvos, E. G., and Bock, W. D., 1976, Massive long-distance transport and redeposition of Upper Cretaceous planktonic foraminifers in Quaternary sediments: Journal of Sedimentary Research, v. 46, no. 4, p. 978-984.

Parona, C., 1890, Radiolarie nei noduli selciosi del calcare giurese di Cittiglio presso Laverno: Bolettino Della Societa Geologica Italiana, v. 9, p. 132-175.

Perşoiu, A., Ionita, M., and Weiss, H., 2019, Atmospheric blocking induced by the strengthened Siberian High led to drying in west Asia during the 4.2 ka BP event–a hypothesis: Climate of the Past, v. 15, no. 2, p. 781-793.

Pessagno, 1976, Radiolarian zonation and stratigraphy of the Upper Cretaceous portion of the Great Valley sequence, California Coast Ranges: Micropaleontology, Spec. publ., v. 2, p. 1-95.

Pessagno, E. A., 1977, Lower Cretaceous radiolarian biostratigraphy of the Great Valley sequence and Franciscan complex, California coast ranges, Cushman Foundation for Foraminiferal Research.

Pessagno, E. A., Six, W. M., and Yang, Q., 1989, The Xiphostylidae Haeckel and Parvivaccidae, n. fam.,(Radiolaria) from the North American Jurassic: Micropaleontology, p. 193-255.

Pettijohn, F. J., Potter, P. E., and Siever, R., 1972, Sand and sandstone, Springer Science & Business Media.

Riedel, W., 1967, Some new families of Radiolaria: Proc. Geol. Soc. London, v. 1640, p. 148-149.

Roser, B., and Korsch, R., 1986, Determination of tectonic setting of sandstone-mudstone suites using SiO2 content and K2O/Na2O ratio: The Journal of Geology, v. 94, no. 5, p. 635-650.

Saura, E., Garcia-Castellanos, D., Casciello, E., Parravano, V., Urruela, A., and Vergés, J., 2015, Modeling the flexural evolution of the Amiran and Mesopotamian foreland basins of NW Zagros (Iran-Iraq): Tectonics, v. 34, no. 3, p. 377-395.

Sepehr, M., Cosgrove, J., and Moieni, M., 2006, The impact of cover rock rheology on the style of folding in the Zagros fold-thrust belt: Tectonophysics, v. 427, no. 1-4, p. 265-281.

Sherkati, S., and Letouzey, J., 2004, Variation of structural style and basin evolution in the central Zagros (Izeh zone and Dezful Embayment), Iran: Marine and petroleum geology, v. 21, no. 5, p. 535-554.

Singer, A., 1979, Palygorskite in sediments: detrital, diagenetic or neoformed—a critical review: Geologische Rundschau, v. 68, no. 3, p. 996-1008.

-, 1980, The paleoclimatic interpretation of clay minerals in soils and weathering profiles: Earth-Science Reviews, v. 15, no. 4, p. 303-326.

-, 1984, The paleoclimatic interpretation of clay minerals in sediments—a review: Earth-Science Reviews, v. 21, no. 4, p. 251-293.

-, 1989, Palygorskite and sepiolite group minerals: Minerals in soil environments, v. 1, p. 829-872.

Soulié-Märsche, I., 1993, Diversity of Quarternary aquatic environments in NE Africa as shown by fossil Charophytes, *in* Schandelmeier, H., and Thorweihe, U., eds., Geoscientific Research in Northeast Africa: Rotterdam, Balkerma.

Soulié-Märsche, I., and García, A., 2015, Gyrogonites and oospores, complementary viewpoints to improve the study of the charophytes (Charales): Aquatic botany, v. 120, p. 7-17.

Stoecklin, J., 1968, Structural history and tectonics of Iran: a review: AAPG bulletin, v. 52, no. 7, p. 1229-1258.

Suárez, M., Pozas, J. M., Robert, M., and Elsass, F., 1994, Evidence of a precursor in the neoformation of palygorskite—New data by analytical electron microscopy: Clay Minerals, v. 29, no. 2, p. 255-264.
Surdam, R. C., and Eugster, H. P., 1976, Mineral reactions in the sedimentary deposits of the Lake Magadi region, Kenya: Geological Society of America Bulletin, v. 87, no. 12, p. 1739-1752.
Takahashi, K., and Honjo, S., 1983, Radiolarian skeletons: size, weight, sinking speed, and residence time in tropical pelagic oceans: Deep Sea Research Part A. Oceanographic Research Papers, v. 30, no. 5, p. 543-568.
Tardy, Y., Bocquier, G., Paquet, H., and Millot, G., 1973, Formation of clay from granite and its distribution in relation to climate and topography: Geoderma, v. 10, no. 4, p. 271-284.
Vergés, J., Goodarzi, M., Emami, H., Karpuz, R., Efstathiou, J., and Gillespie, P., 2011a, Multiple detachment folding in Pusht-e Kuh arc, Zagros: Role of mechanical stratigraphy.
Vergés, J., Sandra, E., Casciello, E., Fernandez, M., Villaseñor, A., Jimenez-Munt, I., and García-Castellanos, D., 2011b, Crustal-scale cross-sections across the NW Zagros belt: implications for the Arabian margin reconstruction: Geological Magazine, v. 148, no. 5-6, p. 739-761.
Vicente, A., Expósito, M., Sanjuan, J., and Martín-Closas, C., 2016, Small sized charophyte gyrogonites in the Maastrichtian of Coll de Nargó, Eastern Pyrenees: An adaptation to temporary floodplain ponds: Cretaceous Research, v. 57, p. 443-456.
Wrobel-Daveau, J.-C., Ringenbach, J.-C., Tavakoli, S., Ruiz, G. M., Masse, P., and De Lamotte, D. F., 2010, Evidence for mantle exhumation along the Arabian margin in the Zagros (Kermanshah area, Iran): Arabian Journal of Geosciences, v. 3, no. 4, p. 499-513.
Yang, Q., 1993, Taxonomic studies of Upper Jurassic (Tithonian) radiolaria from the Taman Formation, east-central Mexico: Palaeoworld, v. 3, p. 164.

Appendix

Arabian Journal of Geosciences (2023) 16:343
https://doi.org/10.1007/s12517-023-11407-z

ORIGINAL PAPER

Using clay mineralogy and micropalaeontological observations to unravel Neogene climate variations in Northern Arabia

Christian A. F. Dietzel[1] · Christoph Berthold[2] · Uwe Kirscher[1,3] · Mahmoud Reza Majidifard[4] · Madelaine Böhme[1,5]

Received: 30 January 2023 / Accepted: 2 April 2023 / Published online: 2 May 2023

Abstract

The Zagros Mountain belt in Iran comprises an extensive record of Mesozoic and Cenozoic deposits uplifted by collision of the Arabian and Iranian continental plates. This area has been shown to provide important information to decipher the climatic history of Western Asia, especially regarding the evolution of deserts in Mesopotamia and Northern Arabia. In a high-resolution geological record of 84 samples, we combine clay mineralogy and micropalaeontological observations to refine the late Neogene climate record in Northern Arabia. We investigated a 2.6-km-thick sedimentary profile from the Simply Folded Zagros Mountain belt spanning ca. 10.2 myrs from the late Middle Miocene (Serravallian) to earliest Pleistocene (Gelasian) comprising floodplain sediments and saline mudstones with a strong aeolian contribution. The clay fraction < 2 µm reveals palygorskite, smectite, illite, chlorite and the zeolite mineral erionite. Using clay mineralogy, arid conditions during the Serravallian and early Tortonian in Northern Arabia are identified, followed by semi-arid conditions during the late Tortonian. Clay mineralogy suggests a transition to sustained arid conditions during the early Messinian and provides a more complex picture on a previously proposed period of hyperaridity (NADX) in Northern Arabia penecontemporaneous with the apex of the Messinian salinity crisis.

Keywords Clay minerals · Palygorskite · Erionite · Neogene climate Arabia

Introduction

Clay minerals form a main constituent of soils and result from the weathering of primary minerals such as feldspar or micas (Allen & Hajek 1989). The exact composition of a clay mineral assemblage developing in soils is dependent on a variety of factors such as the composition of parent rocks, weathering conditions (temperature, precipitation, drainage of soils) and geomorphology and relief of the landscape. Furthermore, the clay mineral assemblages can be altered by subsequent transport and diagenetic processes (Allen & Hajek 1989; Chamley 1989; Singer 1980). In palaeoclimatic studies, other proxies such as stable oxygen isotopes, magnetic susceptibility and micropalaeontology should be employed alongside the analysis of the clay mineral assemblage to overcome factors not directly related to climatic parameters (John et al. 2012; Singer 1984b). Using multi-proxy approaches, the analysis of clay minerals has been used to reconstruct changes in climate and weathering conditions across a wide range of marine and terrestrial settings worldwide (Bolle et al. 2000; Chamley et al. 1986; Li et al. 2000). In areas once covered by the Neotethys ocean such as southern Iran, the clay mineral fraction of Cenozoic and recent sediments was found to comprise smectite, palygorskite, illite, chlorite and kaolinite (Hashemi et al. 2013). However, detailed high-resolution studies of the chronostratigraphic distribution of climate-sensitive clay minerals such as palygorskite in western Iran and Northern Arabia are missing (Hojati & Khademi 2011).

Responsible Editor: Attila Ciner

✉ Christian A. F. Dietzel
christian.dietzel@uni-tuebingen.de

[1] Department of Geosciences, Eberhard Karls University of Tübingen, Tübingen, Germany

[2] Competence Center Archaeometry Baden-Wuerttemberg, Eberhard Karls University of Tübingen, Tübingen, Germany

[3] Earth Dynamics Research Group, The Institute for Geoscience Research (TIGeR), School of Earth and Planetary Sciences, Curtin University, Bentley, Western Australia, Australia

[4] Research Institute for Earth Science, Geological Survey of Iran, Tehran, Iran

[5] Senckenberg Centre for Human Evolution and Palaeoenvironment, Tübingen, Germany

Study aims

This study aims to use clay mineralogy to refine palaeoclimatic trends for the late Neogene in Northern Arabia between 12.6 Ma and 2.4 Ma. New data on clay mineralogy of 84 sediment samples is compared to previously published data of fluctuations in magnetic susceptibility, highly soluble salts and sulphate taken from the same samples by Böhme et al. (2021). While soluble salts can be used to reconstruct palaeoclimate in arid and hyper-arid environments, they can be sensitive to post-depositional leaching (Ewing et al. 2006; Rosenthal et al. 1987). Clay mineralogy will hereby help to independently test the robustness of the previously employed soluble salt-based proxy as samples from the combined geological profile were taken at two different profiles, which vary in recent mean annual precipitation. This way the influence of differing post-depositional leaching of highly soluble salts can be tested. As the ratio of smectite/illite + chlorite was suggested as indicative for soil available moisture in palygorskite bearing recent soils by Hashemi et al. (2013), we will try to establish its utility for reconstructing palaeo-aridity along a sedimentary profile. Comparison of different proxies is expected to increase our understanding of long-term responses of clay mineral associations to complex changes in climatic forcing and detrital parent material composition in semi- to hyper-arid environments.

Background

Previous work

Based on clay mineralogical analysis of rock samples from the Cretaceous to Quaternary, Khormali et al. (2005) reconstructed a long-term warm and arid climate from the Eocene to Pliocene in southern Iran. It is suggested that climate in the Afro-Eurasian domain has been affected by the retreat of the Neotethys ocean since the Late Miocene (Zhang et al. 2014). Using thresholds of soluble nitrate, chlorite and bromide as well as end-member modelling of grain size-distributions along a sedimentary profile, Böhme et al. (2021) suggested transient periods of Arabian hyperaridity at 8.75, 7.78, 7.5 and 6.25 Ma as well as a sustained hyper-arid period between 5.6 Ma and 3.3 Ma (Neogene Arabian Desert Climax, NADX). While transient periods of hyperaridity and NADX match with significant Ponto Caspian low stands, periods of Ponto Caspian high stands corresponded well to a more humid (semi-arid) climate in Mesopotamia (Böhme et al. 2021). NADX was initiated at peak of desiccation of the Mediterranean during the Messinian Salinity Crisis (MSC, stage 2) at 5.59 Ma (Manzi et al. 2013). Hyperaridity correlates with the > 2 myr long separation of the Caspian Sea from the Black Sea basin. Hereby, sea levels of the Mediterranean Sea fell by > 1500 m, furthermore by two steps at 5.6 Ma and 5.38 Ma Caspian Sea level dropped by at least 200 m (Roveri et al. 2014; Ryan 2009; van Baak et al. 2016). A possible mechanism to account for changes in aridity is the influence of Paratethys shrinkage, which shifted climate conditions from temperate to continental in central Asia, by establishing the Siberian Pressure High in winter (Ramstein et al. 1997). This strengthening and expanding Siberian Pressure High blocked the moisture-carrying westerlies from reaching Western Asia and Northern Arabia leading to increased aridity in that region during sea level low stands (Böhme et al. 2021; Perşoiu et al. 2019).

Overview of formation conditions of common clay minerals

S*mectites* are common in many soils of temperate regions, and they are stable in poorly drained environments where leaching of Si and bases are restricted (Borchardt 1989). Smectites are also an important constituent of soils in semi-arid and arid climate zones such as in aridisols in the USA (Dregne 1976; Wilson 1999), Iraq (AI-Rawi et al. 1969), Saudi Arabia (Aba-Husayn et al. 1980) or Israel, where Singer (1984a) presented evidence for neoformation of smectite in saprolites. In southern Iran, Khormali and Abtahi (2003) found most smectite in semi-arid and arid soils to have originated from transformation of palygorskite and illite. The transformation from palygorskite generally occurred at P/ET (ratio of mean annual precipitation to evapotranspiration) > 0.4.

Palygorskite is a fibrous clay mineral that can be formed under semi-arid or arid climate conditions (Singer 1989). Its authigenic formation by chemical precipitation has generally been reported from evaporative basins such as lakes and shallow saline lagoons, soils or in open oceans by hydrothermal alteration of basaltic glass or volcanic sediments (Al-Juboury 2009; Callen 1984; Chamley 1989; Millot 1970; Singer 1979). The conditions of palygorskite formation and stability are characterized by alkaline fluids with high Mg and Si activities (Singer 1980, 1989). Under these conditions, the neoformation of palygorskite is possible from illite and smectite with a loss of K and Al and a relative increase in Si and Mg (Suárez et al. 1994). While arid conditions favour the formation of palygorskite in soils, it is often associated with pedogenic carbonates in semi-arid regions (Al-Juboury 2009). Palygorskite and gypsum content were also shown to have a significant correlation in saline-alkaline soils in southern Iran (Khormali & Abtahi 2003). Shallow

lakes and intra-montane lagoons in the post-Neotethyan era (Oligocene–Miocene) provided a suitable evaporative environment for extensive palygorskite formation in central and southern Iran (Khademi & Mermut 1998; Khormali et al. 2005) and Iraq (Al-Juboury 2009) with the first palygorskite detected in the late Palaeocene.

Illite describes clay-sized micaceous minerals similar to muscovite usually containing more Si, Mg, H_2O and K than ideal muscovite. Also, illite usually constitutes a mixture of micaceous minerals of different origins (Chamley 1989). Illite in soils is often inherited from parent rocks such as shales, siltstones, limestones, loess and a variety of alluvial sediments or may result from alteration of coarser muscovite particles during pedogenesis (Allen & Hajek 1989). According to Singer (1988), illite may also form pedogenically in the surface horizon of aridic and semi-aridic soils from desert dust rich in K-bearing minerals during wetting–drying cycles. Juvenile desert dust deposits resulting from aridic weathering of bedrocks contains only low to moderate amounts of illite (typically in the Middle East), whereas mature dust originating from aridic soils and loess deposits having undergone repeated cycles of deflation and deposition contain relatively high illite contents (typically in Central Asia). Like illite, *chlorite* in soils is generally inherited and is markedly unstable in pedogenic environments; it is commonly reported in relatively unaltered substrata (Allen & Hajek 1989).

Kaolinite originates from weathering in near-surface environments. Its formation is most pronounced where weathering is intense, as in the humid tropics, with alternate wet and dry seasons. Kaolinite also occurs in humid temperate zones, in areas of unimpeded drainage (Allen & Hajek 1989; Tardy et al. 1973). While kaolinite is the dominant clay mineral in late Cretaceous sedimentary rocks in southern Iran, it has gradually disappeared by the Eocene reflecting more arid climate conditions (Khormali et al. 2005).

Erionite is not a clay mineral but a zeolite, it has been described to form from weathered volcanic glass in saline and alkaline soils and lakes (Hay 1964; Surdam & Eugster 1976) as in Cappadocia, Central Turkey, where volcanoclastic tuffs were deposited in a lacustrine environment in the late Miocene-Pliocene.

Geological setting

The formation of the SE-NW trending Zagros Mountain belt can be related to the collision of the Arabian and Eurasian plates, during the closure of the Neotethys ocean (Alavi 1994; Berberian 1995). While some models suggest that the collision of Arabia and Eurasia occurred prior to 18 Ma already, a collision between ~ 11.2 and 5 Ma is indicated by zircon provenance analysis (Zhang et al. 2017). The belt is divided from the NE to the SW into four zones: (1) the Sanandaj-Sirjan metamorphic zone, (2) the Imbricated Belt dominated by thrusting, (3) the Simply Folded Belt characterized by folding, and (4) the Mesopotamian foreland basin with buried folds, extending to the SE into the Persian Gulf (Colman-Sadd 1978; Falcon 1974; Homke et al. 2004) (Fig. 1).

The study area near the Iraq-Iran border is part of the Push t-e Kuh Arc in the Simply Folded Zagros belt where syntectonic deformation of foreland sediments started between 8.1 and 7.2 Ma and was active for at least 5 Ma (Böhme et al. 2021; Homke et al. 2004). The studied sections comprise the Gachsaran Formation, lower Agha Jari Member, Lahbari Member and Bakhtyari Formation. The continuous profiles of up to 3 km are exposed in the two syncline-anticline structures of Changuleh and Zarrinabad (Homke et al. 2004) (Fig. 1). All samples from this study were taken at georeferenced sampling points previously sampled by Homke et al. (2004) for magnetostratigraphy, thus giving them a robust temporal control. The lithological succession in the study area described by Böhme et al. (2021) is summarized as follows:

Lithology

The *Gachsaran Formation* (equivalent to Fatah Fm. in Iraq, lower Fars Fm. in Syria) comprises well-bedded evaporites, metric sized red silty clay beds and green to brown sandstones 10 cm to 2 m thick (Homke et al. 2004). The sandstone beds show symmetrical wave ripples on top as well as mud flat-type trace fossils (faecal pellets and cf. *dactyloides*). The mudstones contain pedogenic gypsum concretions, gypcrete and redox mottling suggesting fluctuating sea levels between shallow marine shoreface and terrestrial backshore depositions. The top of Gachsaran Fm. is marked by a sandy 0.25-m limestone containing the bivalve *Clausinella amidae*.

The *Agha Jari Formation*, covering wide areal extension of the Mesopotamian foreland basin (equivalent to the Injana Fm. in Iraq, upper Fars Fm. in Syria) is characterized by a 2.4-km-thick depositional profile of fine-clastic to fluvial sediments in the study area and has been dated to range from the late Middle Miocene (12.3 Ma) to the base of the Pleistocene (~ 2.5 Ma) by magnetostratigraphy (Homke et al. 2004). It comprises two members: the lower Agha Jari Member and the Lahbari Member. In the study area, the lower part of the Agha Jari Mb. (12.3–11.5 Ma) is characterized by greyish to reddish silty clays rich in pedogenic gypsum concretions with interbedded sandstone channels. At 11.5 Ma, the fine clastic sediments show a reduction of pedogenic gypsum concretions and the occurrence of rubified and lessivized palaeosol horizons. At 11.5 Ma, the fluvial sandstones thicken to > 5 m showing first cross-bedding structures. At 10.8 Ma, the thickness of the distinctly cross-bedded fluvial sandstone

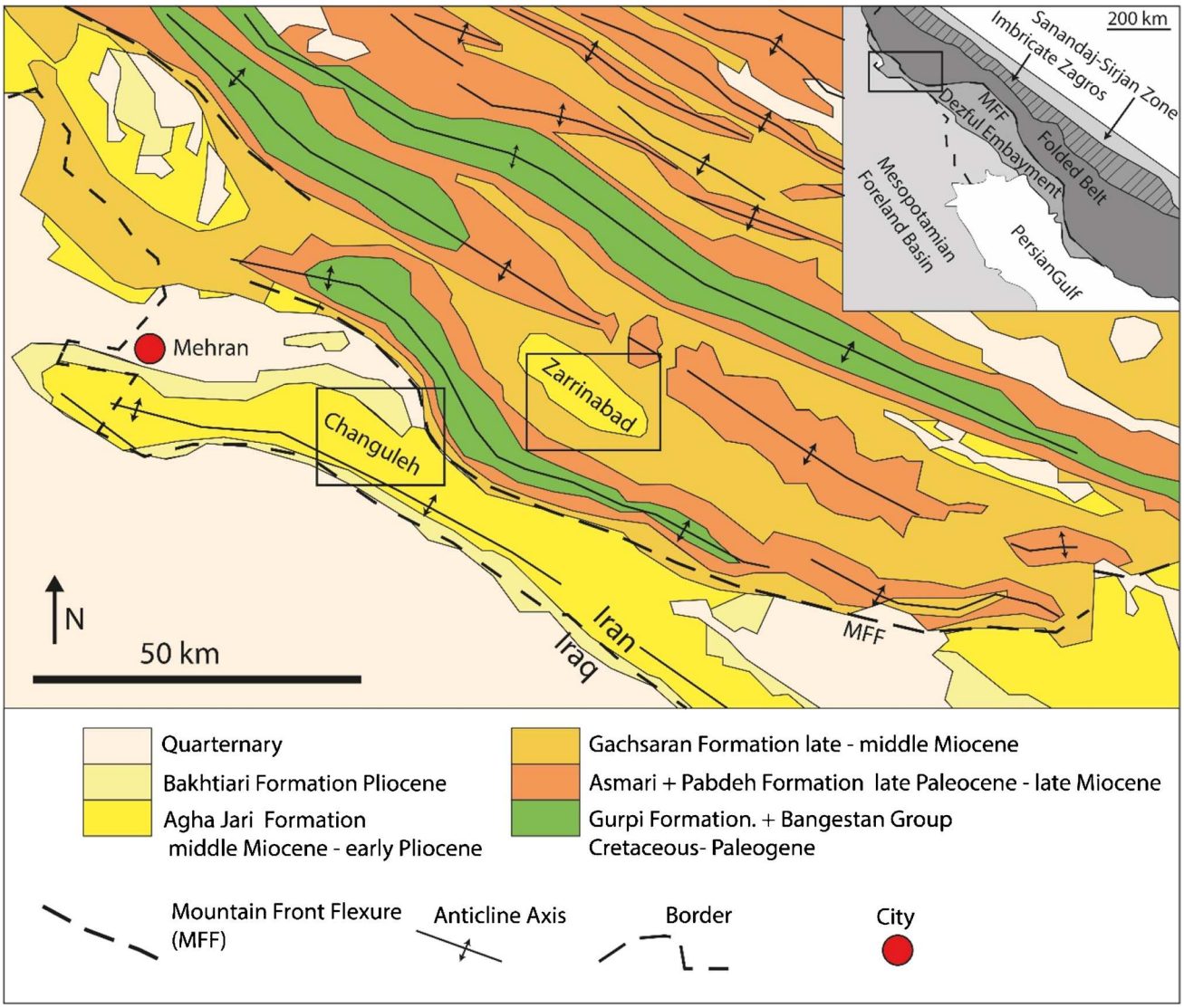

Fig. 1 Geologic map of the Push-e Kush Arc in the Simply Folded Zagros belt, showing the sampling area with boxes. Boxes show limits of sample area. Samples from 12.6 to 9.38 Ma were taken at Zarrinabad anticline and from 9.02 to 2.4 Ma at Changuleh syncline-anticline structure. Map modified from Homke et al. (2004)

strata increases to > 10 m with heavy mineral composition, indicating a (palaeo-) Tigris origin and a palaeo-flow direction pointing towards the southeast (Homke et al. 2004). The fine-grained calcareous palaeosols show intense reddish-green mottling as well as root halos. At 9.7 Ma, sandstone bodies are thin, with calcareous rhizocretes occurring between 9.78 and 6.9 Ma. A thickening of cross- and through-bedded sandstone channels is observed at 8.8 Ma as well as mud-ball erosion. Higher soil moisture within the alluvial plains is indicated between 8.75 and 7.5 Ma by Mn-staining on clay cutans, root halos, gastropods at 8.78 Ma and mass occurrence of small charophyte gyrogonites at 8.69 and 8.56 Ma. At 8.4 Ma, the thickness of sandstones decreases. At 6.25 Ma a, 1-m-thick mudstone horizon showing the efflorescence of salt marks the first transient phase of hyperaridity. It is followed by a 60-m unit of fluvial sandstones dated between 6.15 and 5.95 Ma, marking the youngest deposits of the lower Agha Jari.

The following *Lahbari Member* consists of beige saline mud sediments without visible palaeo-soil development. The sediments are rich in leachable sulphate, nitrate and chloride and contain infrequent channels of very fine-grained fluvial sandstones of less than 5-m thickness. While fluvial sandstones are almost absent between 5.59 and 5.1 Ma, their frequency increases after 5.1 Ma. At 3.5 Ma, small-scale interfingering channels contain cobble-sized limestone clasts with a general coarsening upward trend in conglomerates. Böhme et al. (2021) suggested a higher dust accumulation

rate during the Lahbari Mb is by grain-sized end-member modelling as well as a more westerly source of the sediments by heavy mineral composition. A possible sediment source for the Lahbari Member is also found in the softer Gachsaran and Agha Jari deposits regionally uplifted above the proposed low-angle blind thrust, generating the Push-e Kush Arc rise (Emami et al. 2010).

The transition to the *Bakhtiari Formation* is marked by the appearance of the first boulder-sized clasts in conglomerates just after the beginning of the Pleistocene at 2.5 Ma documenting the progression of the Zagros Mountain Flexure Front (Emami et al. 2010; Homke et al. 2004).

Materials and methods

The 84 evenly distributed mudstone samples were taken from silty horizons along the 2600-m-thick sedimentary profile. Samples from 12.6 to 9.38 Ma were taken at the Zarrinabad anticline and from 9.02 to 2.4 Ma at the Changuleh syncline-anticline structure. As this profile was previously analysed regarding the grain size distribution and the geochemistry of soluble salts, the age model and sample number are identical to the samples used in the study of Böhme et al. (2021). Wherever palaeosols occurred, samples were taken from the B-horizon. Clay minerals sampled from the foreland sediments can be both of detrital and pedogenic origin; thus, the clay mineral record is influenced by the composition of eroded parent material and weathering conditions at time of deposition (Singer 1984b).

For each sample, 5 g of sediment was dried at 110 °C in a drying cabinet and then carefully dispersed by submerging the bottom of the sample in a porcelain crucible in deionized water to gently disaggregate the mineral particles using the swelling properties of the smectitic clay minerals (procedure known as "unterschichten"). Some samples with a higher carbonate and gypsum content required a repetition of this gentle disaggregation process. The samples were then treated with a Dr. Hielscher UP 400S ultrasonic processor (200 W, 50% cycle-time, 30 s) to obtain a homogeneous suspension and to destroy soft agglomerates. Afterwards, sand and potential micro-fossils were removed with a 63-µm sieve (Lehmann et al. 2004). The fraction < 63 µm of each sample was left to flocculate in a 2 l beaker, caused by the cations from the solvable minerals still existing in the sample, with the electrolyte-rich clean water on top being decanted after one night. The decantation process was repeated several times to remove the remaining cations until a stable suspension started to develop. After that, the suspension was stabilized with 25 ml of 0.1 M sodium pyrophosphate solution, and clay minerals < 2 µm were separated from silt by repeated sedimentation in Atterberg columns. Unfortunately, coarse-grained crystalline calcium phosphate hydrate crystallites precipitated in the suspension, which formed by reaction of sodium pyrophosphate with calcium cations from dissolving gypsum in the sample. They were removed from the clay suspension by additional sieving using a sieve with 63-µm mesh size and decantation of the suspension from the sediment of the crystallites. The clay was then concentrated from the suspension using a 0.8-µm vacuum filter to a 40-ml volume. Thereafter, 1 ml of the clay mineral suspension was transferred onto 2 glass slides each and air-dried as oriented clay samples for XRD analysis, with one of the samples being re-measured after treatment with ethylene glycol vapour in an exicator for at least 72 h. A Bruker D8 advance diffractometer with a Cu-sealed tube running at 40 kV/20 mA, a Göbel mirror parallel beam optics, a 0.2-mm divergence slit, a fixed knife edge to suppress air scatter and a 1D-VÅNTEC 1-detector in scanning mode with a step size of 0.008° 2θ and 360 s/step was used for the XRD analysis resulting in a measurement time of approximately 2 h for the range from 2°2 Theta to 55°2 Theta. Mineral identification was performed using the 2006 PDF-4 database from the International Centre for Diffraction Data-Joint Committee of Power Diffraction Standards (ICDD-JCPDS). As there are six or more mineral phases present in the clay-sized fraction and mineral texture, mineral grain orientation, reflex overlap as well as swelling of smectites and background extraction can lead to significant errors and uncertainties in exact clay mineral quantification (Brindley & Brown 1980). A comparison of the integrated reflex intensities was not deemed suitable for the task of clay mineral quantification along the sedimentary column due to the clay minerals on the samples being oriented as well as multiple broad reflex overlaps (Fig. 2). As an alternative, a semi-quantitative approach was chosen by comparing the height only of the main reflex of glycolated oriented samples (001 chlorite; 002 smectite, illite; 110 palygorskite; 100 erionite) (Johns et al. 1954). The following correction factors were applied to account for the broad 002 reflex overlap of smectite with 001 chlorite, 110 palygorskite with 002 illite and 110 palygorskite with 100 erionite. The correction factors were chosen by careful comparison of the relative overlap of intensities for each mineral. They are chlorite, − 0.25 *smectite; illite, − 0.25*palygorskite; erionite, − 0.1*palygorskite. For the estimation of the kaolinite content, a selection of samples was additionally heated at 550 °C for 3 h. The resulting percentage ratios of intensities of clay minerals thus do not represent the exact weight percentage of each clay minerals in the sample, but their comparison can be used to reflect the relative change in clay mineral ratios between different samples. The ratio of smectite/(illite + chlorite) was then used to assess changes of soil available moisture. To check for a potential correlation with concentration of clay minerals with previously analysed data of soluble salts and sulphate, correlation plots and Spearman's correlation were obtained using the software JMP.

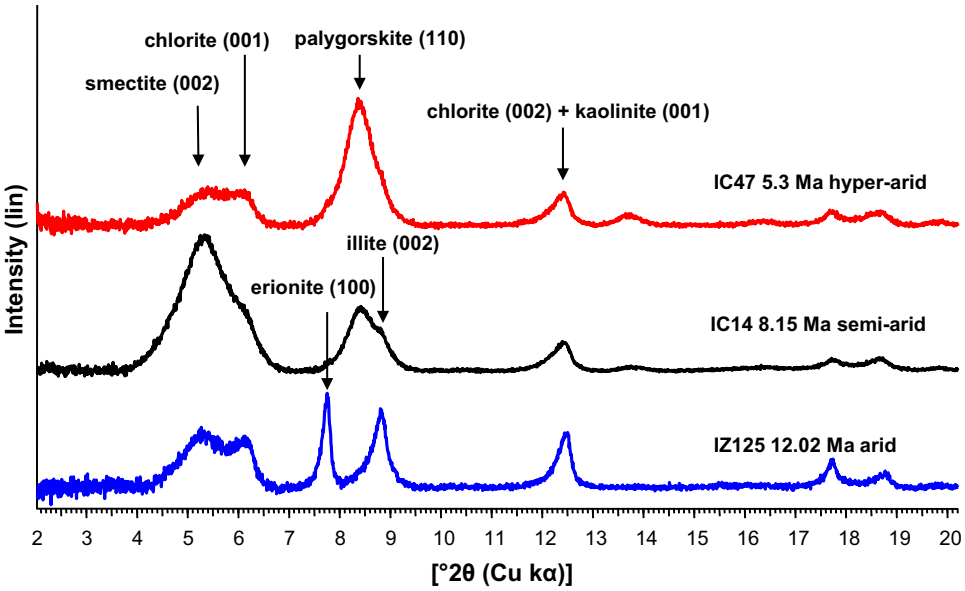

Fig. 2 Three exemplary x-ray diffractograms of three glycolated clay mineral samples representing clay mineral assemblages from semi-arid (black curve), arid (blue curve) and hyper-arid (red curve) conditions. Background has been subtracted of all three samples for better comparability of reflex intensities

A Phenom XL C2 desktop SEM with a 15 kV acceleration voltage was used to analyse charophyte (green algae) fossils as well as pedogenic concretions at University of Tübingen.

Clay mineralogy was compared to bulk magnetic susceptibility previously published as supplementary information by Böhme et al. (2021). Magnetic susceptibility was obtained for all samples using an MFK-1 AGICO Kappabridge on weighted portions of the samples.

Results

The clay fraction of the studied samples consists of highly variable proportions of smectite, illite, chlorite, palygorskite as well as the zeolite mineral erionite (Fig. 2) and was plotted next to the corresponding magnetic susceptibility, salt and sulphate data for better comparability (Fig. 3). Small amounts of kaolinite were present in some samples albeit quantification was not possible due to a varying overlap of the 001 intensity of kaolinite with the 002 reflex of chlorite upon heating to 550 °C. Erionite was only detectable in the clay fraction < 2 µm by XRD. It was not identifiable by follow-up SEM analysis probably due to its small size. Some samples of the fraction < 2 µm also contained accessory quartz, calcite as well as dolomite. Bivariate plots for individual clay minerals, Na^+, Cl^- and SO_4^{2-} are shown in Fig. 4, and Spearman's correlation coefficients among clay minerals are in Table 1. Among the clay minerals, palygorskite exhibited a moderate negative correlation with illite and smectite while the correlation with chlorite was weak and statistically insignificant. The correlation among illite, chlorite and smectite was also found to be weak. Bivariate plots showed that samples obtained from the Zarrinabad section of the lower Agha Jari Fm. exhibited Na^+, Cl^- and SO_4^{2-} concentrations that were generally one or two orders of magnitude lower than samples obtained from the Changuleh section of the lower Agha Jari Member Formation. Clay mineralogy at the same time did not show a distinct clustering between same samples obtained from the two sampling localities. In terms of clay mineralogy and soluble salt geochemistry, samples from the Lahbari Member clustered distinct from those from the lower Agha Jari Member, with higher palygorskite, Na+, Cl− and SO_4^{2-} concentrations than samples from the Gachsaran Formation and lower Agha Jari Formation.

Gachsaran Formation

The lowermost sample dated to 12.6 Ma, which is the only one belonging to the Gachsaran Formation, contains illite, erionite as well as minor smectite and chlorite and accessory dolomite. Magnetic susceptibility is the lowest of the whole profile. The presence of small gyrogonites of *Chara* sp. is indicative of freshwater or brackish conditions at the time of sediment deposition (Soulié-Märsche 2008).

Lower Agha Jari Member

The six stratigraphic lowest samples from 12.02 to 11.2 Ma comprise smectite, illite, chlorite and often erionite as well as accessory quartz, while palygorskite is absent. First traces of palygorskite are present at 10.88 Ma; its content increases to a first maximum at 8.75 Ma and then decreases to a new minimum at 7.1 Ma (Fig. 3B). Later on, palygorskite shows a long-term increase towards the onset of the Lahbari Member. While smectite contents are generally high throughout the lower Agha Jari Member, long-term maxima can be

distinguished around 10 and 8 Ma. The amount of smectite starts to generally decrease after 7 Ma to reach a minimum at the onset of the Lahbari Member (Fig. 3A). Illite shows a long-term decrease from 12.02 to 7.25 Ma (Fig. 3C). Its percentage is then temporarily elevated at around 7 Ma and decrease again at the onset of the Lahbari Member. The intra-sample variation of illite is relatively high. While chlorite content (Fig. 3D) is generally lower than illite, a strong intra-sample variability throughout the lower Agha Jari Member is noted too. Erionite occurs rather unsystematically in low amounts in many samples between 12.02 and 7.25 Ma (Fig. 3E). Between 7.1 and 5.5 Ma, the strong variation as well as a total increase of erionite is clearly noticed. The resulting ratio of smectite/(illite + chlorite) has both a strong variability in between samples but also on a longer time-scale (Fig. 3H). After gradually increasing until 9.54 Ma, it drops moderately for about 0.75 myrs. Between 8.75 and 6.9 Ma, it reaches on average the highest values throughout the sedimentary column and then sharply drops, to remain relatively low until the onset of the Lahbari Member at 5.59 Ma with a minimum at 6.25 Ma. The initial increase in palygorskite between 10.88 and 8.75 Ma coincides with an increase of magnetic susceptibility (Fig. 3G) of the sediment. Magnetic susceptibility then fluctuates around a median of 2^{-7} SI until the onset of the Lahbari Member. Small gyrogonites of *Chara* sp. were observed in samples at 10.25 Ma and 9.51 Ma. The presence of dwarfed gyrogonites of *Chara* sp. at 8.69 and 8.56 Ma was previously described by Böhme et al. (2021). The gyrogonites at 8.56 Ma were now identified to likely comprise *Chara vulgaris*, *Chara globularis* and *Chara* sp. (Fig. 5d-h). Three gyrogonites showing strong dissolution etching of calcite at the surface were identified as *Nitellopsis obtusa* at 7.5 Ma (Fig. 5i-j). SEM analysis revealed the overgrowth of palygorskite fibres onto calcified charophyte thalli at 8.56 Ma (Fig. 5a-c). Palygorskite overgrowth can also be seen on pellet-shaped carbonate concretions with possible halite pseudomorphs at 7.1 Ma (Fig. 6). At 8.78 Ma, tube-shaped aggregates of gypsum likely resembling rhizocretes, similar to those reported by Khalaf et al. (2014) in a fluvial playa, were observed (Fig. 7a).

Lahbari Member

The base of the Lahbari Member at 5.59 Ma is generally characterized by higher palygorskite and lower smectite contents than the lower Agha Jari Member. The clay mineral assemblage of the Lahbari Member can be divided into three intervals: (1) 5.59–4.6 Ma; (2) 4.44–4.33 Ma; (3) 4.25–2.4 Ma. During the first interval, the amount of smectite is the lowest of the entire sedimentary column, while the content of palygorskite is very high. Illite and smectite are also comparatively low, and smectite/(illite + chlorite) reaches the lowest values of all the investigated samples. The second interval is characterized by an increase in illite, smectite, chlorite and smectite/(illite + chlorite) ratio, while the amount of palygorskite is cut in half. In the third interval, the amounts of illite and chlorite are again reduced, while palygorskite sharply increases. Smectite and smectite/(illite + chlorite) are slightly higher than in the second interval. Erionite is generally rare in the Lahbari Member in comparison to the lower Agha Jari Member. Magnetic susceptibility sharply decreases at the onset of the Lahbari Member, then increases until 4.7 Ma and then moderately decreases until 4.25 Ma. During the third interval, it stays high again. A single gyrogonite of *Chara* sp. was observed in 10 g of sediment from 5.50 Ma additionally to several ostracod fragments (Fig. 5k-l). Fragments of ostracods were also found at 3.55 Ma. Fine-grained gypsum comprises a major component of the sand fraction of the Lahbari Member, a potential gypsum rhyzocrete measuring around 1 mm in diameter being observed in one sample at 4.44 Ma (Fig. 7b).

Discussion

General discussion

While clay minerals provide an integrated record of overall climate impact, they do not provide direct indications of climate parameters. Levels relatively rich in chlorite, illite, palygorskite and quartz correspond to relatively dry periods, while humid periods are dominated by more stable clay minerals such as kaolinite. Smectite can indicate a climate with contrasting seasons and a pronounced dry season (Singer 1984b). The distinction between detritic and authigenic clay minerals is problematic as extra-climatic factors such as parent rock material, differentiation during transport, topography and diagenetic changes can influence clay mineral assemblages (Singer 1984b). As detrital clay minerals will have been transported and repositioned by aeolian and fluvial processes along the catchment area of the Mesopotamian foreland basin, the palaeoclimate record of this study will therefore be indicative of palaeoclimatic impact in a larger integrated area. In areas exceeding 300 mm of annual precipitation, palygorskite is unstable and can weather to other clay minerals such as smectite (Paquet & Millot 1972), making the presence of palygorskite a good indicator for relatively dry climate. As palygorskite can only form from smectite and illite in the presence of alkaline fluids rich in Mg and Si (Singer 1989), palygorskite might not form in arid soils lacking sufficient Mg and Si. In a recent study, Hashemi et al. (2013) found parent rock material composition to be the most important factor on clay mineral distribution in different moisture regimes in gypsiferous palygorskite-rich soils of various geological origins in the semi-arid to arid

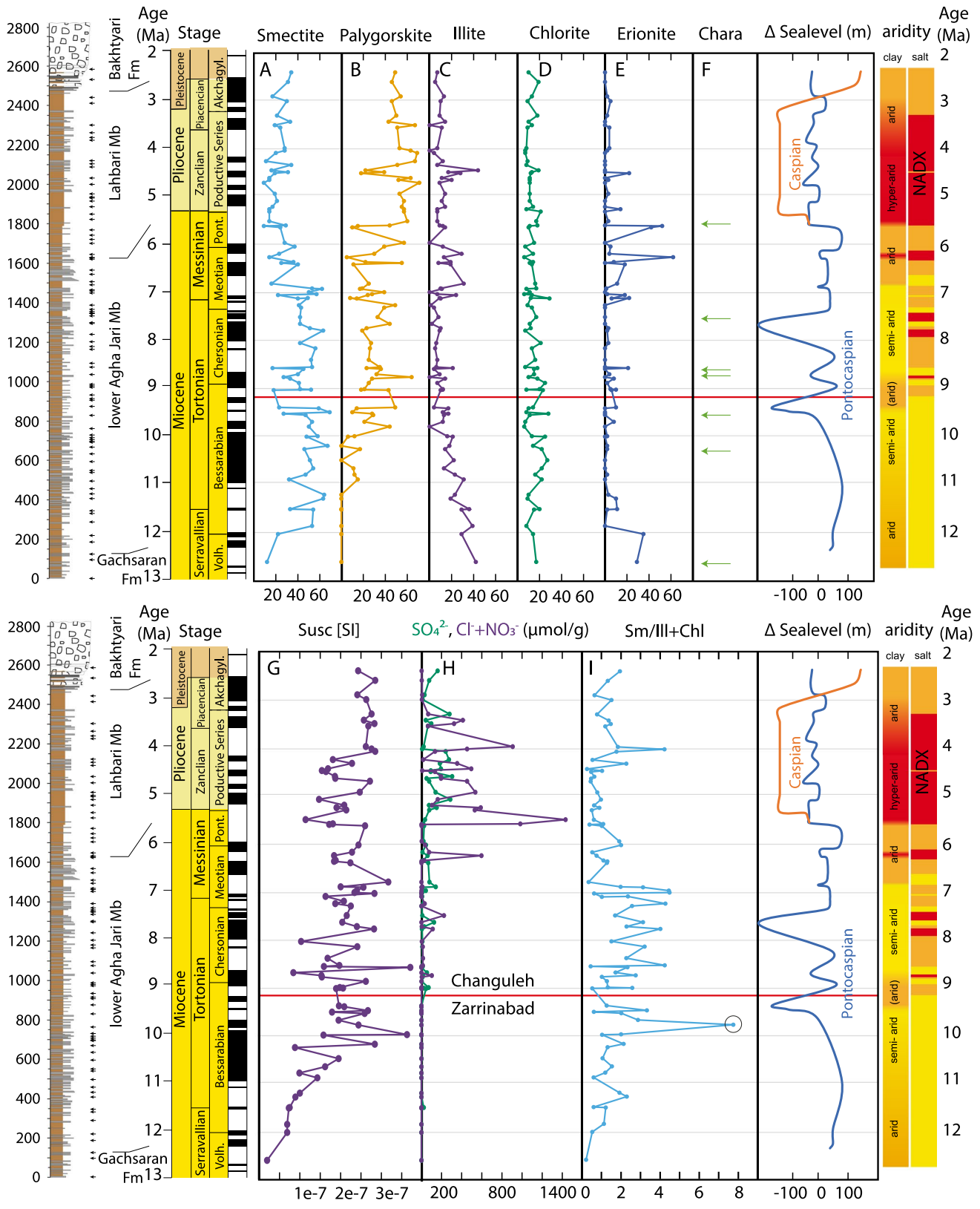

Fars Province in Iran. Besides the influence of parent material onto the clay mineral assemblage, it was demonstrated that the ratio of smectite/(illite + chlorite) increased with soil moisture. Hereby, the lowest ratio of smectite/(illite + chlorite) was found in soils with aridic moisture regime (mean 0.38) and the highest ratio in a xeric moisture regime (mean

◂**Fig. 3** Variability plot of clay minerals (A-D) and erionite (E) in % as function of XRD reflex intensity. (F) Occurrence of charophytes. Stratigraphic profile, sea level variations, magnetic susceptibility (G), soluble salt and sulphate data (H) adapted from Böhme et al. (2021). (I) smectite/(illite + chlorite) ratio as indicator for soil moisture availability with higher ratios indicating higher moisture (encircled sample represents a statistical outlier due to lack of illite). Right columns: new long-term aridity interpretation based on clay mineral ratios beside soluble salt-based interpretations of Böhme et al. (2021). Horizontal red line marking different sampling localities at Zarrinabad and Changuleh syncline-anticline structures, note the lack of soluble salts at Zarrinabad sampling site with no apparent change in clay mineralogy

1.26, max 2.12). We assumed that the correlation between soil moisture and smectite/(illite + chlorite) was indicative of changes in the palaeo-soil moisture regime in this study because it was demonstrated across pedons formed on parent material from various geological origins; however, changes in detrital parent material will have an effect on clay mineral assemblages.

Clay transformation

In our study, we observed an almost linear anticorrelation across all samples between palygorskite and illite suggestive of neoformation of the former at the expense of the latter (Table 1, Fig. 4). This relationship also seems to hold true between palygorskite and smectite albeit to a lesser extent. Similar neoformation and transformation between clay minerals were reported in recent arid Iranian soils by Khormali and Abtahi (2003). Further detailed geochemical studies will be helpful in getting a deeper insight into the geochemical controls of palygorskite genesis along this sedimentary profile.

Magnetic susceptibility

The changes in clay mineralogy were also compared to changes in magnetic susceptibility. The magnetic susceptibility of soils is affected by geological parent material composition and soil forming processes (Dearing et al. 1996). In a study of subtropical Chinese soils, a trend of mafic volcanic rocks > felsic rocks > metamorphic rocks > sedimentary rocks was shown for magnetic susceptibility (Shenggao 2000). Magnetic susceptibility of soils was analysed by Sanjari et al. (2021) along a xeric-aridic climolithotoposequence in central Iran. Hereby, it was shown that magnetic susceptibility values were increased with depth in soils with igneous parent material due to primary ferrimagnetic particles, but the opposite trend was found in soils with a sedimentary origin indicating a stronger influence of pedogenic magnetic particles. Increasing weathering in more developed soils of igneous parent material causes the destruction of inherited primary magnetic minerals through time, decreasing magnetic susceptibility. However, formation of pedogenic ferrimagnetic particles in soils with sedimentary parent material increased magnetic susceptibility with the soil development (Fine et al. 1989; Sanjari et al. 2021; Shenggao 2000). Looking at the complete sedimentary profile, we could not establish a clear positive correlation between enhanced weathering, indicated by a high proportion of smectite or kaolinite compared to illite and chlorite or geological indicators such as manganese staining or redox mottling that would correspond to strongly elevated magnetic susceptibility by pedogenic ferrimagnetic particles in the sediments. Therefore, we assume the contribution of inherited primary magnetite grains to be larger than the contribution of pedogenically formed ferrimagnetic minerals such as magnetite or maghemite.

Gachsaran Formation and lower Agha Jari Member

The clay mineral suite between 12.6 and 9.54 Ma likely reflects a gradual transition from arid to semi-arid climate conditions. A more intense transformation of illite to smectite and starting at 10.88 Ma palygorskite indicates increased amounts of soil available water. The enhanced chemical weathering of illite to smectite might also be indicating a climate with increasingly contrasting seasons and a pronounced dry season (Singer 1984b). An increase in mafic input sourced from tectonically exhumed, allochthonous slices the Kermanshah radiolarite-ophiolite complex in the high Zagros is regionally observed in Zagros foreland sediments from the Dezful Embayment to the SE of this study area in the middle Tortonian (Etemad-Saeed et al. 2020). Thus, the co-increase in palygorskite and magnetic susceptibility after 10.88 Ma can best be explained by enhanced input of more mafic parent material rich in magnetite and Mg-rich minerals, providing the necessary magnesium for palygorskite formation. Fine-grained sediments of this section also show indicators of soil development such as redox mottling and carbonate rhizocretes (Böhme et al. 2021), which might partially contribute to the increase in magnetic susceptibility in palaeosols. However, a contemporaneous increase in sedimentation rate along the floodplain between 12.8 and 9.5 Ma from 13 to 30.5 cm/ka (Homke et al. 2004) would indicate the accelerated subsidence of soils giving less time for intense pedogenic formation of ferrimagnetic minerals. The sample taken at 9.78 Ma giving an excessively high smectite/(illite + chlorite) ratio of 7.7 appears to be a statistical outlier probably due to complete lack of illite potentially due to transformation to palygorskite (encircled sample in Fig. 3H). Between 9.51 and 8.78 Ma, a drop in smectite/(illite + chlorite) ratio suggests a slight intermittent aridification which is corroborated by field observations of a decrease in fluvial channel thickness and therefore fluvial run-off rate. This aridification is roughly contemporaneous

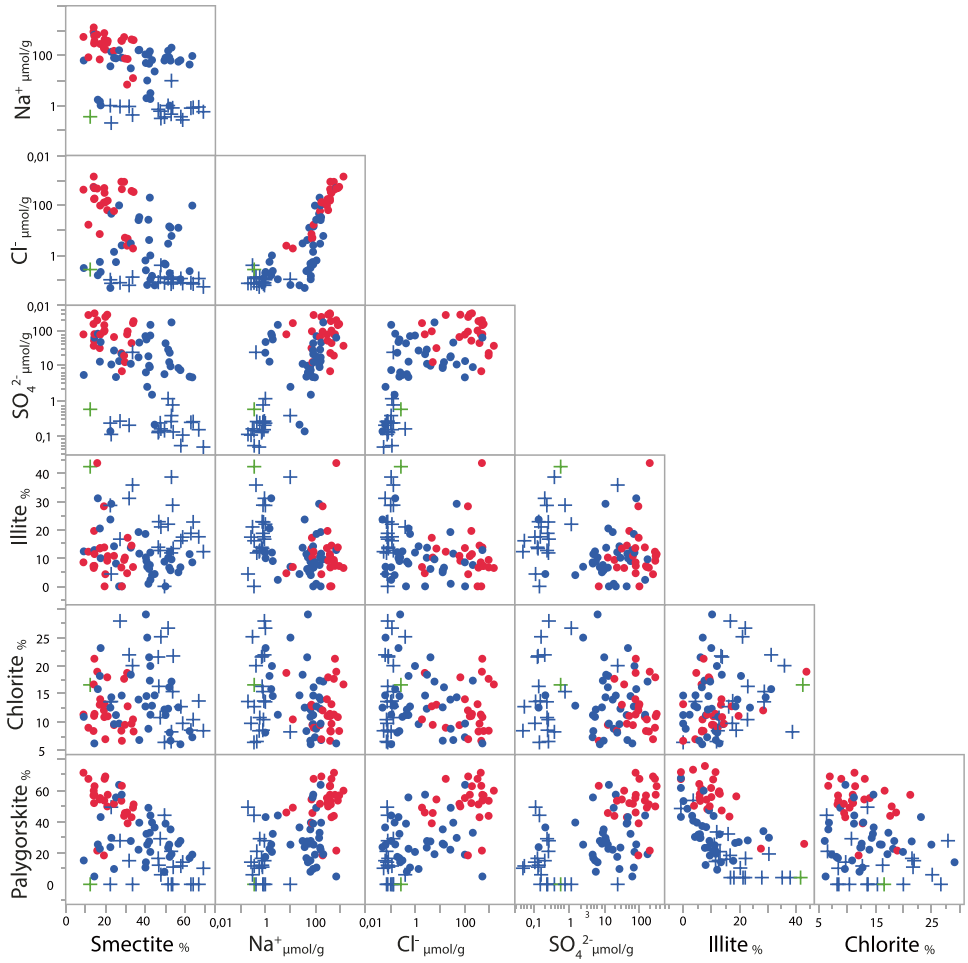

Fig. 4 Bivariate plots of clay minerals illite, smectite, chlorite, palygorskite in % of clay fraction < 2 µm and soluble salts Na^+, Cl^- and SO_4^{2-} in µmol/g. Crosses, samples from Zarrinabad section of the profile; dots, samples from the Changuleh section of the profile. Gachsaran Fm. in green, lower Agha Jari Fm. in blue and Lahbari Mb. in red. Na^+, Cl^- and SO_4^{2-} data from Böhme et al. (2021)

Table 1 Spearman correlation coefficient for clay minerals

Variable 1	Variable 2	Spearman ρ	Probability. > |ρ|	Correlation strength
Chlorite	Illite	0.24	0.0293	Weak or none
Smectite	Illite	−0.04	0.6926	Weak or none
Smectite	Chlorite	−0.12	0.2782	Weak or none
Palygorskite	Chlorite	−0.19	0.0819	Weak or none
Palygorskite	Smectite	−0.53	< 0.0001	Moderate
Palygorskite	Illite	−0.63	< 0.0001	Moderate

with a temporary Paratethys low stand which might have led to decreased precipitation in Northern Arabia (Böhme et al. 2021). The general increase in soil available moisture reflected in the highest average high smectite/(illite + chlorite) ratios recorded throughout the profile between 8.75 and 7.25 Ma is also noted by field observation of pedogenic features such as manganese staining, plant-root halos and a thickening of fluvial channels (Böhme et al. 2021 Fig. 3 E–H). As the continuous presence of palygorskite and lack of kaolinite excludes humid climate conditions, a semi-arid climate conditions appear to be most probable. While two clay mineral samples between 7.1 and 7.04 Ma indicate more arid conditions at the beginning of the Messinian already, a permanent drop in smectite/(illite + chlorite) ratio is only observed after 6.9 Ma. No systematic change in magnetic susceptibility is observed during this transition indicating a stronger signal of inherited magnetite grains than pedogenically formed magnetic minerals in the sediments. A possible trigger for the aridification indicated at 6.9 Ma could be provided by the Intra-Maeotian event, leading to a significant Eastern Paratethys base-level drop (Palcu et al. 2019). The shrinking extend of the Caspian Sea hereby may have enforced the Siberian Pressure High, deflecting the moisture laden westerlies from Arabia (Böhme et al. 2021).

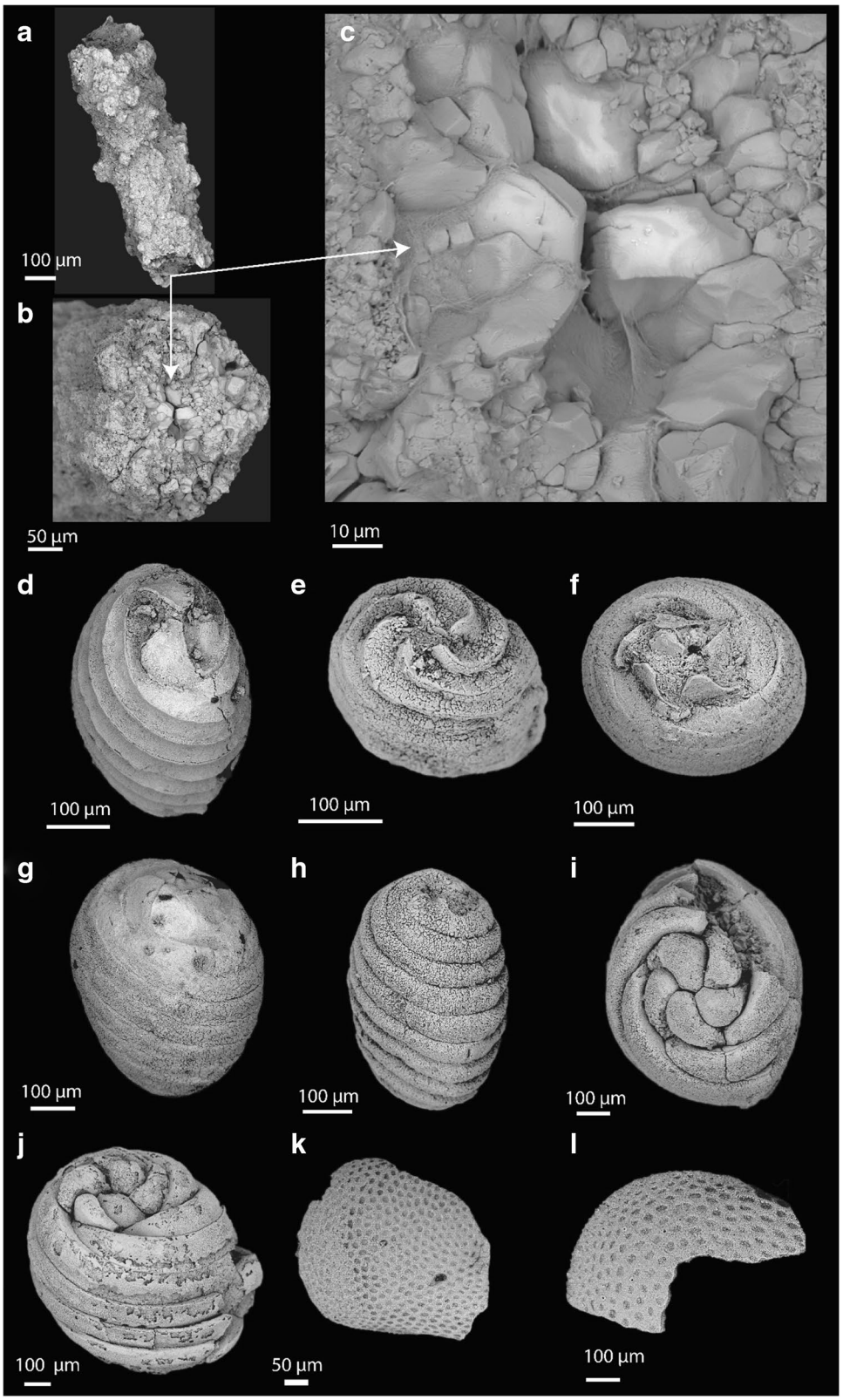

Fig. 5 a–c Calcified charophyte thallus with on-growth of fibrous palygorskite; d–e gyrogonites likely *Chara vulgaris*, sample IC10 (8.56 Ma); f apex of sprouted gyrogonite of *Chara vulgaris*, sample IC10 (8.56 Ma); g gyrogonite likely *Chara globularis*, sample IC10 (8.56 Ma); h gyrogonite *Chara* sp., sample IC10 (8.56 Ma); i–j gyrogonites of *Nitellopsis obtusa* with calcite dissolution structures, sample IC21 (7.5 Ma); k–l ostracod fragments, sample IC45 (5.5 Ma).

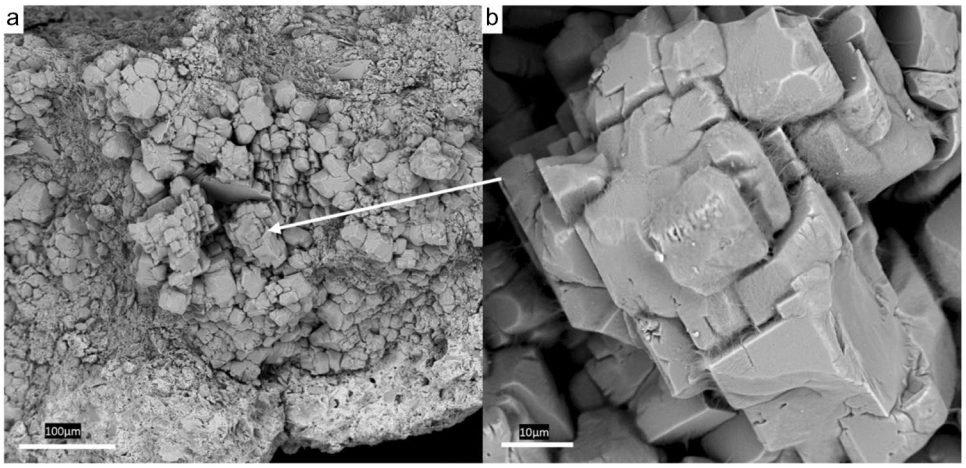

Fig. 6 **a**, **b** Pedogenic concretion comprising carbonate and clay minerals with potential halite pseudomorphs showing an on-growth of fibrous palygorskite, sample IC 25X (7.1 Ma).

Lahbari Member

The Lahbari Member samples from 5.59 to 4.6 Ma show a further decrease in the average smectite/(illite + chlorite) ratio; the dominance of palygorskite indicates highly evaporative, arid conditions. Because gypsiferous soils can provide buffered alkaline media with necessary anions and cations for palygorskite crystallization (Birsoy 2002; Owliaie et al. 2006), the observation of very high palygorskite content is possibly linked to an increase in sulphate and gypsum (Fig. 3 B, H, Fig. 4). Elevated gypsum, halite and palygorskite content in the samples might also be partially derived from other evaporative sediments due to a strong increase in aeolian dust input (Böhme et al. 2021). This detrital material could possibly be regionally sourced from tectonically exposed evaporitic sediments of the Gachsaran Formation within the folded Zagros (Emami et al. 2010). The short reduction in palygorskite and increase in smectite and illite between 4.44 and 4.33 Ma might reflect unfavourable geochemical palygorskite formation conditions, a decrease in aeolian dust input or potential short-term cooling leading to a reduction in chemical weathering. A general increase from 4.33 to 2.4 Ma in the smectite/(illite + chlorite) ratio suggests a slight raise in soil water availability compared to the lower parts of the Lahbari Member. However, it might also reflect changes in parent materials due to the progression of the Zagros Mountain Front Flexure, characterized by the Bakhtiari Formation starting at 2.5 Ma (Homke et al. 2004).

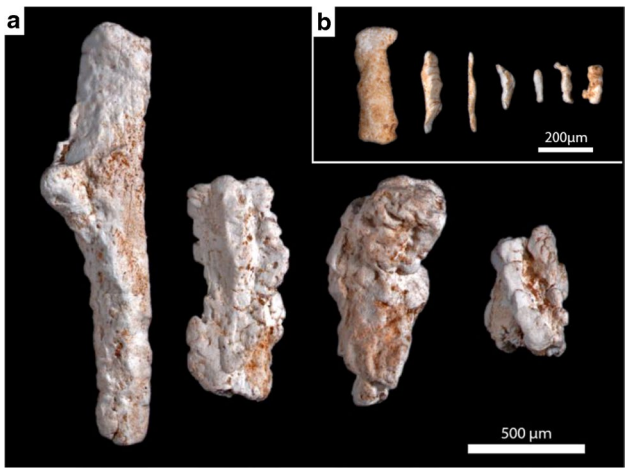

Fig. 7 **a** Gypsum rhizocrete sample IC 5b (8.78 Ma), **b** gypsum rhizocrete, sample IC 63 (4.44 Ma).

Comparison with soluble salt data

The extremely low salt and sulphate concentrations of the samples taken in the Zarrinabad section of the geological profile (12.6–9.38 Ma) (Fig. 4) are highly indicative of post-depositional leaching processes, rendering the previous palaeoclimatic interpretation in Böhme et al. (2021) in this part of the profile by soluble salt geochemistry as semi-arid unreliable. The very low salt and sulphate concentrations are in disagreement with the frequent observation of palygorskite in the same samples, which has been shown to form in evaporative soils at high pH after the increase of Mg/Ca ratio by initial gypsum precipitation (Khademi & Mermut 1998). Arid conditions are also strongly suggested by a very low smectite/(illite + chlorite) ratio and an absence of kaolinite in the samples lacking palygorskite between 12.02 and 11.2 Ma. As clay mineralogy in the Zarrinabad Sect. (12.6–9.38 Ma) of the lower Agha Jari Fm does not cluster distinctively different from the Changuleh Sect. (9.02–5.6 Ma), clay minerals do not seem to have been affected by post-depositional leaching unlike soluble salts and sulphate. The observation of post-depositional leaching at the Zarrinabad sampling site (150–250 mm/a annual precipitation) is probably caused by comparatively higher mean annual precipitation than at the Changuleh sampling site (85–150 mm/a annual precipitation) (Nikpour et al. 2022).

The transient hyper-arid events suggested by soluble salt geochemistry at 8.75, 7.78 and 7.50 Ma, which should correspond to Paratethys low stands are not clearly discernible in the clay mineral paragenesis. This might be due to short duration of the events, other factors affecting regional climate or a stronger overprint of parent material of the weathered clays. However, the transient hyper-arid event at 6.25 Ma suggested by soluble salt geochemistry is also reflected in the clay mineral assemblage. While a continuous signal of enhanced aridity after 6.9 Ma is indicated by clay minerals and in sulphate data, it does not show in soluble salts possibly due to post-diagenetic leaching of highly soluble salts. In the lower Lahbari Member, the clay mineral assemblage is very rich in palygorskite with a low smectite/(illite + chlorite) ratio which is congruent with the previous interpretation of hyperaridity during NADX based on the geochemistry of soluble salts and palynology (Böhme et al. 2021). Nevertheless, it is not possible to draw a clear threshold between merely arid and hyper-arid conditions using clay mineralogy.

Erionite

As erionite is formed by the weathering of volcanic glass under alkaline-saline conditions (Hay 1964; Surdam & Eugster 1976), its occurrence in the sediments along palygorskite supports the presence of alkaline or saline-alkaline soil solutions or ponds at time of deposition. It is unclear whether the volcanic glass found in the analysed sediments is related to reworked volcanoclastic material or syndepositional ashfall events.

Charophytes

As biota have a much quicker, seasonal, response time to environmental change than clay mineral assemblages, which should take longer timeframes to respond to new equilibrium conditions (cf. Hillier & Pharande 2008), they can give an inside into sub-annual climatic changes. The observation of small charophyte gyrogonites of *Chara vulgaris* and *Chara globularis* along palygorskite cutans on calcified charophyte thalli in a sediment sample at 8.56 Ma as well as the occurrence of *Chara* sp. along ostracod fragments in saline mudstones at 5.5 Ma suggests a strong seasonal fluctuation in surface water availability and salinity. While extant charophytes require at least 3 months of fresh to brackish water conditions to complete their growth cycle (Soulié-Märsche 1991), authigenic palygorskite formation usually occurs in alkaline or alkaline-saline shallow lakes or lagoons with elevated Mg and Si activities (Draidia et al. 2018; Singer 1979). Suitable conditions to explain both the small size of the observed charophyte gyrogonites (Böhme et al. 2021; Vicente et al. 2016) and the authigenic palygorskite formation could be created by occasional seasonal desiccation of shallow fresh ponds within the floodplain under highly evaporative conditions resulting in a contemporaneous increase in alkalinity and salinity. Therefore, palygorskite found on charophyte thalli at 8.56 Ma would only have precipitate after charophytes had succumbed to a stressful, increasingly saline environment. While *Chara vulgaris* is commonly found in shallow floodplain ponds, the presence of gyrogonites of *Nitellopsis obtusa* in arid environments is usually an indicator of permanent, oligohaline freshwater bodies of 4–12 m depth (Kröpelin & Soulié-Märsche 1991; Soulié-Märsche 1993). The presence of three gyrogonites of *Nitellopsis obtusa* at 7.5 Ma showing calcite dissolution in weakly consolidated, carbonate-poor, fine-grained floodplain sediments without sedimentological indications palaeolake or oxbow development such as laminations or marl-banks can possibly be interpreted as allochthonous redeposition of gyrogonites of older lake sediments. An autochthonous presence of *N. obtusa* in this sample also seems implausible by the soluble salt geochemistry, as it has previously been classified to belong to a transient hyper-arid climate based on an elevated halite content of 1.07 wt %.

Conclusions

Clay mineralogy of the lower Agha Jari Fm suggests arid climate conditions in Northern Arabia during the Late Serravallian and early Tortonian, which were not indicated in a previous soluble salt-based study due to post-depositional leaching of sediments in one part of the stratigraphical section of the previous investigation. While conditions during the late Tortonian are generally suggested to be semi-arid, clay mineralogy argues towards aridification during the early Messinian. A sharp transition in clay mineralogy is visible at the onset of the Lahbari Mb at 5.59 Ma, where high palygorskite content and low smectite/(illite + chlorite) ratio characterise a phase of hyper-arid sediment deposition, that was previously proposed based on soluble salt chemistry. The onset is contemporaneous with the apex of the Messinian salinity crisis. Clay mineralogy of the mid-late Pliocene suggests an increase in soil moisture with arid climate conditions. While magnetic susceptibility data provided useful indirect information on changing parent material mineralogy, further detailed geochemical studies would be helpful for establishing better control on the total influence of parent material composition and detrital clay minerals onto the clay mineral paragenesis. As transient hyper-arid phases proposed based on soluble salt geochemistry at 8.75, 7.78 and 7.50 Ma were not sufficiently resolved in changing clay mineralogy, it is indicated that soluble salts could be more sensitive in distinguishing short-term aridity thresholds between semi-arid, arid and hyper-arid conditions than

clay mineralogy. However, we also found that soluble salt geochemistry should always be employed along with other proxies such as clay mineralogy in palaeoclimate studies of continental sediments due to the possibility of post-depositional leaching of individual samples or entire sections. The geographical distribution of erionite was found to be much larger than previously known. High resolution palynological and micropalaeontological studies along this reference profile are warranted to better resolve inconsistencies between the clay and soluble salt-based climate reconstruction of individual samples and to enhance the understanding of temperature and precipitation variations and the associated evolution of the semi-arid to hyper-arid ecosystems.

Supplementary Information The online version contains supplementary material available at https://doi.org/10.1007/s12517-023-11407-z.

Acknowledgements The authors are thankful for fruitful discussions that greatly helped improving the manuscript with Haytham El Atfy (University of Tübingen). Ingeborg Soulié-Märsche (Université de Montpellier) is thanked for invaluable help with the identification of charophytes. Support at the SEM was provided by Tatiana Miranda and Martin Ebner (University of Tübingen). Anette Flicker (University of Tübingen) is acknowledged for technical support during sample preparation in the XRD lab. Sample photography was kindly provided by Agnes Fatz (University of Tübingen). Martin Gross (Naturkundemuseum Graz) is thanked for help with the identification of ostracods.

Funding Open Access funding enabled and organized by Projekt DEAL.

Declarations

Conflict of interest The authors declare no competing interests.

References

Aba-Husayn M, Dixon J, Lee S (1980) Mineralogy of Saudi Arabian soils: southwestern region. Soil Sci Soc Am J 44(3):643–649

AI-Rawi, A., Jackson, M., & Hole, F. (1969) Mineralogy of some arid and semi-arid land soils of Iraq. Soil Sci 107:480486

Al-Juboury AI (2009) Palygorskite in Miocene rocks of northern Iraq: environmental and geochemical indicators. Acta Geol Pol 59(2):269–282

Alavi M (1994) Tectonics of the Zagros orogenic belt of Iran: new data and interpretations. Tectonophysics 229(3–4):211–238

Allen B, Hajek B (1989) Mineral occurrence in soil environments. Minerals in Soil Environments 1:199–278

Berberian M (1995) Master "blind" thrust faults hidden under the Zagros folds: active basement tectonics and surface morphotectonics. Tectonophysics 241(3–4):193–224

Birsoy R (2002) Formation of sepiolite-palygorskite and related minerals from solution. Clays Clay Miner 50(6):736–745

Böhme M, Spassov N, Majidifard MR, Gärtner A, Kirscher U, Marks M, Dietzel C, Uhlig G, El Atfy H, Begun DR (2021) Neogene hyperaridity in Arabia drove the directions of mammalian dispersal between Africa and Eurasia. Communications Earth & Environment 2(1):1–13

Bolle M-P, Pardo A, Hinrichs K-U, Adatte T, Von Salis K, Burns S, Keller G, Muzylev N (2000) The Paleocene-Eocene transition in the marginal northeastern Tethys (Kazakhstan and Uzbekistan). Int J Earth Sci 89(2):390–414

Borchardt G (1989) Smectites Minerals in Soil Environments 1:675–727

Brindley G, Brown G (1980) Quantitative X-ray mineral analysis of clays. Crystal Structures of Clay Minerals and Their X-Ray Identification 5:411–438

Callen RA (1984) Clays of the palygorskite-sepiolite group: depositional environment, age and distribution. In Developments in Sedimentology 37:1–37

Chamley H (1989) Clay sedimentology. Clay Sedimentology

Chamley H, Meulenkamp J, Zachariasse W, Vanderzwaan G (1986) Middle to late miocene marine ecostratigraphy-clay-minerals, planktonic-foraminifera and stable isotopes from Sicily. Oceanol Acta 9(3):227–238

Colman-Sadd S (1978) Fold development in Zagros simply folded belt. Southwest Iran AAPG Bulletin 62(6):984–1003

Dearing JA, Hay KL, Baban SM, Huddleston AS, Wellington EM, Loveland P (1996) Magnetic susceptibility of soil: an evaluation of conflicting theories using a national data set. Geophys J Int 127(3):728–734

Draidia S, El Ouahabi M, Daoudi L, Havenith H-B, Fagel N (2018) Occurrences and genesis of palygorskite/sepiolite and associated minerals in the Barzaman formation. United Arab Emirates Clay Minerals 51(5):763–779. https://doi.org/10.1180/claymin.2016.051.5.06

Dregne HE (1976) Soils of arid regions. Elsevier

Emami H, Vergés J, Nalpas T, Gillespie P, Sharp I, Karpuz R, Blanc E, Goodarzi M (2010) Structure of the Mountain Front Flexure along the Anaran anticline in the Push-e Kush Arc (NW Zagros, Iran): insights from sand box models. Geological Society, London, Special Publications 330(1):155–178

Etemad-Saeed N, Najafi M, Vergés J (2020) Provenance evolution of Oligocene-Pliocene foreland deposits in the Dezful embayment to constrain Central Zagros exhumation history. J Geol Soc 177(4):799–817

Ewing SA, Sutter B, Owen J, Nishiizumi K, Sharp W, Cliff SS, Perry K, Dietrich W, McKay CP, Amundson R (2006) A threshold in soil formation at Earth's arid–hyperarid transition. Geochim Cosmochim Acta 70(21):5293–5322

Falcon NL (1974) Southern Iran: Zagros Mountains. Geological Society, London, Special Publications 4(1):199–211

Fine P, Singer M, La Ven R, Verosub K, Southard R (1989) Role of pedogenesis in distribution of magnetic susceptibility in two California chronosequences. Geoderma 44(4):287–306

Hashemi S, Baghernejad M, Najafi GM (2013) Clay mineralogy of gypsiferous soils under different soil moisture regimes in Fars Province. Iran Journal of Agricultural Science and Technology 15:1053–1068

Hay RL (1964) Phillipsite of saline lakes and soils. American Mineralogist: Journal of Earth and Planetary Materials 49(9–10):1366–1387

Hillier S, Pharande A (2008) Contemporary pedogenic formation of palygorskite in irrigation-induced, saline-sodic, shrink-swell soils of Maharashtra. India Clays and Clay Minerals 56(5):531–548
Hojati S, Khademi H (2011) Genesis and distribution of palygorskite in Iranian soils and sediments In. Developments in Clay Science 3(201):218
Homke S, Vergés J, Garcés M, Emami H, Karpuz R (2004) Magnetostratigraphy of Miocene-Pliocene Zagros foreland deposits in the front of the Push-e Kush arc (Lurestan Province, Iran). Earth Planet Sci Lett 225(3–4):397–410
John CM, Banerjee NR, Longstaffe FJ, Sica C, Law KR, Zachos JC (2012) Clay assemblage and oxygen isotopic constraints on the weathering response to the Paleocene-Eocene thermal maximum, east coast of North America. Geology 40(7):591–594
Johns WD, Grim RE, Bradley WF (1954) Quantitative estimations of clay minerals by diffraction methods. J Sediment Res 24(4):242–251
Khademi H, Mermut A (1998) Source of palygorskite in gypsiferous Aridisols and associated sediments from central Iran. Clay Miner 33(4):561–578
Khalaf FI, Al-Zamel A, Gharib I (2014) Petrography and genesis of Quaternary coastal gypcrete in North Kuwait, Arabian Gulf. Geoderma 226:223–230
Khormali F, Abtahi A (2003) Origin and distribution of clay minerals in calcareous arid and semi-arid soils of Fars Province, southern Iran. Clay Miner 38(4):511–527. https://doi.org/10.1180/0009855023740112
Khormali F, Abtahi A, Owliaie H (2005) Late Mesozoic—Cenozoic clay mineral successions of southern Iran and their palaeoclimatic implications. Clay Miner 40(2):191–203
Kröpelin S, Soulié-Märsche I (1991) Charophyte remains from Wadi Howar as evidence for deep mid-Holocene freshwater lakes in the Eastern Sahara of Northwest Sudan. Quatern Res 36(2):210–223
Lehmann M, Berthold C, Pabst W, Gregorová E & Nickel K (2004) Particle size and shape characterization of Kaolins-comparison of settling methods and laser diffraction. Key Engineering Materials
Li L, Keller G, Adatte T, Stinnesbeck W (2000) Late Cretaceous sea-level changes in Tunisia: a multi-disciplinary approach. J Geol Soc 157(2):447–458
Manzi V, Gennari R, Hilgen F, Krijgsman W, Lugli S, Roveri M, Sierro FJ (2013) Age refinement of the Messinian salinity crisis onset in the Mediterranean. Terra Nova 25(4):315–322
Millot G (1970) Geology of clays: weathering, sedimentology, geochemistry. Springer-Verlag
Nikpour N, Fotoohi S, Hosseini SZ, Negaresh H, Bahrami S (2022) An assessment of land degradation and its effects on geomorphology using LADA model: a case study of Ilam Province, west of Iran. Environmental Earth Sciences 81(10):274
Owliaie H, Abtahi A, Heck R (2006) Pedogenesis and clay mineralogical investigation of soils formed on gypsiferous and calcareous materials, on a transect, southwestern Iran. Geoderma 134(1–2):62–81
Palcu DV, Vasiliev I, Stoica M, Krijgsman W (2019) The end of the Great Khersonian Drying of Eurasia: magnetostratigraphic dating of the Maeotian transgression in the Eastern Paratethys. Basin Res 31(1):33–58
Paquet H & Millot G (1972) Geochemical evolution of clay minerals in the weathered products in soils of Mediterranean climate. Proceedings of the International Clay Conference
Perşoiu A, Ionita M, Weiss H (2019) Atmospheric blocking induced by the strengthened Siberian High led to drying in west Asia during the 4.2 ka BP event-a hypothesis. Climate of the past 15(2):781–793
Ramstein G, Fluteau F, Besse J, Joussaume S (1997) Effect of orogeny, plate motion and land–sea distribution on Eurasian climate change over the past 30 million years. Nature 386(6627):788–795
Rosenthal E, Magaritz M, Ronen D, Roded R (1987) Origin of nitrates in the Negev Desert. Israel Applied Geochemistry 2(3):347–354
Roveri M, Flecker R, Krijgsman W, Lofi J, Lugli S, Manzi V, Sierro FJ, Bertini A, Camerlenghi A, De Lange G (2014) The Messinian Salinity Crisis: past and future of a great challenge for marine sciences. Mar Geol 352:25–58
Ryan WB (2009) Decoding the Mediterranean salinity crisis. Sedimentology 56(1):95–136
Sanjari S, Farpoor MH, Mahmoodabadi M (2021) Magnetic susceptibility of soils as affected by lithology, geomorphology and climate in Jazmoorian Watershed, central Iran. Geosci J 25(6):903–913
Shenggao L (2000) Lithological factors affecting magnetic susceptibility of subtropical soils, Zhejiang Province. China Catena 40(4):359–373
Singer A (1979) Palygorskite in sediments: detrital, diagenetic or neoformed—a critical review. Geol Rundsch 68(3):996–1008
Singer A (1980) The paleoclimatic interpretation of clay minerals in soils and weathering profiles. Earth Sci Rev 15(4):303–326. https://doi.org/10.1016/0012-8252(80)90113-0
Singer A (1984a) Clay formation in saprolites of igneous rocks under semiarid to arid conditions, Negev, southern Israel. Soil Sci 137(5):332–340
Singer A (1984b) The paleoclimatic interpretation of clay minerals in sediments—a review. Earth Sci Rev 21(4):251–293
Singer A (1988) Illite in aridic soils, desert dusts and desert loess. Sed Geol 59(3–4):251–259
Singer A (1989) Palygorskite and sepiolite group minerals. Minerals in Soil Environments 1:829–872
Soulié-Märsche I (1991) Charophytes as lacustrine biomarkers during the Quaternary in North Africa. Journal of African Earth Sciences (and the Middle East) 12(1–2):341–351
Soulié-Märsche I (1993) Diversity of quaternary aquatic environments in NE Africa as shown by fossil charophytes. In H. Schandelmeier & U. Thorweihe (Eds.), Geosci Res Northeast Afr. Balkerma
Soulié-Märsche I (2008) Charophytes, indicators for low salinity phases in North African sebkhet. J Afr Earth Sc 51(2):69–76
Suárez M, Pozas JM, Robert M, Elsass F (1994) Evidence of a precursor in the neoformation of palygorskite—new data by analytical electron microscopy. Clay Miner 29(2):255–264
Surdam RC, Eugster HP (1976) Mineral reactions in the sedimentary deposits of the Lake Magadi region. Kenya Geological Society of America Bulletin 87(12):1739–1752
Tardy Y, Bocquier G, Paquet H, Millot G (1973) Formation of clay from granite and its distribution in relation to climate and topography. Geoderma 10(4):271–284
van Baak CG, Stoica M, Grothe A, Aliyeva E, Krijgsman W (2016) Mediterranean-Paratethys connectivity during the Messinian salinity crisis: the Pontian of Azerbaijan. Global Planet Change 141:63–81
Vicente A, Expósito M, Sanjuan J, Martín-Closas C (2016) Small sized charophyte gyrogonites in the Maastrichtian of Coll de Nargó, Eastern Pyrenees: an adaptation to temporary floodplain ponds. Cretac Res 57:443–456
Wilson MJ (1999) The origin and formation of clay minerals in soils: past, present and future perspectives. Clay Miner 34(1):7–25
Zhang Z, Ramstein G, Schuster M, Li C, Contoux C, Yan Q (2014) Aridification of the Sahara desert caused by Tethys Sea shrinkage during the Late Miocene. Nature 513(7518):401–404
Zhang Z, Xiao W, Majidifard MR, Zhu R, Wan B, Ao S, Chen L, Rezaeian M, Esmaeili R (2017) Detrital zircon provenance analysis in the Zagros Orogen, SW Iran: implications for the amalgamation history of the Neo-Tethys. Int J Earth Sci 106(4):1223–1238

Rivista Italiana di Paleontologia e Stratigrafia
(*Research in Paleontology and Stratigraphy*)
vol. 130(1): 35-46. **March 2024**
DOI: https://doi.org/10.54103/2039-4942/20461

REWORKED MESOZOIC RADIOLARIANS IN MIOCENE-PLIOCENE FORELAND SEDIMENTS IN THE ZAGROS BELT, IRAN

CHRISTIAN A.F. DIETZEL[1]*, HAYTHAM EL ATFY,[1,2,3] CHRISTOPH BERTHOLD[4], MAHMOUD REZA MAJIDIFARD[5] & MADELAINE BÖHME[1,6]

[1]Terrestrial Palaeoclimatology, Department of Geosciences, Eberhard-Karls-University of Tübingen, Germany.
E-mail: christian.dietzel@uni-tuebingen.de
[2]Palaeobotany Group, Institute for Geology and Palaeontology University of Münster, 48149 Münster, Germany.
[3]Geology Department, Faculty of Science, Mansoura University, 35516 Mansoura, Egypt.
[4]Competence Center Archaeometry – Baden-Wuerttemberg, Eberhard-Karls-University of Tübingen, Germany.
[5]Research Institute for Earth Sciences, Geologic Survey of Iran, Teheran, Iran.
[6]Section Palaeontology, Senckenberg Centre for Human Evolution and Palaeoenvironment, Tübingen, Germany.
*Corresponding author.

Associate Editor: Silvia Gardin.

To cite this article: Dietzel C.A.F., El Atfy H., Berthold C., Reza Majidifard M. & Böhme M. (2024) - Reworked Mesozoic radiolarians in Miocene-Pliocene foreland sediments in the Zagros Belt, Iran. *Riv. It. Paleontol. Strat.*, 130(1): 35-46.

Keywords: Radiolaria; Zagros; sedimentary transport; Cretaceous; Miocene; Pliocene; Iran.

Abstract. Micropaleontology can give important insights into the provenance and paleoenvironmental conditions in terrestrial sedimentary archives. For the current study, 84 samples representing a 2.6 km thick sedimentary profile from the Simply Folded Zagros Mountain Belt were investigated. They span ca. 10.2 my from the late Middle Miocene (Serravallian) to the earliest Pleistocene (Gelasian), and comprise floodplain sediments and saline mudstones with an aeolian contribution. The samples revealed a unique Cretaceous radiolarian assemblage comprising largely of cryptothoracic nassellarians and spherical spumellarians. This record highlights the reworking of sediments derived from Cretaceous Qulqula-Kermanshah radiolarian claystones and radiolarites in the Imbricated Zagros Belt into distal Neogene Zagros foreland sediments in Lurestan (Lurestan Arc). The high abundance of *Holocryptocanium barbui* (Dumitrica) and other cryptothoracic taxa compared to the Qulqula-Kermanshah radiolarian claystones and radiolarites potentially indicates a preferred erosion of softer units such as the Red Radiolarian Claystone Unit (RRCU) compared to harder radiolarian cherts. The observation of a reworked largely cryptothoracic assemblage might also point to additional sorting effects during fluvial and aeolian transport as well as during redeposition, depending on the morphology and hydrodynamic properties of individual radiolarian taxa.

Introduction

In previous paleoclimatic studies, a 2.800 m thick sedimentary succession of Miocene-Pliocene foreland sediments in the Zagros Mountain Belt (Iran) was investigated by soluble salt geochemistry (Böhme et al. 2021) and clay mineralogical analysis (Dietzel et al. 2023). Within the studied profile, the oldest sample (12.6 Ma, Serravallian) taken from the Gachsaran Formation was of coastal-marine origin. In contrast, samples from the lower Aghajari Member (12.02–5.6 Ma, Serravallian-Messinian) show a

Received: June 26, 2023; accepted: February 06, 2024

fluvial-alluvial origin. On top of the studied succession, samples from the Lahbari Member (5.59–2.5 Ma, Messinian-Gelasian) were derived from both aeolian and fluvial-alluvial provenance where soluble salt geochemistry and palynological observations point to a period of sustained hyper-arid climate between 5.6 and 3.3 Ma. This phenomenon was described as the Neogene Arabian Desert climax (NADX), the onset contemporaneous with the acme of the Messinian Salinity Crisis (Böhme et al. 2021). Clay mineralogical investigations throughout the profile (Dietzel et al. 2023) revealed prominent occurrences of autochthonous charophytes in several samples, which were visible even with the naked eye within the sand fraction (> 63 μm), next to few radiolarians. These findings instigated a detailed micropaleontological investigation of all samples to check for further microfossils which could have reliable implications for paleoclimate interpretations as well as sediment provenance. For this purpose, a detailed investigation of the sand fraction in all remaining samples was carried out. The investigation revealed the widespread occurrence of a unique allochthonous Cretaceous radiolarian assemblage throughout the whole sedimentary profile. This reworked radiolarian record closes a gap in understanding the Neogene tectonic obduction of Mesozoic radiolarites in the Zagros mountain belt. Furthermore, it could enhance our knowledge on the effect of erosion and secondary transport on microfossil assemblages such as radiolarians. Henceforth, the current study ultimately aims to detect erosional and transport sorting effects on a reworked radiolarian assemblage and highlight its environmental and ecological impact through time and space throughout the studied material.

Geological overview

The SE–NW trending Zagros Fold and Thrust Belt (ZFTB) resulted from the collision between the Arabian and the Eurasian plates. This collision led to crustal shortening and accommodation of thick sedimentary cover. Deformation intensity is decreasing from the Zagros Suture Zone to the present deformation front, located near the Iran-Iraq border (Alavi 1994; Berberian 1995). The ZFTB belt is tectonically divided, from the SW to the NE, into four zones; (1) the Mesopotamian Foreland Basin with buried folds, extending into the Persian Gulf, (2) the Folded Belt characterized by simple folds, (3) the Imbricated Zone characterized by thrusting, including ophiolite sequences with radiolarites of Jurassic to Cretaceous age (Gharib & De Wever 2010; Al-Qayim et al. 2018); and (4) the Sanandaj–Sirjan metamorphic and magmatic zone (Homke et al. 2004; 2010). The Zagros foreland sediments were, next to an aeolian contribution (Böhme et al. 2021), largely deposited by axial and radial fluvial systems in the Miocene and alluvial fan systems in the Pliocene, derived from the Zagros mountain belt (Koshnaw et al. 2020). Systematic clast analysis revealed the presence of radiolarian chert likely to be derived from erosion of deep marine Qulqula – Kermanshah radiolarites into the Neogene Zagros foreland basin. These clastic sediments have been reported from the proximal conglomerates at the Kirkuk Embayment NNE of the study area (Koshnaw et al. 2017) as well as from the Dezful Embayment towards SE (Etemad-Saeed et al. 2020) and have also been documented in channel-lags from a restricted interval of the Lower Aghajari Member (see below) in the present study area (Böhme et al. 2021) (Fig. 1). However, these clasts have not been comprehensively investigated and there is only limited information on the contribution of radiolarites to other stratigraphic levels as well as to the more distal foreland available sediments, where a finer grain size hampers clast analysis.

The study area near the Iran-Iraq border is part of the Lurestan Arc in the Simply Folded Zagros Belt where syndepositional deformation of foreland sediments has initiated in the Tortonian, possibly between 8.1 and 7.2 Ma (Homke et al. 2004). The investigated mudstone samples cover the Gachsaran Formation, Lower Aghajari Member, Lahbari Member and Bakhtyari Formation. The continuous profiles with a thickness of nearly 2.6 km were sampled in two localities including the Zarrinabad and Changuleh syncline-anticline structures (Fig. 1). The studied samples have robust temporal control, as they were taken at georeferenced sampling points that have been previously dated using magnetostratigraphy by Homke et al. (2004). The sampling points were resampled by Böhme et al. (2021) and are interpolated with numerical age data along the stratigraphic profile. While the clastic rocks from the Zarrinabad profile

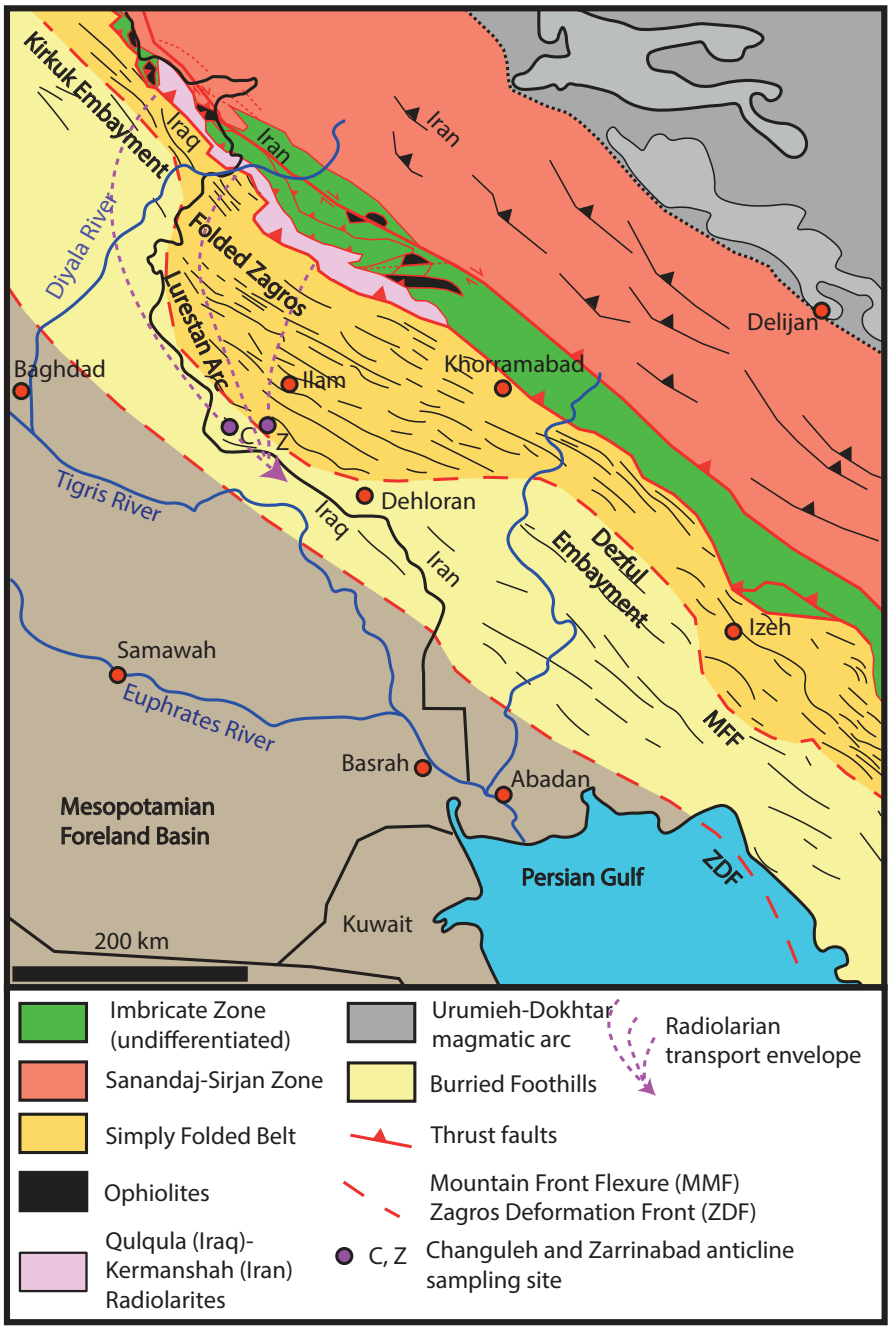

Fig. 1- Structural overview map of the northeastern Mesopotamian Foreland basin. Regional geotectonic map modified from Vergés et al. (2011) with distribution of radiolarites in the Iran-Iraq border region adapted from Ali et al. (2014).

are of late Serrvallian-early Tortonian age (12.6–9.38 Ma), samples from the Changuleh profile are of mid-Tortonian to Pleistocene age (9.02–2.4 Ma). A brief summary of the geological description of the sedimentary profile in (Böhme et al. 2021) is presented here:

In the study area, the upper part of the **Gachsaran Formation** is characterized by alternating reddish mudstones rich in pedogenic gypsum and sandstones with wave ripples, typical of a depositional environment alternating between shallow marine shoreface and terrestrial backshore facies.

The **Aghajari Formation** is divided into the Lower Aghajari Member and the Lahbari Member. The Lower Aghajari Member (12.02–5.6 Ma; Serravallian - Messinian) represents roughly 1.5 km thickness of the sedimentary profile. It is composed of fine-clastic mudstones alternating with and thick fluvial sandstone deposits often showing cross-bedding structures. Channel-lags, between stratigraphic meter 520-770 (10.8 to 9.8 Ma), contain pebble-sized radiolarite-cherts (Fig. 2), which have been not observed in both older or younger horizons. In the Lower Aghajari Member, pedogenic features such

as rhizocretes from carbonate and gypsum as well as manganese staining are commonly observed. Fluvial sandstone channels often feature mud ball erosion at their base. Previous paleoclimate analysis indicates arid conditions during the Serravallian and early Tortonian, followed by semi-arid conditions during the late Tortonian (Böhme et al. 2021; Dietzel et al. 2023), based on soluble salt geochemistry and clay mineralogy. A transition to sustained arid conditions is suggested during the early Messinian. While the sedimentary environment of this rock unit in Khuzestan and Lurestan is characterized by river and lake sedimentation, it represents a coastal-marine facies in Fars.

The **Lahbari Member** (5.59–2.4 Ma; Messinian-lower Gelasian) in the Changuleh anticline is characterized by saline mudstones lacking the pedogenic features observed in the Lower Aghajari Member. Fluvial sandstones are less frequent and generally much thinner than in the underlying member Sediment found in the fine grained Lahbari Member were possibly redeposited locally from the Gachsaran and Aghajari Sediments, which were regionally uplifted in the Lurestan Arc (Emami et al. 2010). The occurrence of structureless, thick silts together with the geochemistry of soluble salts has furthermore been interpreted to indicate an increased aeolian sediment deposition during a hyper-arid period between 5.59 and 3.3 Ma (NADX) (Böhme et al. 2021). Coarse grained alluvial conglomerates can be observed in the upper Lahbari Mb. signifying the progression of the Zagros Mountain Front Flexure near the transition to the conglomeratic Bakhtyari Formation around 2.5 Ma (Homke et al. 2004).

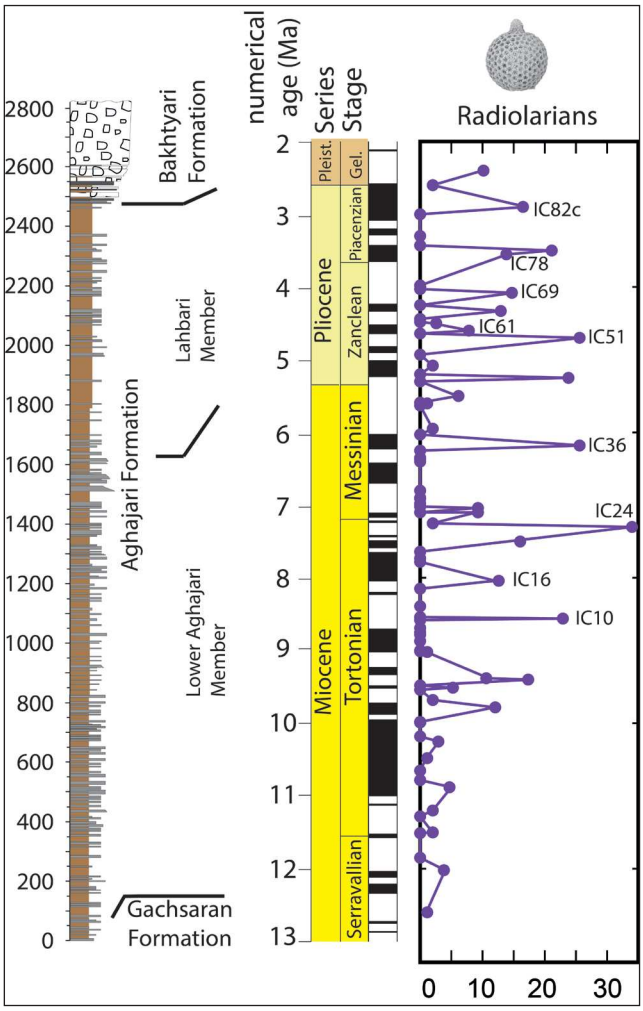

Fig. 2 - Combined stratigraphic profile of the sampling sites at the Zarrinabad anticline and Changuleh syncline-anticline structure. Sedimentary profile and magnetostratigraphic timescale adapted from Homke et al. (2004), sampling points adapted from Böhme et al. (2021). Lines and points represent the numbers of radiolarians found under the binocular in 5g of sediment sample. Number marks sample ID and position of illustrated radiolaria within the profile.

Material and methods

A few kilometres N from the Iran-Iraq border in the Ilam province, Iran, a number of 84 evenly distributed mudstone samples were collected from silty horizons along the 2600 m thick sedimentary profile. Sediments from 12.6 to 9.38 Ma were sampled at the Zarrinabad anticline and from 9.02 to 2.4 Ma at the Changuleh syncline-anticline structure (Fig. 1). As the same samples were previously investigated for paleoclimate analysis, the age model and sample number is identical to Böhme et al. (2021). For the purpose of the current investigation, 5 grams of each sample were dried overnight at 110 °C and then gently disaggregated by hydrating the samples with de-ionized water, utilizing the swelling properties of clay minerals. The samples were then treated with ultrasound for 30 s, to achieve complete separation of clay, silt and sand. The sand fraction was then separated from silt and clay by rinsing the sample through a 63 µm sieve for further micropaleontological investigation (Dietzel et al. 2023). The cleaned samples of the sand fraction were then analysed using a 80 x magnification LEICA S8AP0 binocular. Radiolarians were identified and picked from the sand fraction in 36 samples using a fine brush. 15 selected samples spanning the whole sedimentary profile were then transferred onto a carbon coated sample mount and analysed by a Phenom XL C2 Desktop SEM with 15 kV acceleration voltage.

Results

Thirty-six samples collected throughout the sedimentary profile yielded in total 359 radiolarian specimens (Tab. 1 supplement, Fig. 2). A general increase of radiolarians per productive sample is observed after ~10 Ma. The retrieved radiolarians were found in sediment samples from the Gachsaran Formation, Lower Aghajari Member and Lahba-

ri Member. Their size varied from 90–360 μm and comprised Nassellaria with a large spherical abdomen and Spumellarians. The majority of all recognizable skeletons showed hexagonal surface ornamentations. Specific identification to a species level was only possible for few specimens due to surface damage, recrystallization and abrasion likely related to secondary transport. This is aggravated by the general similarities of the surface morphology of Nassellarian taxa such as, *Cryptamphorella* sp. or *Holocryptocanium barbui* (Dumitrica) (Pl. 2). Furthermore, identification was hampered by the fact, that the allochthonous nature of the radiolarians did not allow for age cross-referencing between individual radiolarians in one individual sample. Their lowest and highest occurrence ranges were compiled after previous works. The known stratigraphic range of specifically identified radiolarians was plotted next to the age span of the Kermanshah-Qulqula radiolarites as a possible source (Gharib & De Wever 2010; Al-Qayim et al. 2018) (Fig. 3). Furthermore, the presence of other marine taxa represented by foraminifera was noted in sample IC10 (8.56 Ma) and in IZ157 (9.54 Ma), IC69 (4.08 Ma) and IC 82c (2.9 Ma), that are beyond the scope of this investigation.

Systematic paleontology

Class RADIOLARIA Müller, 1858
Subclass POLYCYSTINEA Ehrenberg, 1839, emend. Riedel, 1967
Order **Nassellaria** Ehrenberg, 1875
Family Archaeodictyomitridae Pessagno, 1976
Genus *Tharnala* Pessagno, 1977

Tharnala sp.
Plate 1, fig. a

Occurrence: sample IC21 7.5 Ma.

Family Artostrobiidae Riedel, 1967
Genus *Rhopalosyringium* Campbell & Clark, 1944

Rhopalosyringium sp.
Plate 1, fig. b

Occurrence: sample IC69, 4.08 Ma.

Family Williriedellidae Dumitrica, 1970
Genus *Cryptamphorella* Dumitrica, 1970

Cryptamphorella conara Foreman, 1968
Plate 1, fig. c

Occurrence: sample IC51, 4.7 Ma.
Stratigraphic range of the taxon: Albian-Maastrichtian (Bandini et al. 2008).

Cryptamphorella sp. cf. ***C. conara*** Foreman, 1968
Plate 1, fig. d; Plate 2, fig. h

Occurence: sample, IC21, 7.5 Ma; IC51 4.7 Ma.

Cryptamphorella**?** sp.
Plate 1, fig. e

Occurrence: sample IC82c, 2**.**9 Ma.

Genus *Holocryptocanium* Dumitrica, 1970

Holocryptocanium barbui Dumitrica, 1970
Plate1, fig. f; Plate 2, figs. a-c, f

Occurrence: samples IC36 6.18 Ma; IC 51, 4.7 Ma; IC61, 4.6 Ma.
Stratigraphic range of the taxon: Tithonian-Turonian (Bragina & Bragin 2021; Baumgartner et al. 2023).

Holocryptocanium sp. cf. ***H. astiense*** Pessagno, 1977
Plate 1, fig. g

Occurrence: sample IC 61, 4.6 Ma.
Stratigraphic range of the taxon: Cenomanian-Coniacian (Bragina & Bragin 2021).

Order **Spumellaria** Ehrenberg, 1875
Family Dactyliosphaeridae Squinabol, 1904
Genus *Dactyliosphaera* Squinabol 1904

Dactyliosphaera**?** sp.
Plate 1, fig. h

Occurrence: sample IC10, 8.56 Ma.

Family Parvivaccidae Pessagno & Yang, 1989, emend. Dumitrica & Caulet, in De Wever et al. (2001)
Genus *Praeconosphaera* Yang, 1993

Praeconosphaera sp. cf. ***P. antiqua*****?** Parona, 1890
Plate 1, fig. i

Occurrence: samples IC16, 8.04 Ma; IC51, 7.7 Ma; IC78, 3.55 Ma.
Remarks. Possibly a cryptocehalic nasselarian.

Family Praeconocaryommidae Pessagno, 1976

Genus *Praeconocaryomma* Pessagno, 1976

Praeconocaryomma sp. cf. ***P californiensis*** Pessagno, 1976

Plate 1, fig. j

Occurrence: sample IC10, 8.56 Ma; sample IC 24, 7.3 Ma.
Stratigraphic range of the taxon: Upper Cenomanian-Campanian (Bragina 2004).

Family Xiphostylidae Haeckel, 1881
Genus *Archaeocenosphaera* Pessagno, 1989

***Archaeocenosphaera*?** sp.

Plate 1, fig. k; Plate 2, fig. i

Occurrence: sample IC26, 7.04 Ma, IC21, 7.5 Ma.

Archaeocenosphaera clathrata Parona, 1890

Plate 1, fig. l

Occurrence: IC78, 3.55 Ma.
Stratigraphic range of the taxon: Lower Devonian-Eocene (Ozsvárt et al. 2020).

Archaeocenosphaera*? *mellifera O'Dogherty, 1994

Plate 1, fig. m

Occurrence: sample IC16, 8.04 Ma.
Stratigraphic range of the taxon: Albian-Campanian (Bragina et al. 2022).

Gen. et spec. indet. 1

Plate 1, fig. n

Occurrence: sample IC 21 at 7.5 Ma.
Remarks. This taxon describes a spherical internal mold of a radiolarian skeleton.

Gen. et spec. indet. 2

Plate 1, fig. o

Occurrence: sample IC61, 4.6 Ma.
Remarks. This taxon describes a spherical mould of 80 µm diameter and displays protruding imprints of pore structure.

Gen. et spec. indet. 3

Plate 2, fig. d

Occurrence: sample IC36 6.18 Ma.

Gen. et spec. indet. 4

Plate 2, fig. e

Occurrence: sample IC36 6.18 Ma.

Gen. et spec. indet. 5

Plate 2, fig. g

Occurrence: sample IC36 6.18 Ma.

Discussion

Sediment provenance and tectonic implications

Regarding mineralogical composition, the sediments of the Aghajari Member are mostly composed of quartz, feldspar, volcanic, and metamorphic lithoclasts sourced from Eurasia. The composition of detrital Cr-spinels also indicates a contribution of mafic to ultramafic ophiolites of the Arabia-Eurasia suture zone to the foreland sediments (Cai et al. 2021). The ophiolites of the Zagros suture zone are currently exposed alongside radiolarite nappes in Kermanshah and Neyriz in Iran (Stoecklin 1968; Cai et al. 2021) and can also be found NW along strike in Iraq and Turkey (Jassim & Goff 2006; Ismail et al. 2010). The Zagros radiolarites found within the Imbricate Zagros have been described in the literature as Qulqula radiolarites in Iraq and Kermanshah radiolarites in Iran. They have been micropaleontologically constrained to the lower Pliensbachian up to the Turonian at Kermanshah, Iran (Gharib & De Wever 2010) and Bajocian to the end of the Cenomanian at Qulqula, Iraq (Al-Qayim et al. 2018). Reworked radiolarians identified in this study in the Zagros foreland sediments are generally of Cretaceous age while Jurassic ones are poorly represented. Although the Qulqula – Kermanshah radiolarites of the Arabia-Eurasia suture zone 200-300 km north of the study area (Fig. 1) are indicated as the general source area, the limited presence of reworked Jurassic taxa might be either due to a better preservation potential of Cretaceous taxa or a minor occurrence of Jurassic radiolarites in the direct erosional area. The assumed source area agrees with paleoflow directions in the floodplain sediments and radiolarian claystones of the Aghajari Member in the study area pointing towards SE as the present-day Tigris river (Homke et al. 2004). The presence of radiolarite clasts have been described throughout the Zagros Foreland Basin (Koshnaw et al. 2017; Etemad-Saeed et al. 2020; Böhme et al. 2021). Radiolarians from these clasts

PLATE 1

SEM-Illustrations of allochthonous Jurassic and Cretaceous Radiolaria found in Lower Aghajari Member and Lahbari Member.
a) *Tharnala* sp. sample IC21 7.5 Ma; b) *Rhopalosyringium* sp. sample IC69, 4.08 Ma; c) *Cryptamphorella conara* Foreman, 1968 sample IC51, 4.7 Ma; d) *Cryptamphorella* sp. cf. *C. conara* Foreman, 1968, sample IC21, 7.5 Ma; e) *Cryptamphorella*? sp. 2 sample IC82c, 2.9 Ma; f) *Holocryptocanium barbui* Dumitrica, 1970 sample IC 51, 4.7 Ma; g) *Holocryptocanium* sp. cf. *H. astiense* Pessagno, 1977 sample IC 61, 4.6 Ma; h) *Dactyliosphaera*? sample IC10, 8.56 Ma; i) *Praeconosphaera* sp. cf. *P. antiqua*? Parona, 1890 sample IC51 4.7 Ma; j) *Praeconocaryomma* sp. cf. *C. californiensis* Pessagno, 1976, sample IC 24, 7.3 Ma; k) *Achaeocenosphaera*? sp. sample IC26, 7.04 Ma; l) *Archaeocenosphaera clathrata* Parona, 1890 sample IC78, 3.55 Ma; m) *Archaeocenosphaera*? *mellifera* O'Dogherty 1994 sample IC16, 8.04 Ma; n) Gen. et spec. indet. 1 sample IC 21 7.5 Ma o) Gen. et sp. indet. 2, sample IC61, 4.6 Ma.

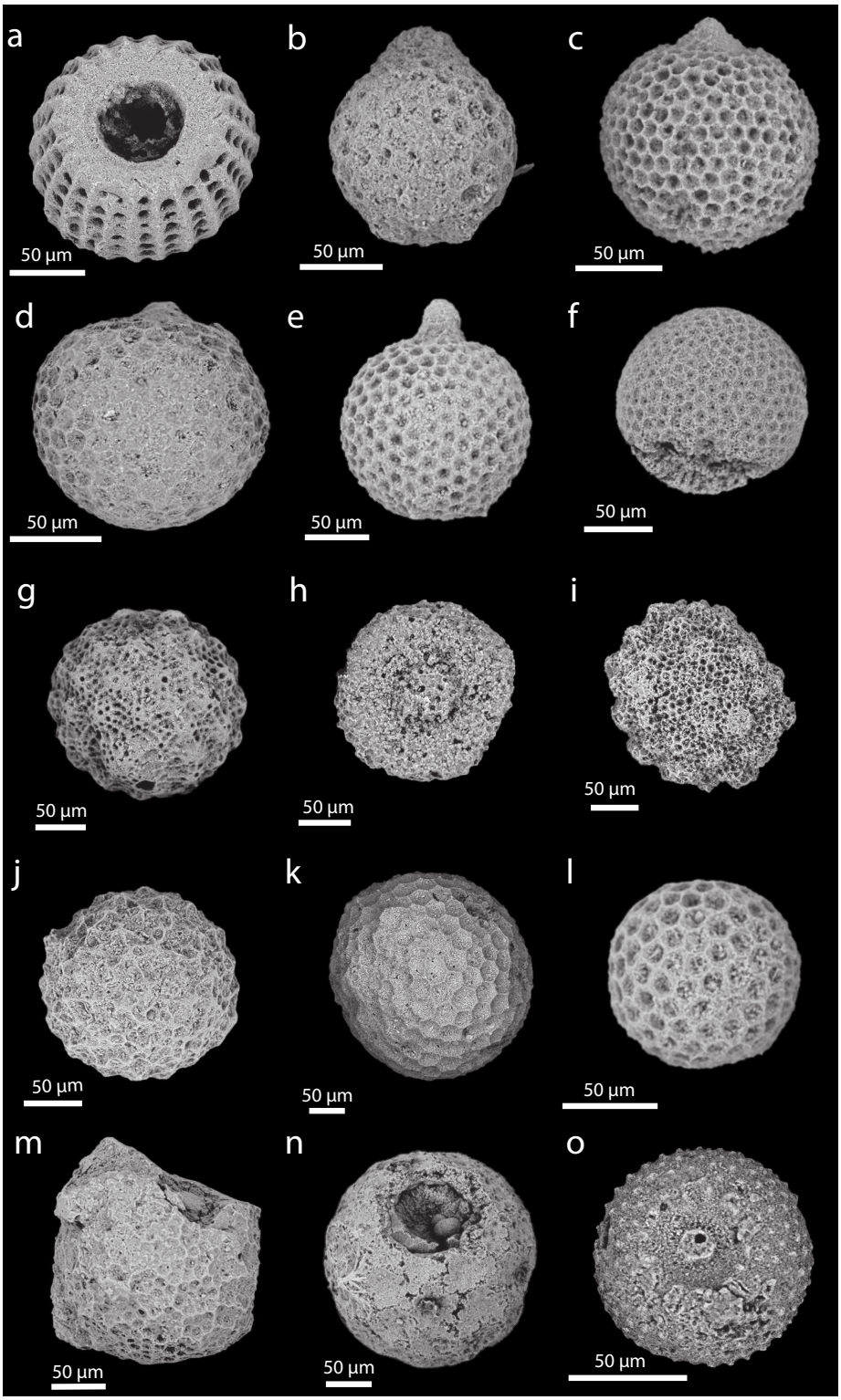

would likely be better suited for age determination due to a higher preservation potential; however, no clasts were available for comparison in this study. An increase in the proportion of radiolarite clasts has been reported in conglomerates from the Zagros foreland sediments in the Dezful embayment, 200 km SE of this study area, in the mid-Tortonian ~ 9 Ma and was linked to tectonic exhumation and erosion of the Kermashah radiolarites in the Imbricated Zagros NE of the Dezful Embayment (Etemad-Saeed et al. 2020). An earlier increase in the radiolarians per sample is observed in the samples of this study at ~ 10 Ma (Fig. 2), possibly indicative of an earlier increased tectonic exposure of

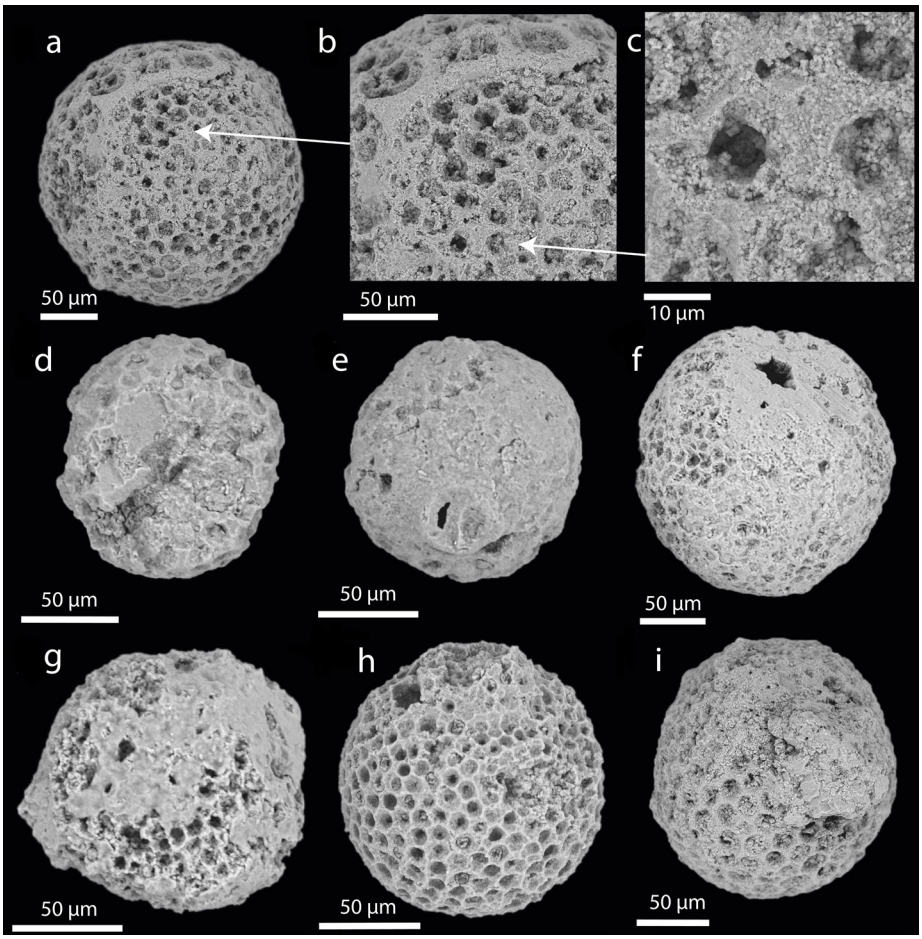

PLATE 2

SEM-Illustrations of typical preservation allochthonous radiolarians with hexagonal pore structure found in Miocene-Pliocene foreland sediments of the Pust-e Kuh arc.

a-c) *Holocryptocanium barbui* Dumitrica, 1970 recrystallization and partial overgrowth of radiolarian skeleton with SiO_2 infill of pore spaces and abdomen with fine grained quartz crystals sample IC61, 4.6 Ma; d) Gen. et sp. indet. 3, complete recrystallization of pore-space with SiO_2 extremely poor preservation of surface, potential transport damage, sample IC36 6.18 Ma; e) Gen. et sp. indet. 4 hollow radiolarian skeleton showing recrystallization of surficial pore space with SiO_2, with abrasion damage on the surface, sample IC36 6.18 Ma; f) *Holocryptocanium barbui* Dumitrica, 1970 hollow skeleton showing recrystallization of surficial pore space and limited infill of the abdomen with SiO_2, some abrasion damage on the surface, sample IC36 6.18 Ma; g) Gen. et sp. indet. 5, a recrystallized skeleton with growth of clay minerals and carbonate, sample IC36 6.18 Ma; h) *Cryptamphorella* sp. cf. *C. conara* Foreman, 1968 abraded cephalo-thoracic portion. partial infill of pores with SiO_2, sample IC51 4.7 Ma.; i) *Archaeocenosphaera*? sp., recrystallized skeleton with fine-grained SiO_2 infill of pore spaces, overgrowth of coarse-grained SiO_2 on the surface, sample IC21 7.5 Ma.

the Qulqula – Kermanshah radiolarites NE of the Lurestan Arc compared to the Dezful embayment.

The presence of allochthonous radiolarians likely derived from Qulqula – Kermanshah radiolarites throughout the uppermost part of the Gachsaran Formation, Lower Aghajari Member, and the Lahbari Member indicates a continuous sediment input originating from the Imbricated Zagros to the North and East of the study area during the Miocene and Pliocene. In the Lahbari Member, between 5.59 and 3.3 Ma, Böhme et al. (2021) suggested enhanced aeolian input from a westerly sediment source based on the heavy mineral spectrum during the hyper-arid NADX phase. In the case of a long-range-aeolian sediment transport from a sediment source in the west, a change in microfossil assemblage would also be expected compared to the fluvial deposits of the Lower Aghajari Member. The sustained observation of radiolarians likely derived from Qulqula – Kermanshah radiolarites is, however, more indicative of a sediment origin to the NNE. Therefore, the presence of radiolarians in the Lahbari Member is better explained by the redeposition of the local Gachsaran and Aghajari sediments regionally uplifted in the Pusht-e Kuh Arc to the North and East of the Changuleh Anticli-

ne, according to the model of Emami et al. (2010). Hereby aeolian processes likely played an important role in regional sediment redeposition leading to the formation of thick, structureless, saline siltstones of the Lahbari Member in front of the Lurestan Arc (cf. Böhme et al. 2021).

Impact of erosion and redeposition on radiolarian assemblages

Erosion

While frequent radiolarian chert clasts were described by Etemad-Saeed et al. (2020), clasts of radiolarite chert were only recognized between 10.8 to 9.8 Ma in the Zarrinabad section of the profile (Böhme et al. 2021). Unfortunately, no sample of these cherts was taken in the field for analysis. Only single radiolarians without major chert attachments were observed throughout the fine-grained sandstones and mudstones of this study. This could correspond to the mobilization of single radiolarians from softer claystones such as the Red Radiolarian Claystone Unit (RRCU). *Holocryptocanium barbui* (Dumitrica) is the most commonly observed taxon in this study. In the Qulqula – Kermanshah radiolarites *H. barbui* (Dumitrica) has so been observed in the RRCU (Al-Qayim et al. 2018), where it has been reported alongside *Archaeodictyomitra mitra* (Dumitrica), *Angulobracchia portmanni* s.l. (Baumgartner) and *Pseudodictyomitra carpatica* (Lozyinak). The radiolarian claystones of the RRCU are of Berriasian to early Aptian age (Al-Qayim et al. 2018). They possibly represent the "Crypto-Archaeo" Assemblage, comprising low diversity, ecologically tolerant forms (chiefly cryptocephalic and cryptothoracic nassellarians and *Archeodictyomitra* spp.) which have been interpreted to originate in the Subtropical Gyre (Baumgartner et al. 2023). Enhanced erosion of radiolarians from these softer low-diversity radiolarian claystones compared to interbedded harder radiolarian cherts or limestones is therefore possibly a prime factor accounting for the high percentage of cryptothoracic nassellarians observed in this study, while other radiolarian taxa described from radiolarites Gharib and De Wever (2010) and Al-Qayim et al. (2018) are missing. The RRCU with a thickness of 80-100 m has only been analysed by a single sediment sample so far (KN-32), therefore the age span covered given by Al-Qayim et al. (2018) might possibly be too short.

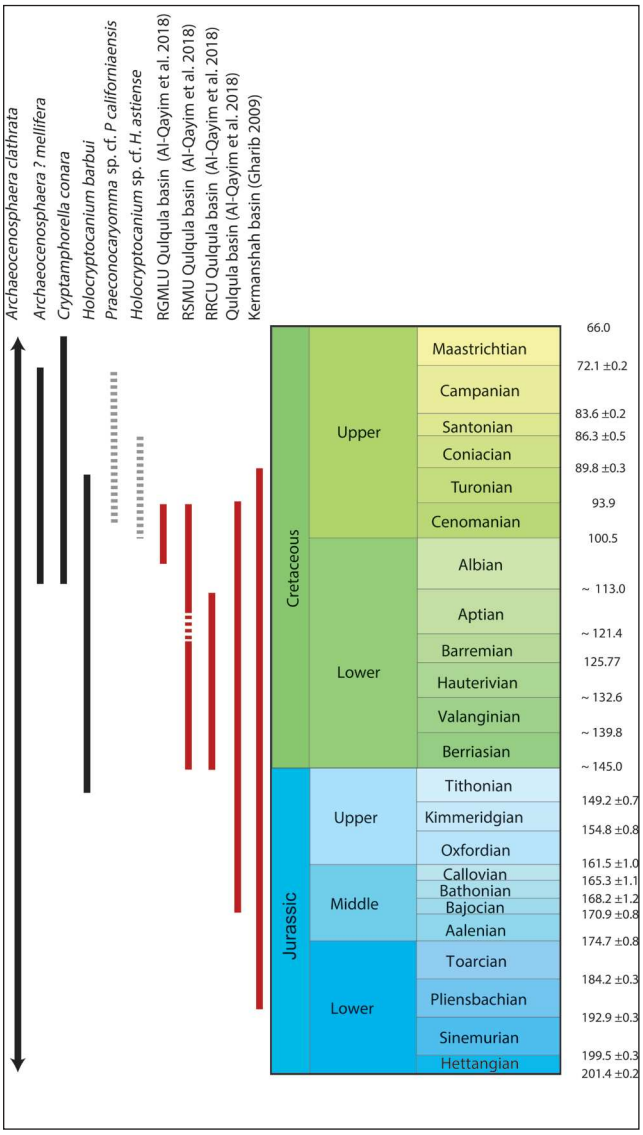

Fig. 3 - Stratigraphic chart marking the total range of occurrence of Mesozoic radiolarian taxa identified in Zagros foreland sediments and the age of radiolarites in the Qulqula – Kermanshah basins as potential source area. Grey dotted bars indicate a higher level of uncertainty in the determination of taxon.

This might explain the missing age range overlap between the RRCU and some of the cryptothoracical taxa observed in this study such as *Cryptamphorella conara* (Foreman) (Fig. 3). A temporal overlap for mid- to Late Cretaceous radiolarian taxa found in this study is found in the Red Siliceous Mudstone Unit (RSMU) of up to 50 m thickness comprising thin to medium bedded radiolarian mudstone and shale alternating with siliceous shale, and minor limestone and chert, as well as the Reddish-Green Mudstone and Limestone Unit (RGMLU) of up to 20 m thickness comprising alternation of red and green marly mudstones and claystones, with thin to

medium beds of calcilutite to calcisiltite bioclastic to peloidal limestone (Al-Qayim et al. 2018). While the RSMU and RRCU have been interpreted to have been deposited the distal abyssal plane, the RGMLU has been interpreted to represent the proximal slope of the Afro-Arabian Margin. A single radiolarian bearing pelagic limestone sample (KN-2) of the middle Albian to Cenomanian RGMLU and a single middle Aptian-Cenomanian radiolarian shale sample (KN-3) of the RSMU were assessed in Al-Qayim et al. (2018). While the described assemblages did contain *Tharnala praeveneta* (Pessagno) and *Tharnala pulchra* (Squinabol) in sample KN-2, they do not match well with the reworked Middle-Upper Cretaceous cryptothoracic Nasselarians observed in this study. No taxonomic data was available on the radiolarian assemblages of the interbedded softer mudstones and claystones found within the RGMLU and RSMU. Further future high-resolution studies in the Qulqula – Kershmanshah radiolarites and radiolarian claystones are therefore warranted.

Transport

Additionally, compact spherical radiolarians could have been enriched during transport. It seems possible that compact spherical taxa show more resistance to breaking during turbulent fluvial erosion and transport than complexly branched taxa with long-producing spines. A turbulent transport history is implied by the evidence of surface abrasion and chipped-off surface structure visible on many radiolarian skeletons (Pl. 2) All radiolarians observed in this study show a varying degree of recrystallization of SiO_2 (Pl. 2). If this infill of diagenetic SiO_2 predates the erosion of the primary radiolarites during the Miocene and Pliocene, it might have further strengthened the structure of the individual radiolarians giving more resistance against erosional processes. An additional model for preferential transport could be provided by the sorting processes of aeolian transport, such as dust storms, which preferentially transport well-rounded silt and sand grains (Mazzullo et al. 1992) along the semi-arid to the hyper-arid flood plain.

Deposition

Furthermore, settling velocities of different radiolarian taxa need to be considered. For this study only mudstones were analyzed, while the interbedded coarser grained sandstones were not tested. It is therefore possible that larger taxa could have been deposited preferentially within the coarser sandstones along the floodplain. The departure of a grain from a spherical shape causes a decrease in its settling velocity within a fluid (Komar & Reimers 1978). Experimental work by Takahashi and Honjo (1983) on extant radiolarian skeletons indicated a variation in sinking speed in seawater between 13 and 416 m per day. The observed sinking speeds are generally lower than those predicted by Stokes Law and systematically deviate from it. In the experimental study the weight per shell showed the highest correlation with sinking speed, while some taxa with a large spine surface demonstrated significantly reduced sinking rates. Compact, spherical taxa filled with recrystallized silica might therefore be expected to settle to the ground quicker in a slowly flowing river, than radiolarians of a more complex structure with a higher surface-weight ratio.

It cannot be ruled out, however, that fragile radiolarians have been damaged further during the sample dispersion process. However, no obvious fragments were found during the picking of radiolarians. Smaller fragments might also have been lost during the sieving process in a 63 μm sieve. The observation of strong sorting of radiolarians contrasts with a report of reworked Upper Cretaceous radiolarians described in the Eocene marine London clay formation, where no such sorting has been observed (Fer et al. 2016). While the authors described a generally poor preservation of radiolarians as also found in this study, the source and mode of transport of these reworked radiolarians was uncertain. Differences could also apply as the radiolarians in this study were deposited within a mudstone of a fluvial environment. In contrast, the assemblage reported by Fer et al. (2016) was deposited in a marine environment.

Conclusion

Cretaceous radiolarians throughout the uppermost part of the Gachsaran Formation, Lower Aghajari Member, and Lahbari Member is a unique record for terrestrial sediments. This indicates a continuous contribution of eroded Mesozoic radiolarites from the tectonically obducted Kermanshah – Qulqua radiolarite complex located in the Imbricated Zagros to the Foreland sediments in the Lu-

restan arc during the Late Miocene and Pliocene, which increased during the Tortonian at ~ 10 Ma. The allochthonous radiolarian assemblage is mainly characterized by several taxa of recrystallized, compact, spherical Nassellarians and Spumellarians. This assemblage is distinct from the autochthonous assemblage reported from the Kermanshah-Qulqula radiolarites as a potential source region and shows some similarities to the assemblage described from the Red Radiolarian Claystone Unit (RRCU) of the Qulqula radiolarites. This observation might suggest a selectively enhanced erosional mobilization of radiolarians from the softer radiolarian claystones compared to harder radiolarites. Furthermore, it seems possible that compact spherical taxa provide more stability during transport than more elongated or branched-shaped radiolarian skeletons. It is also possible that these taxa have a higher Stokes settling velocity in slow-flowing fluvial systems than taxa with a higher surface-to-weight ratio, leading to an increased deposition in fluvial sediments.

Acknowledgements: We would like to thank Tatiana Miranda and Hartmut Schulz for supervision the SEM work and Martin Ebner for his fruitful discussions. It is a pleasure to acknowledge Silvia Spezzaferri for the valuable input regarding the identification of microfossils. We are most grateful to Peter Baumgartner and three anonymous reviewers for their constructive reviews, which greatly improved the manuscript.

References

Al-Qayim B.A., Baziany M.M. & Ameen B.M. (2018) - Mesozoic Tethyan Radiolarite age determination, Zagros suture zone, Kurdistan, NE Iraq. *The Iraqi Geological Journal*: 17-33.

Alavi M. (1994) - Tectonics of the Zagros orogenic belt of Iran: new data and interpretations. *Tectonophysics,* 229(3-4): 211-238, 234.

Ali S.A., Mohajjel M., Aswad K., Ismail S., Buckman S. & Jones B. (2014) - Tectono-stratigraphy and structure of the northwestern Zagros collision zone across the Iraq-Iran border. *Faculty of Science, Medicine and Health - Papers*: part A. 2058.

Bandini A.N., Flores K., Baumgartner P.O., Jackett S.-J. & Denyer P. (2008) - Late Cretaceous and Paleogene radiolaria from the Nicoya Peninsula, Costa Rica: a tectonostratigraphic application. *Stratigraphy,* 5(1): 3-21.

Baumgartner P.O., Li X., Matsuoka A. & Vérard C. (2023) - Austral and Subtropical Gyre Radiolaria-latest Jurassic to Early Cretaceous Leg 123, Site 765, Argo Abyssal Plain revisited: Southern Hemisphere paleobiogeography and global climate change. *Micropaleontology,* 69(6).

Berberian M. (1995) - Master "blind" thrust faults hidden under the Zagros folds: active basement tectonics and surface morphotectonics. *Tectonophysics,* 241(3-4): 193-224, 200.

Böhme M., Spassov N., Majidifard M.R., Gärtner A., Kirscher U., Marks M., Dietzel C., Uhlig G., El Atfy H. & Begun D.R. (2021) - Neogene hyperaridity in Arabia drove the directions of mammalian dispersal between Africa and Eurasia. *Communications Earth & Environment,* 2(1): 1-13.

Bragina L. (2004) - Cenomanian-Turonian radiolarians of northern Turkey and the Crimean Mountains. *Paleontological Journal,* 38: S325-S456.

Bragina L. & Bragin N. (2021) - Radiolaria from the lower Cenomanian (Upper Cretaceous) of Crimea. Part 2. Nassellaria. *Revue de Micropaléontologie,* 71: 100482.

Bragina L., Proshina P., Bragin N., Tsiolakis E., Symeou V. & Papadimitriou N. (2022) - Radiolaria and planktonic foraminifera from Sarama composite section of the Kannaviou Formation (Campanian, Upper Cretaceous, Cyprus). *Palaeoworld,* 31(4): 704-722.

Cai F., Ding L., Wang H., Laskowski, A.K., Zhang L., Zhang B., Mohammadi A., Li J., Song P. & Li Z. (2021) - Configuration and timing of collision between Arabia and Eurasia in the Zagros collision zone, Fars, southern Iran. *Tectonics,* 40(8): 1-21, 18.

Campbell A.S. & Clark B.L. (1944) - Radiolaria from upper Cretaceous of middle California. *Geological Society of America, Special Papers*. 57: 1-61.

De Wever P., Dumitrica P., Caulet J.P., Nigrini C. & Caridroit M. (2001) - Radiolarians in the sedimentary record. CRC Press, 28 feb 2002, 533 pp.

Dietzel C.A., Berthold C., Kirscher U., Majidifard M.R. & Böhme M. (2023) - Using clay mineralogy and micropalaeontological observations to unravel Neogene climate variations in Northern Arabia. *Arabian Journal of Geosciences,* 16(5): 343.

Dumitrica P. (1970) - Cryptocephalic and cryptothoracic Nassellaria in some Mesozoic deposits of Romania. *Revue Roumaine de Géologie Géophysique et Géographie*, 14(1): 45-124.

Ehrenberg C.G. (1875) - Fortsetzung der mikrogeologischen Studien als Gesammt-Ubersicht der mikroskopischen Palaontologie gleichartig analysirter Gebirgsarten der Erde, mit specieller Rucksicht auf Polycystinen-Mergel von Barbados. *Abhandlungen der Koniglichen Akademie der Wissenschaften zu Berlin* 1875 (1875): 1-226.

Emami H., Vergés J., Nalpas T., Gillespie P., Sharp I., Karpuz R., Blanc E. & Goodarzi M. (2010) - Structure of the Mountain Front Flexure along the Anaran anticline in the Pusht-e Kuh Arc (NW Zagros, Iran): insights from sand box models. *Geological Society, London, Special Publications,* 330(1): 155-178, 173.

Etemad-Saeed N., Najafi M. & Vergés J. (2020) - Provenance evolution of Oligocene–Pliocene foreland deposits in the Dezful embayment to constrain Central Zagros exhumation history. *Journal of the Geological Society,* 177(4): 799-817.

Fer T., Danelian T. & Bailey H.W. (2016) - Upper Cretaceous radiolarians reworked in the Eocene London Clay Formation, SE England. *Journal of Micropalaeontology,* 35(2): 133-142.

Foreman H.P. (1968) - Upper Maastrichtian Radiolaria of California. *Special Papers in Palaeontology* 3: 1-82.

Gharib F. & De Wever P. (2010) - Radiolaires mésozoïques de la formation de Kermanshah (Iran). *Comptes Rendus Palevol,* 9(5): 209-219.

Haeckel E. (1881) - Prodromus systematis radiolarium, Entwurf eines Radiolarien-Systems auf Grund von Studien der challenger-radiolarien. *Jenaische Zeitschrift für Naturwissenschaft,* 15: 418.

Homke S., Vergés J., Garcés M., Emami H. & Karpuz R. (2004) - Magnetostratigraphy of Miocene–Pliocene Zagros foreland deposits in the front of the Push-e Kush arc (Lurestan Province, Iran). *Earth and Planetary Science Letters,* 225(3-4): 397-410.

Homke S., Vergés J., Van Der Beek P., Fernandez M., Saura E., Barbero L., Badics B. & Labrin E. (2010) - Insights in the exhumation history of the NW Zagros from bedrock and detrital apatite fission-track analysis: Evidence for a long-lived orogeny. *Basin Research,* 22(5): 659-680, 660.

Ismail S.A., Mirza T.M. & Carr P.F. (2010) - Platinum-group elements geochemistry in podiform chromitites and associated peridotites of the Mawat ophiolite, northeastern Iraq. *Journal of Asian Earth Sciences,* 37(1): 31-41, 33.

Jassim S.Z. & Goff J.C. (2006) - Geology of Iraq. DOLIN, s.r.o., distributed by Geological Society of London, 2006, 341 pp.

Komar P.D. & Reimers C. (1978) - Grain shape effects on settling rates. *The Journal of Geology,* 86(2): 193-209.

Koshnaw R.I., Horton B.K., Stockli D.F., Barber D.E., Tamar-Agha M.Y. & Kendall J.J. (2017) - Neogene shortening and exhumation of the Zagros fold-thrust belt and foreland basin in the Kurdistan region of northern Iraq. *Tectonophysics,* 694: 332-355.

Koshnaw R.I., Horton B.K., Stockli D.F., Barber D.E. & Tamar-Agha M.Y. (2020) - Sediment routing in the Zagros foreland basin: Drainage reorganization and a shift from axial to transverse sediment dispersal in the Kurdistan region of Iraq. *Basin Research*, 32(4): 688-715, 709.

Matsuoka A. (1984) - Late Jurassic four-segmented nassellarians (radiolaria) from Shikoku, Japan. *Journal of Geosciences, Osaka City University,* 27: 143-153.

Mazzullo J., Alexander A., Tieh T. & Menglin D. (1992) - The effects of wind transport on the shapes of quartz silt grains. *Journal of Sedimentary Research,* 62(6): 961-971, 970.

Müller J. (1858) - Über die Thalassicollen, Polycystinen und Acanthometren des Mittelmeeres. F. Dümmler.

O'Dogherty L. (1994) - Biochronology and paleontology of mid-Cretaceous radiolarians from northern Apennines (Italy) and Betic Cordillera (Spain). *Section des sciences de la terre, Université de Lausanne*, 1994, 413 pp.

Ozsvárt P., Bahramnejad E., Bagheri S. & Sharifi M. (2020) - New Albian (Cretaceous) radiolarian age constraints for the Dumak ophiolitic mélange from the Shuru area, Eastern Iran. *Cretaceous Research,* 111: 104451.

Parona C. (1890) - Radiolarie nei noduli selciosi del calcare giurese di Cittiglio presso Laverno. *Bollettino della Socieà Geologica Italiana*, 9: 132-175.

Pessagno E.A. (1976) - Radiolarian zonation and stratigraphy of the Upper Cretaceous portion of the Great Valley sequence, California Coast Ranges. *Micropaleontology, Spec. publ.,* 2: 1-95.

Pessagno E.A. (1977) - Lower Cretaceous radiolarian biostratigraphy of the Great Valley sequence and Franciscan complex, California coast ranges. Cushman Foundation for Foraminiferal Research, 1977, 87 pp.

Pessagno E.A., Six W.M. & Yang Q. (1989) - The Xiphostylidae Haeckel and Parvivaccidae, n. fam. (Radiolaria) from the North American Jurassic. *Micropaleontology*: 193-255.

Riedel W. (1967) - Some new families of Radiolaria. *Proceedings of the Geological Society of London*, 1640: 148-149.

Squinabol S. (1904) - Radiolarie cretacee degli Euganei. *Atti e Memorie della Reale Accademia di Scienze Lettere ed Arti in Padova*, Nuova Serie 20: 171-244.

Stoecklin J. (1968) - Structural history and tectonics of Iran: a review. *AAPG Bulletin,* 52(7): 1229-1258, 1230.

Takahashi K. & Honjo S. (1983) - Radiolarian skeletons: size, weight, sinking speed, and residence time in tropical pelagic oceans. Deep Sea Research Part A. *Oceanographic Research Papers,* 30(5): 543-568.

Vergés J., Sandra E., Casciello E., Fernandez M., Villaseñor A., Jimenez-Munt I. & García-Castellanos D. (2011) - Crustal-scale cross-sections across the NW Zagros belt: implications for the Arabian margin reconstruction. *Geological Magazine,* 148(5-6): 739-761.

Yang Q. (1993) - Taxonomic studies of Upper Jurassic (Tithonian) radiolaria from the Taman Formation, east-central Mexico. *Palaeoworld,* 3: 164.

Received: 10 September 2023 | Revised: 27 February 2024 | Accepted: 11 March 2024

DOI: 10.1111/bre.12861

Basin Research IAS EAGE WILEY

RESEARCH ARTICLE

A revised model for Neogene Zagros foreland sedimentation in the Lurestan arc based on new geochemical data

Christian A. F. Dietzel[1] | **Uwe Kirscher**[1,2] | **Christoph Berthold**[3] | **Mahmoud Reza Majidifard**[4] | **Madelaine Böhme**[1,5]

[1]Department of Geosciences, Terrestrial Paleoclimatology, Eberhard-Karls-University of Tübingen, Tübingen, Germany

[2]Earth Dynamics Research Group, The Institute for Geoscience Research (TIGeR), School of Earth and Planetary Sciences, Curtin University, Bentley, Western Australia, Australia

[3]Competence Center Archaeometry – Baden-Wuerttemberg, Eberhard-Karls-University of Tübingen, Tübingen, Germany

[4]Research Institute for Earth Sciences, Geologic Survey of Iran, Teheran, Iran

[5]Senckenberg Centre for Human Evolution and Palaeoenvironment, Tübingen, Germany

Correspondence
Christian A. F. Dietzel, Department of Geosciences, Terrestrial Paleoclimatology, Eberhard-Karls-University of Tübingen, Tübingen, Germany.
Email: christian.dietzel@uni-tuebingen.de

Abstract

The Zagros foreland basin is an important sedimentary archive for the tectonic and paleoclimatic evolution of the Zagros Mountains and the entire Neotethyan Arabia–Iran collision zone. By combining new geochemical high-resolution whole rock XRF data with clay mineralogy and soluble salt geochemistry we propose an evolution of the sedimentary environment in the Lurestan arc from the Serravallian to the early Pleistocene, closing a gap in understanding the complex exhumation history of the central Zagros mountain belt. An increase in ultramafic sedimentary input indicates a shift from provenance 1 to provenance 2 by ophiolite exhumation at ca.10 Ma in the Imbricated Zagros north of the Lurestan arc. Our data further indicates that the sedimentary environment of parts of the Lahbari Mb within the Lurestan arc represents a piedmont deposition of fine-grained alluvial fans and siltstones with aeolian contribution deposited under hyper-arid climate conditions. These represent provenance shift 3 and were likely sourced from evaporites of the underlying Gachsaran Fm and fluvial deposits of the Lower Aghajari Mb (provenance 1 and provenance 2), uplifted by the Mountain Front Flexure at around 5.6 Ma. Combining XRF whole rock data with clay mineral data refines formation conditions of the clay minerals in the foreland basin such as palygorskite, which is revealed to be authigenic in origin in the Lower Aghajari Mb. as a function of varying Mg-content due to variations of erosion of the ultramafic and mafic rocks in the Imbricate Zagros belt. Palygorskite in the Lahbari Member is likely both inherited from the Neogene Gachsaran evaporites as well as of authigenic origin.

KEYWORDS

basin evolution, palygorskite, sedimentary transport, Zagros

2 | INTRODUCTION

Sediments of the Zagros foreland basin have been studied for a long time (Alavi, 2004; Etemad-Saeed et al., 2020; Homke et al., 2004; Koshnaw et al., 2020; Najafi et al., 2021; Stoecklin, 1968; Vergés et al., 2019) as they contain important information about the Zagros orogenesis related to the collision of the Arabian and Iranian plates. Furthermore, they represent a valuable continental archive for paleoclimatic studies, which indicated a relatively dry and arid climate throughout the Miocene (Etemad-Saeed et al., 2020; Khormali et al., 2005).

In a previous paleoclimatic study, a ca. 10.2 Myr sedimentary profile in the Zagros Mountain Belt (Iran) was investigated (Böhme et al., 2021). The age of this profile is of high quality based on an extensive magnetostratigraphic study by Homke et al. (2004). The oldest sample (12.6 Ma) taken from the Gachsaran Fm was evidently of coastal origin, samples from the Aghajari Fm (12.0–5.6 Ma) were derived from fluvial origin. Samples from the Lahbari Mb were considered to be of both aeolian and fluvial provenance. In sediments of the Lahbari Mb, a sustained period of hyper-arid climate conditions was proposed between ca. 5.6 and 3.3 Ma based on soluble salt geochemistry and the observation of thick structureless silt deposits. These authors termed this interval Northern Arabian Desert climax (NADX) and pointed out that its onset is coeval with the start of the Messinian salinity crisis and Pontocaspian sea-level drop was identified as a possible driving force (Böhme et al., 2021). In a follow-up study soluble salt geochemistry and magnetic susceptibility of all of the samples of the reference profile were compared with clay mineralogy of 84 mudstone samples and micropaleontological observations (Dietzel et al., 2023). The clay fraction <2 μm revealed various amounts of smectite, illite, chlorite, palygorskite and the zeolite mineral erionite, where the Lahbari Mb showed the highest concentrations of palygorskite. The variations in clay minerals were linked to changes in soil humidity regimes and changing parent material input provenance. Herby, the ratio smectite/(illite + chlorite) proved particularly useful in the reconstruction of soil available moisture (Hashemi et al., 2013). Clay mineralogy indicated arid conditions in the Serravallian and early Tortonian, followed by semi-arid conditions in the late Tortonian. Permanent aridification seemed to be present during the middle Messinian and Zanclian and clay mineralogy was largely congruent with hyper-arid climate during the deposition of saline sediments of the Lahbari Mb between 5.6 and 3.3 Ma (Dietzel et al., 2023). Alongside requiring arid climate, the occurrence and variability of palygorskite within the sedimentary profile could be linked to changes in magnetic susceptibility, suggesting an influence of changing

Key points

1. XRF Data indicates exhumation of ophiolites in the Imbricated Zagros north of the Lurestan Arc at ca 10 Ma.
2. Mg from Ophiolite exhumation contributes to palygorskite formation in the Lower Aghajari Mb.
3. Combining XRF and clay mineral data gives new insights into the formation of the Lahbari Mb in the Lurestan arc.

of mafic input on palygorskite genesis. However, the influence of compounding factors such as the presence of detrital palygorskite, elevated levels of gypsum and the corresponding relationship to paleoclimate remained insufficiently understood. Furthermore, the information possibly hidden in the observed variations in-between Illite and chlorite remained elusive. In order to better distinguish the competing impact of changing climate factors and variation in sediment sources, whole-rock geochemical analysis using XRF of 83 mudstone samples was performed and combined with the results of the XRD analysis of clay samples and the geochemistry of highly soluble salts from previous studies (Böhme et al., 2021; Dietzel et al., 2023). The comparison of new XRF data with magnetic susceptibility, soluble salt geochemistry, and clay mineralogy aims to create a unique reference for the long-term evolution of an important continental sedimentological archive. The comparison of these proxies provides a unique opportunity to enhance the knowledge of the formation and redistribution of clay minerals like palygorskite in complex terrestrial semi-arid to hyper-arid environments. The age of the samples is well constrained as the samples were taken at georeferenced sampling points of an earlier magnetostratigraphic study by Homke et al. (2004). Böhme et al. (2021), where the sample collection is first presented, took samples at roughly the same position where magnetostratigraphic samples were positioned. The age was determined by the sample position within a certain geomagnetic polarity chron (Raffi et al., 2020) with an assumed constant sediment accumulation rate within each chron. Since the accuracy was slightly overestimated by Böhme et al. (2021), we rounded all ages to just 1 decimal place similar to Homke et al. (2004). Therefore, chronological comparison of geochemical data from the Lurestan arc to geochemical trends from other recent publications from across the Zagros (Etemad-Saeed et al., 2020; Koshnaw et al., 2017, 2020) gives further insights into sediment provenance and the tectonic evolution of the Zagros Mountain Belt in general.

3 | GEOLOGICAL AND TECTONIC DEVELOPMENT OF THE ZAGROS MOUNTAIN BELT

The NW–SE-trending Zagros mountain belt is formed by five different sub-parallel structural domains, from NE to SW: (1) the Urumieh–Dokhtar Magmatic Arc, (2) the metamorphic and magmatic Sanandaj–Sirjan Zone, (3) the Imbricate Zone (also described as High Zagros Thrust Belt or Crush Zone in Iran or Thrust zone and Nappe Zone in Iraq), (4) the Simply Folded Belt (High Folded Zone in Iraq), and (5) the Foothill zone or buried foothills covered by the Mesopotamian–Persian Gulf foreland basin (Low folded Zone in Iraq). These structural domains are separated by major thrust faults (Vergés, Sandra, et al., 2011) (Figure 1). The Sanandaj–Sirjan Zone and the Imbricate Zone are separated by the Main Zagros Fault (also described as Main Zagros Reverse Fault or Main Zagros Thrust) which is traditionally interpreted as the Neo-Tethys suture in Iran (Blanc et al., 2003; Homke et al., 2010; Le Garzic et al., 2019). Towards the Lurestan arc (also known as Pusht-e-Kuh arc) in Iran and the Kurdistan Region of Iraq (KRI) the Main Zagros Fault has been overprinted by an active dextral fault in the last 3 ca.5 Ma, referred to as the Main Recent Fault (Mohajjel & Fergusson, 2013).

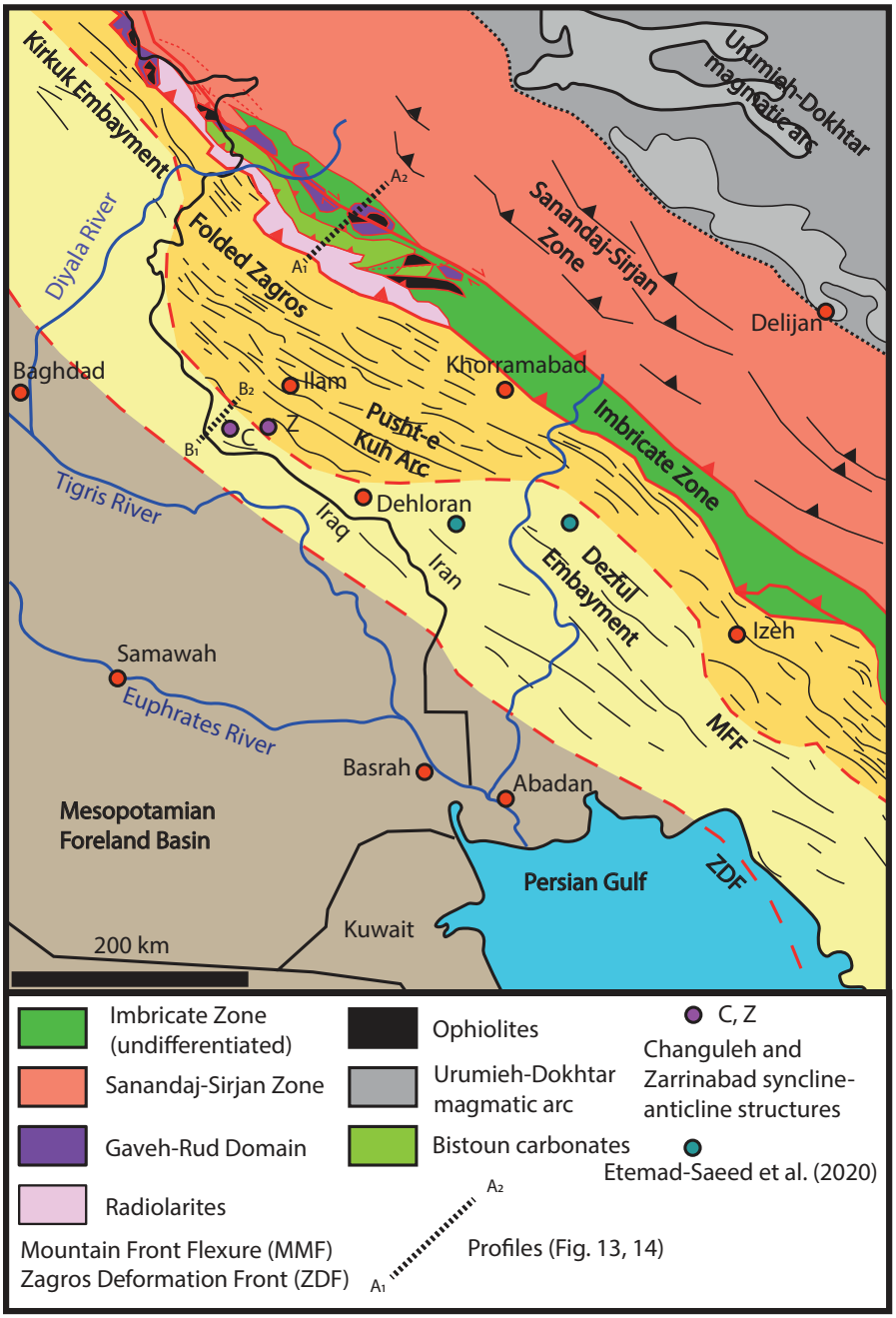

FIGURE 1 Geotectonic overview map of the northeastern Mesopotamian Foreland Basin. Map modified from Vergés, Goodarzi, et al. (2011) and Vergés, Sandra, et al. (2011) with imbricate Zagros modified from Ali et al. (2014) Rivers adapted from Un-Escwa (2013).

The Urumieh–Dokhtar magmatic belt (UDMB) forms a distinctively linear, 150 km wide active margin of the Iranian plate with Andean-type tholeiitic, calc–alkaline, and K-rich alkaline extrusive and intrusive rocks. Pre-Jurassic calc-alkaline intrusive rocks, exposed in the southeastern part of the UDMB, represent the oldest rocks in this magmatic belt. The youngest rocks of this belt are represented by Pliocene pyroclastic rocks and lava flows with alkaline and calc-alkaline composition. Volcanism in the UDMB began and peaked in the Eocene (Berberian et al., 1982; Berberian & King, 1981; Honarmand et al., 2013).

The 150–200 km wide Sanandaj–Sirjan Zone (SSZ) comprises Palaeozoic–Cretaceous sedimentary and metamorphic rocks intruded by Jurassic–Oligocene plutons (Alavi, 1994). The metamorphic rocks of the SSZ experienced greenschist to amphibolite facies metamorphism with main metamorphic episode taking place during the Late Cretaceous (Mohajjel & Fergusson, 2000). The sedimentary and metamorphic rocks of the SSZ have been intruded by numerous calc-alkaline plutons of variable composition ranging from granite to gabbro during the Jurassic and Eocene (Alavi, 1994; Baharifar et al., 2004; Berberian & King, 1981).

The Imbricate Zone is a highly deformed domain comprising multiple tectonic slices including the distal part of the Arabian margin, Cretaceous ophiolites, remains of island arcs accretionary prisms (Blanc et al., 2003; Le Garzic et al., 2019; Vergés, Sandra, et al., 2011). The Lurestan zone is generally composed of the following domains from NNE to SSW: Gaveh-Rud domain (equivalent to Walash-Naopurdan intra-oceanic island arc in Iraq), Cretaceous ophiolites, Late Triassic to middle cretaceous Bisotun-Avroman carbonates, Qulqula-Kermanshah radiolarites of Jurassic-Cretaceous age (e.g., Ali et al., 2014). The Imbricate Zone has been thrusted on top of the Simply Folded Belt in Iran and the High Folded Zone in Iraq above the High Zagros fault (HZF).

The Simply Folded Belt is characterized by a fold and thrust system involving the sedimentary cover of the Arabian Margin subducting Plate. In the Lurestan Arc of Iran, the whole sedimentary succession above the lower Ediacaran-Cambrian- Hormuz salt is affected by folding, which acts as an incompetent detachment plane (Alavi, 2007; Blanc et al., 2003; McQuarrie, 2004; Molinaro et al., 2004; Mouthereau et al., 2007; Sepehr et al., 2006; Sherkati & Letouzey, 2004; Vergés, Goodarzi, et al., 2011). The Simply Folded Zagros Belt is separated from the buried foothills by the Mountain Front Flexure (MFF), which leads to a 3 km structural relief in the Lurestan arc (Berberian, 1995; Emami et al., 2010).

The multi-stage orogeny of the Zagros mountains and associated Mesopotamian Foreland Basin started with the Campanian to Palaeocene obduction of sub-oceanic to oceanic crust above the Arabian margin. It culminated in the Neogene with the collision of the Arabian and Central Iranian blocks (Alavi, 2004; Homke et al., 2010; Saura et al., 2015) In Lurestan the obduction event involved the emplacement of the Jurassic-Cretaceous Qulqula-Kermanshah radiolarites, the Bisotun-Avroman carbonates and the Kermanshah ophiolites (Ali et al., 2014; Wrobel-Daveau et al., 2010). The obduction of ophiolites and radiolarites onto Arabian continental crust is associated with a flexure of the Arabian lithosphere leading to the formation of proto-foreland basins such as the Amiran basin in Lurestan (Homke et al., 2009). The Eocene–Oligocene volcano-sedimentary rocks of the Walash-Naopurdan terrane (Gaveh-Rud domain) developed as an intra-oceanic island-arc within the intervening Neotethys Ocean. They structurally overlie the older ophiolite mélange and radiolarite terranes as a result of continued tectonic convergence onto the margin of the Arabian Plate (Ali et al., 2014). Afterwards, the emplacement of the Sanandaj–Sirjan Zone during the latest Oligocene (Etemad-Saeed et al., 2020) led to the development of the major Mesopotamian foreland Basin as a response to crustal thickening in the hinterland. The later deformation of the foreland basin generally propagated towards the southwest (Lawa et al., 2013; Le Garzic et al., 2019; Wrobel-Daveau et al., 2010) (Figure 2).

4 | GEOLOGICAL DEVELOPMENT AND CHANGING SEDIMENT INPUT IN THE ZAGROS FORELAND BASIN

The Miocene–Pliocene clastic infill of the Zagros basin is highly variable from SW towards NE as different strata were subjected to erosion at the same time. In the *Dezful Embayment* SE of the current study area, Etemad-Saeed et al. (2020) suggested sediment sourcing mainly from igneous and metamorphic rocks derived from the tectonic unroofing of the Sanandaj–Sirjan domain during the Serravallian and early Tortonian. During the mid-Tortonian at ca. 9 Ma sediments of the Aghajari Fm in the Dezful embayment show a strong increase in radiolarite clasts and reduction in volcanic and metamorphic clasts, with coeval reduction in the ratio of incompatible over compatible elements suggesting exposure of subordinate mafic rocks in the source area derived from the exhumed Neo-Tethyan radiolarite-ophiolite allochthonous slices from the Kermanshah Complex in the High Zagros zone. Etemad-Saeed et al. (2020) also reported a further provenance shift during the Messinian ca. 7 Ma. Here an increasing contribution of carbonate clasts (up to 85%) and a decrease of radiolarian cherts (to 15%) characterize the upper Lahbari and Bakhtyari conglomerates.

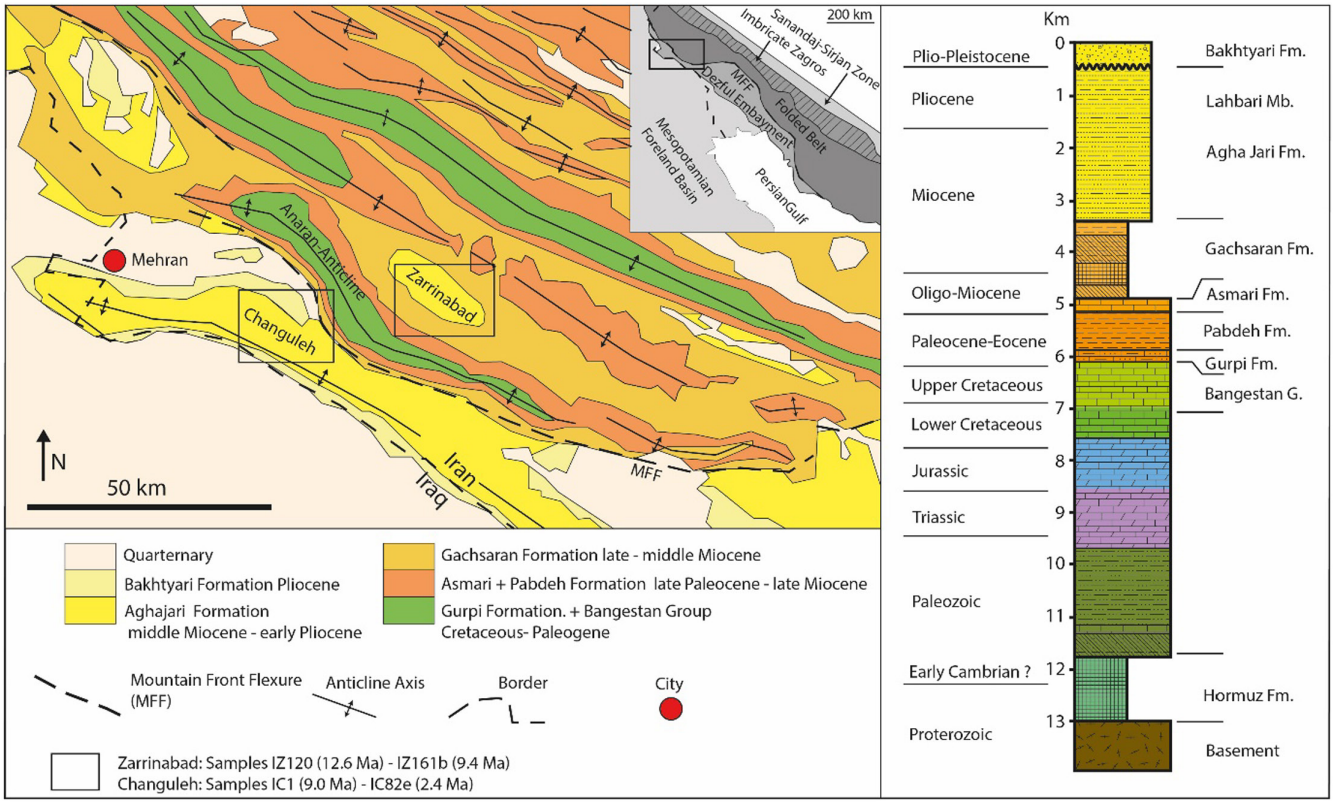

FIGURE 2 Simplified geological map of the sampling area at the Changuleh and Zarrinabad anticlines. Map modified from Homke et al. (2004), stratigraphic column after Emami et al. (2010).

The proximal carbonate clasts were sourced from large anticlines growing in the hanging wall of the Mountain Front Fault involving crystalline basement at depth. In *the Kirkuk Embayment* towards the NW of the Lurestan arc, a different provenance history was reported by Koshnaw et al. (2017) based on detrital zircon geochronology and sandstone mineralogy in foreland sediments from the Miocene to present: Between 18 and 12 Ma sediments were exclusively sourced from the exhuming volcano-sedimentary Walash-Naopurdan Group (Gaveh-Rud domain in Iran) to the NE. Between 12 and 8 Ma sediments are dominantly deposited by axial rivers from Palaeozoic rocks to the North and a lesser degree from the Walash-Naopurdan Group and ophiolites by transverse rivers from NE. Between 8 and 5 Ma sediments are exclusively sourced from the Walash-Naopurdan Group by transverse rivers. At 5 Ma, the fold-thrust belt in the Kurdistan region experienced major basement-involved thrusting, possibly out-of-sequence, that generated the MFF, which initiated gravel deposition of the Bai-Hasan Upper Bakhtyari Fm in the adjacent foreland basin. The sediment source was suggested to comprise the Walash-Naopurdan Group, ophiolites, radiolarite chert, Red Bed Series rocks and carbonate rocks by transverse rivers from the NE.

In the Lurestan arc helium fission track analysis on apatite was performed on four sediment samples from the Zarrinabad and Changuleh syncline anticline structures by Homke et al. (2010): Thereof, one sample was taken at the top of the Zarrinabad syncline sampling site in the Lower Aghajari Mb at profile metre 810 (see Figure 4). Three samples were taken at the Changuleh anticline, the oldest in the Lower Aghajari Mb. before the onset of growth strata at profile metre 840, the second at the onset of the Lahbari Mb. at profile metre 1660 and the youngest at profile metre 2320 within the Bakhtyari conglomerates. All samples display a similar dominant component with mean ages ranging from 33.7 ± 4.1 to 40.1 ± 3.9 Ma. The age distribution of the second population ranges from 61 ± 17.7 to 94.6 ± 22.9 Ma. The helium fission track ages from the Eocene group were likely representative of cooling/denudation event encompassing middle and late Eocene times, which coincides with massive volcanic and magmatic episodes of gabbroic composition in the Sanandaj–Sirjan and Gaveh-Rud domain. The Apatite Fission tracks ages of early-late Cretaceous age are likely sourced from slices scratched from the outer Arabian margin and from the obducted oceanic radiolaritic-ophiolitic complex. Emami et al. (2010) suggested that the fine-grained sediments of the Lahbari Mb could have been sourced from the softer Gachsaran and Aghajari deposits regionally uplifted above the proposed low-angle blind thrust, which generated the Lurestan Arc rise around 5.5 Ma. A strong contribution

of aeolian silts towards the Lahbari Mb from a westerly source during a sustained hyper-arid period (NADX), based on the heavy-mineral composition of 84 sediment samples and grain-size modelling has been suggested by Böhme et al. (2021) (Figure 3).

5 | GEOLOGICAL STRATA OF THE STUDY AREA IN THE LURESTAN ARC

The sedimentary samples used for this study were taken at two localities. The first section was sampled along the southern flank of the Zarrinabad syncline, located NE of the Anaran Anticline and the MFF. The second section was sampled at the Changuleh anticline-syncline pair SW of the Anaran Anticline and the MFF (Figure 2).

5.1 | Gachsaran formation

The uppermost part of the shallow marine Gachsaran Fm consists of thick well-bedded evaporites, blue to red silty-clay beds and green to brown sandstones. In the uppermost part dm-scale carbonate banks alternate with fine-grained

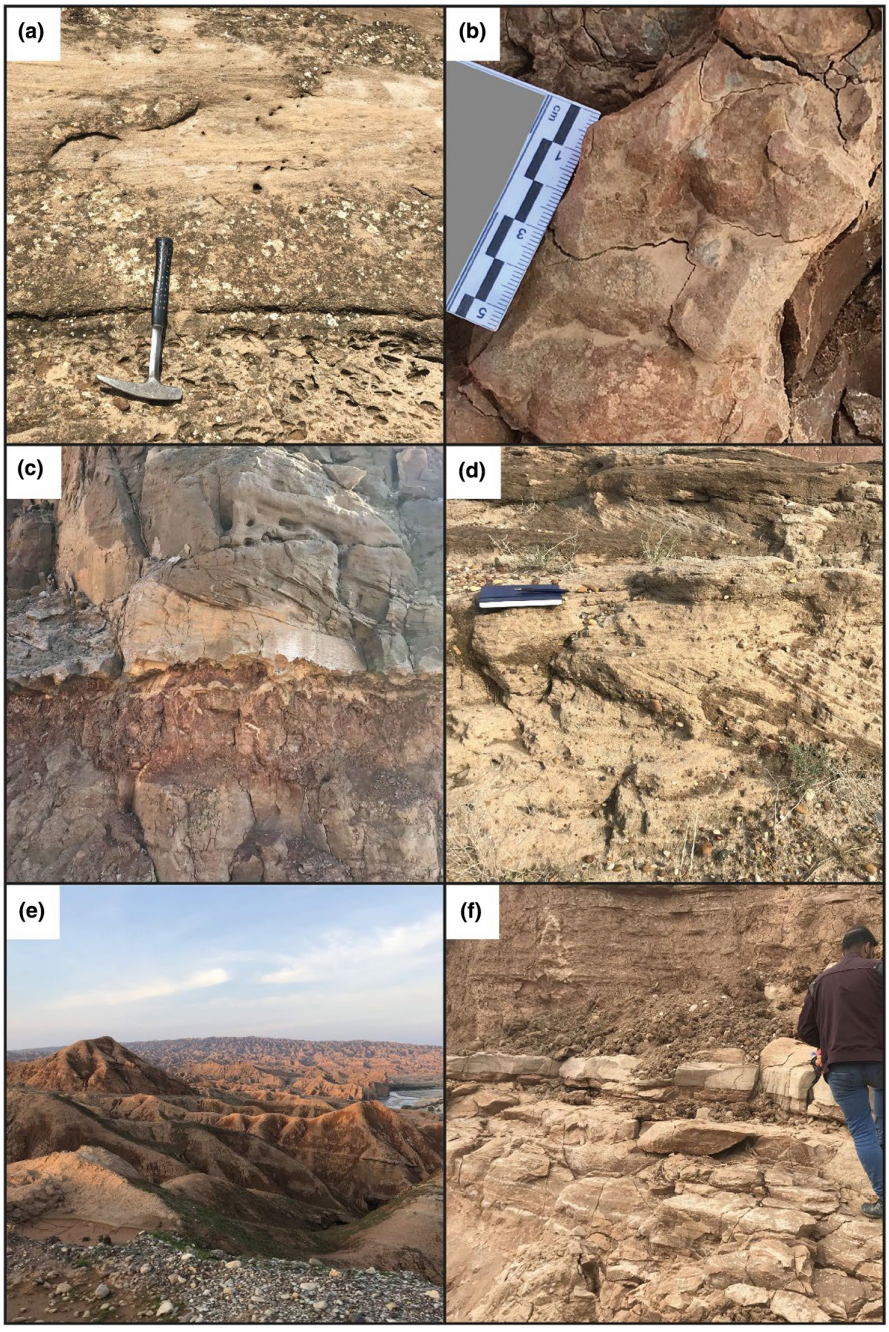

FIGURE 3 (a) Pebble-rich sandstone with softer weathered out clasts 395 m, Lower Aghajari Mb, (b) freshwater gastropod in mudstone 920 m Lower Aghajari Mb, (c) Red mudstone interpreted as overbank sediments eroded by reddish-beige fluvial sandstone channels 925 m, (d) conglomeratic sandstone with cross-bedding structures 1450 m, Lower Aghajari Mb, (e) Lower Aghajari Mb in front with transition to Lahbari Mb in the background, (f) very-fine grained sandstone bed interbedded with mudstones 2030 m Lahbari Mb.

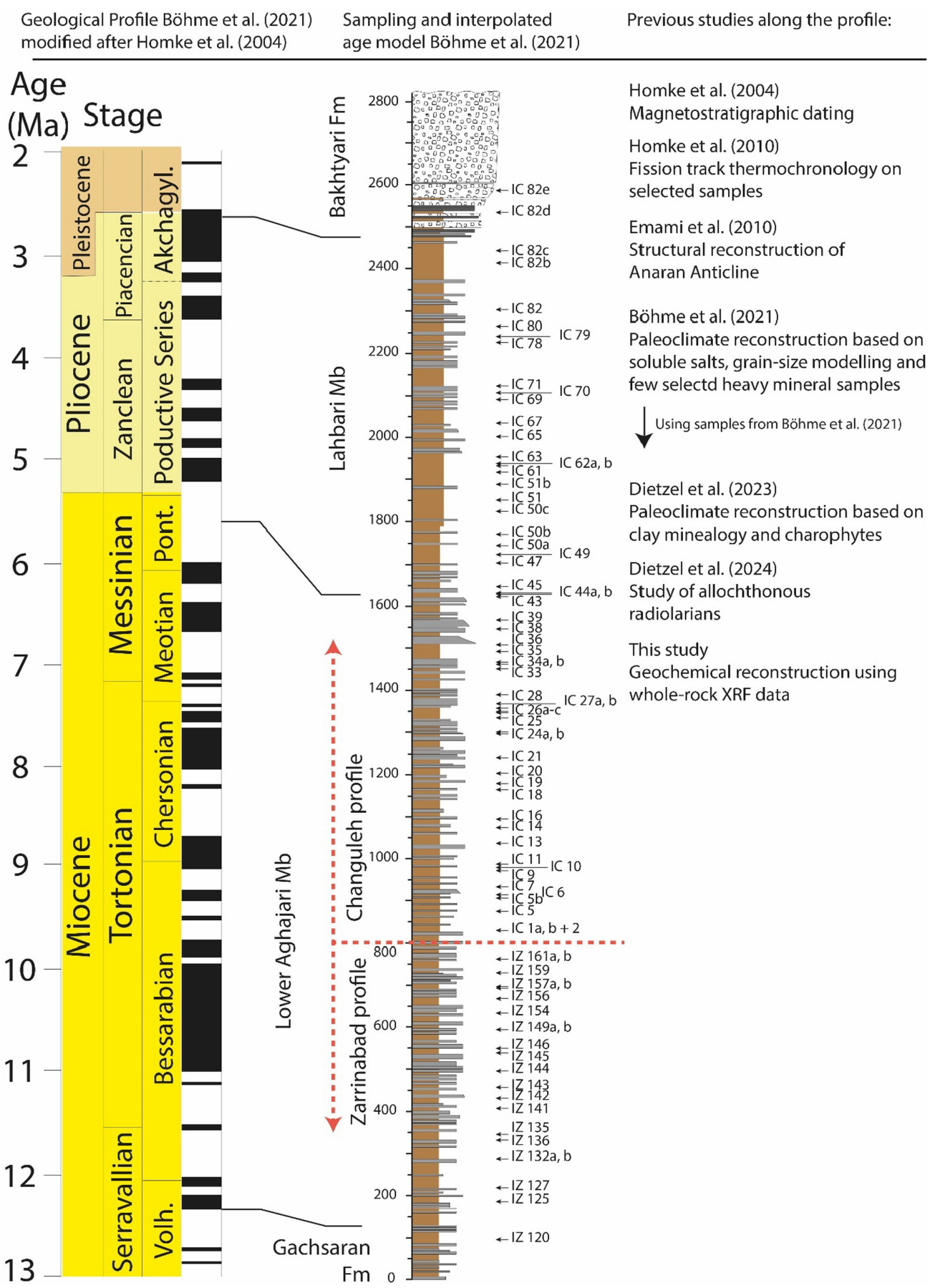

FIGURE 4 Composite sample profile along the Zarrinabad and Changuleh syncline anticline structures with sample numbers.

sandstone beds, often showing wave ripples. The mudstones are rich in pedogenic gypsum concretions and show redox mottling suggesting fluctuating sea levels with the depositional environment changing between marine shoreface and terrestrial backshore facies. While Homke et al. (2004) located the transition towards the Lahbari Mb at 12.8 Ma, Böhme et al. (2021) suggested a transition to the Lower Aghajari Mb. at 12.3 Ma based on the observation of a last bed rich in marine shells found at stratigraphic level 130 m. Salt extrusions have also been described from an unspecified likely deeper stratigraphic level of the Gachsaran Fm at the Anaran Anticline (Emami et al., 2010).

5.2 | Lower Aghajari member

The Aghajari Fm (Upper Fars Fm in Syria, Injana Fm in Iraq and Dibdiba Fm in Kuwait) represents a 2.4 km-thick depositional profile of fine-clastic to fluvial sediments, which is widely distributed in the Mesopotamian Foreland Basin dated by magnetostratigraphy in the Lurestan arc from the late Middle Miocene to the base of the Pleistocene (Homke et al., 2004). It comprises two parts: The Lower Aghajari Mb and the Lahbari Mb. The Lower Aghajari Mb is characterized by the presence of thick sandstone channels often showing cross-bedding structures as well as fine-grained mudstones (Figure 3a–c). The thickness of well-consolidated sandstone beds towards the middle of the section displays thicknesses ranging from several tens to several tens of meters, with thin layers of conglomerates at the bottom of sandstone layers appearing in the last 130 m underneath the transition to the Lahbari Mb (Figure 3d) (Homke et al., 2004). Layers of silty mudstone also frequently appear in the Lower Aghajari Mb likely representing overbank sediments. These mudstones show pedogenic carbonate and redox mottling and the infrequent presence of charophyte gyrogonites (Böhme et al., 2021).

5.3 | Lahbari member

Sandstones of the Lahbari Mb are less consolidated than those of the Lower Aghajari Mb. A large part of sandstone layers, generally thinner than 5 m, is covered by a distinct beige-coloured mud (Figure 3f). Near the top of the formation, several sandstone beds contain thin dark gravel with pebbles smaller than 5 cm (Homke et al., 2004). The mudstones of the Lahbari Mb are furthermore strongly enriched in highly soluble salts such as chlorite and nitrates (Böhme et al., 2021).

5.4 | Bakhtyari formation

The conglomerates of the Bakhtyari Fm have a characteristic rough topography which is often difficult to access. They consist of conglomerates mostly made of grey carbonatic and dark brown clasts with a varying amount of interbedded fine brown sandstones. An increase in clast size is noted towards the top of the formation (Homke et al., 2004).

6 | MATERIALS AND METHODS

The 83 mudstone samples were taken from silty horizons along the 2600 m thick combined sedimentary profile (Figure 4). Twenty-one samples from 12.6 to 9.4 Ma were taken at the Zarrinabad Anticline. The age of the samples is well constrained as the samples were taken at georeferenced sampling points of an earlier magnetostratigraphic study by Homke et al. (2004). Sixty-two samples were taken from 9.0 to 2.4 Ma at the Changuleh syncline-anticline structure. The age model and sample numbers are identical to the paleoclimatic studies of Böhme et al. (2021) and Dietzel et al. (2023), where grain size distribution, soluble salt geochemistry, magnetic susceptibility and clay mineral distribution were obtained using the same sample material as in the current study. Wherever paleo-soils were present, the B-horizon was sampled. Clay mineral distribution on glycolated and non-glycolated oriented samples was determined using A Bruker D8 advance diffractometer with a Cu-sealed tube running at 40 kV/20 mA, Göbel mirror, fixed anti-air scatter screen and a VÅNTEC1-1D-detector (Dietzel et al., 2023). In order to better understand the geochemical driving forces especially regarding palygorskite genesis 15 g of 83 mudstone samples were analysed through x-ray fluorescence (XRF) for major element oxides (SiO_2, TiO_2, Al_2O_3, Fe_2O_3, MnO, MgO, CaO, Na_2O, K_2O and P_2O_5), minor elements (Ba, Ni, Rb, Sr, V, Y, Zn. Zr) and loss on ignition (LOI). One sample (IC161, 9.4 Ma) analysed in previous studies for soluble salt and clay minerals could not be analysed for geochemistry due to a lack of sample material. Fifteen grams of each sample were dried overnight at 110°C and ground up using a zirconia ball mill to a fine powder. XRF analysis was performed at the Department of Geochemistry of the University of Tübingen. Pressed powder pellets were analysed using a Bruker AXS S4 Pioneer with a rhodium X-ray source. Fused disks were prepared, using 7.5 g Merck A12 di-lithium tetraborate/lithium metaborate (66:34) flux and 1.5 g sample. Total Fe is reported as Fe_2O_3 (LOI) was determined after heating powdered samples at 1000°C for an hour. The XRF data can be found in the supplementary information (Data S1).

7 | RESULTS

The bulk geochemistry of major and trace elements of the studied mudrock samples was normalized to Post Archean Australian Shale (PAAS) as reference for upper continental crust (McLennan, 2001) (Figure 5). As some of the sediments analysed for this study contain up to 8% of soluble halite (Böhme et al., 2021), Na_2O (silicate) was calculated by subtracting the amount of highly soluble Na^+ measured by Ion chromatography from the total Na_2O measured by XRF. For better readability the results of 83 samples were summarized in averages of several samples into five distinct groups based on sampling locality, geological formation and distinct changes in geochemistry within the Lower Aghajari Mb: (1) Gachsaran Fm 12.6 Ma (Zarrinabad Anticline) $n=1$; (2) Lower Aghajari Mb 12.0–10 Ma (Zarrinabad Anticline) $n=13$; (3) Lower Aghajari Mb 10–9.4 Ma (Zarrinabad Anticline) $n=7$; (4) Lower Aghajari Mb 9.0–5.6 Ma (Changuleh Anticline) $n=36$; (5) Lahbari Mb 5.6–2.4 Ma (Changuleh Anticline) $n=26$. While most of the mudstones in this study contain some detrital calcite and gypsum, the single sample taken from the Gachsaran Fm is a harder dolomitized marl, which did not-self disperse easily by hydration with de-ionized water during clay-mineral analysis (Dietzel et al., 2023).

7.1 | Major and minor elements

Compared to PAAS, all sample groups are depleted in SiO_2, Al_2O_3, Na_2O, Na_2O (silicate), K_2O, and P_2O_5 (Figure 5). TiO_2 and Fe_2O_3 and TiO_2 are only slightly depleted in the marl from the Gachsaran Fm and similar to PAAS in all the other sample groups. Mn is strongly enriched in the Gachsaran Fm and slightly enriched in the other sample groups. The strongest enrichment in MgO is observed in the Gachsaran Fm (dolomite), and a distinct increase in Mg enrichment is observed within the Lower Aghajari Mb (Group 2 & 3) between ca. 11 and 9.5 Ma. MgO is also enriched in the Lahbari Mb. CaO is enriched in all sample groups.

7.2 | Large Ion Lithophile elements LILE (Ba, Rb, Sr)

While Ba and Rb are depleted in all sample groups compared to PAAS (Figure 5), the highest contents for each element are found in the oldest samples of the Lower Aghajari Mb (Group 2). While Sr is depleted throughout the Gachsaran and Lower Aghajari Mb, it is enriched compared to PAAS in the Lahbari Mb.

7.3 | High field strength elements HFSE (Y, Zr)

Y and Zr are strongly depleted in the dolomitized marl of the Gachsaran Fm. The mudstone samples from the Lower Aghajari Mb show depletion in Y and Zr compared to PAAS and groups 2, 3 and 4 show a systematic decrease in Y and Zr towards younger sediment samples. The Y and Zr content in samples from the Lahbari Mb is similar to younger samples of the Lower Agah Jari Fm (group 4) (Figure 5).

7.4 | Transitional elements (Co, Cr, Ni, V, Zn)

While the more mafic transitional elements Co, Cr and Ni are all enriched throughout the sedimentary section (Figure 5), the content is lowest in the sample taken

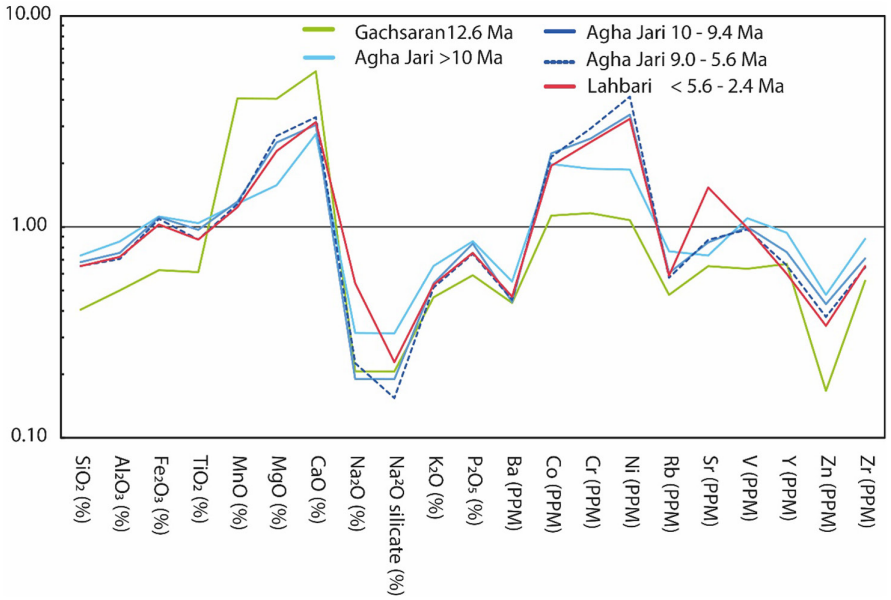

FIGURE 5 Major, minor and trace elements of geochemically distinct sample groups normalized to Post Archaean Australian Shale (PAAS, McLennan, 2001).

from the Gachsaran Fm. The enrichment in Co is similar in the samples taken throughout the Lower Aghajari Mb and the samples from the Lahbari Mb. Compared to group 2, a stronger increase is observed in Ni and Cr in the younger samples of the Aghajari Fm (groups 3 & 4) contemporaneous with Mg (Figure 6). Ni and Cr enrichment of the samples of the Lahbari Mb is in-between groups 2 and 3 of the Lower Aghajari Mb The correlation in-between Ni and MgO is higher than the correlation amongst Ni and Cr or MgO and Cr (Figure 7). While the sample from the Gachsaran Fm is depleted in V, the content of V in all other sample groups is comparable to PAAS. Zn is depleted in all sample groups with the strongest depletion in the sample from the Gachsaran Fm.

7.5 | Geochemical classification of sandstones and mudstones

The SandClass diagram $\log(SiO_2/Al_2O_3)$ versus $\log(Fe_2O_3/K_2O)$ (Herron, 1988) was used for geochemical classification of the mudstones (Figure 8). Compared to the classification scheme by Pettijohn et al. (1972) ($\log(SiO_2/Al_2O_3)$ vs. $\log(Na_2O/K_2O)$) it can discriminate a wider range of sediments and is better suited for iron-rich argillaceous sediments (Herron, 1988). Furthermore, as the sedimentary rocks analysed for this study contain up to 8% of soluble halite (Böhme et al., 2021), the SandClass scheme appears to be better suited for geochemical classification considering the unknown error in correcting total Na_2O measured by XRF for soluble Na^+ measured by Ion chromatography. All 83 mudstones analysed fell into one cluster, with 79 samples being classified as shales and two samples each being marginally classified as Fe-shale and Wacke, respectively (Figure 6). The samples from the Lahbari Mb sub-clustered in-between samples of the Lower Aghajari Mb at 12.0–10 Ma and samples from the Lower Aghajari Mb at 10–5.6 Ma (Figure 8).

8 | GEOCHEMISTRY AS INDICATOR OF SOURCE ROCKS

8.1 | Major elements

The geochemistry of major elements can be used to infer the provenance and tectonic setting of sedimentary basins (Bhatia, 1983) (Figure 9). Sandstones mainly derived from calc-alkaline andesites typically show a higher abundance of TiO_2 and Al_2O_3. Na_2O and Fe_2O_3 and a lower abundance of SiO_2 and K_2O compared to all other sandstones. Continental arc sandstones mainly derived from felsic volcanites are characterized by higher SiO_2, K_2O and K_2O/Na_2O ratios and lower Fe_2O_3+MgO than oceanic island arc sandstones. Sandstones from an active continental margin derived from uplifted continental basement have a higher SiO_2 and K_2O content reflecting the content of the upper continental crust. Sandstones derived from

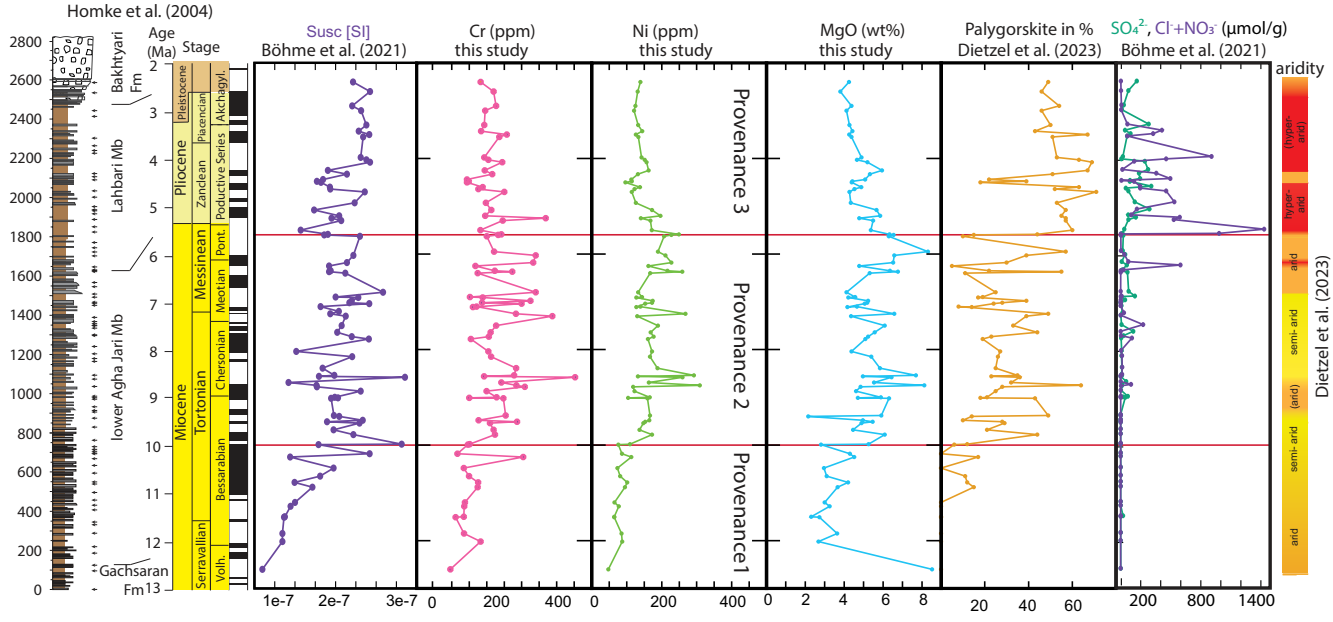

FIGURE 6 Variations of magnetic susceptibility, Cr, Ni and MgO and palygorskite content along the combined stratigraphic profile of the Zarrinabad and Changuleh synclines. Stratigraphic profile modified by Böhme et al. after Homke et al. (2004). Magnetic susceptibility and soluble salt data modified from Böhme et al. (2021), palygorskite and clay-based aridity interpretations from Dietzel et al. (2023).

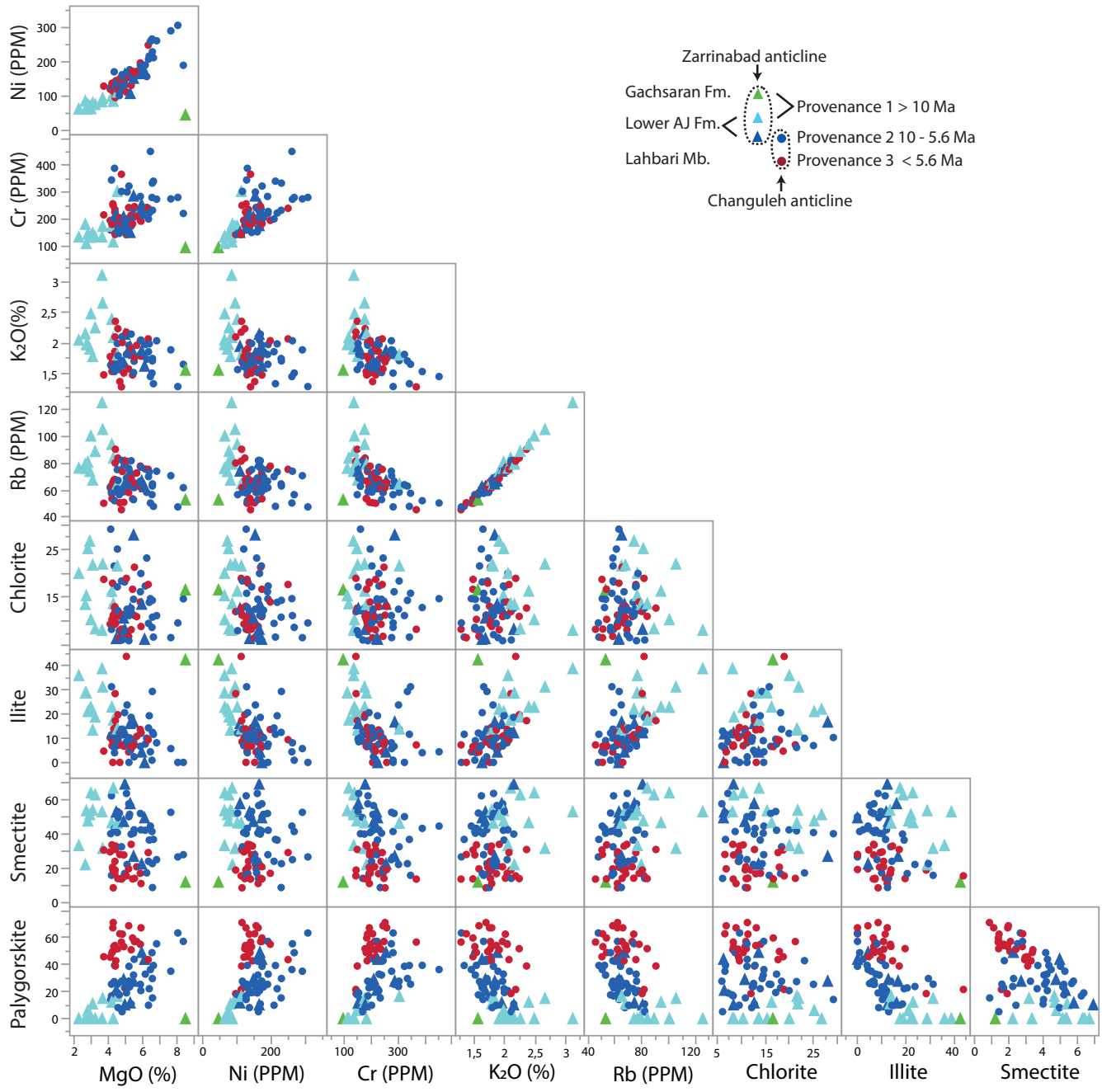

FIGURE 7 Bimodal plots of MgO, K_2O, Rb, Ni, Cr and illite, chlorite, smectite and palygorskite. Geochemical data from this study clay mineral data from Dietzel et al. (2023).

a passive margin are highly variable, but generally enriched in SiO_2 and depleted Al_2O_3, TiO_2, Na_2O and CaO (Bhatia, 1983). Apart from sandstones, systematic variations in SiO_2 content and K_2O/Na_2O are also useful in discriminating different tectonic settings in siltstones and mudstones (Roser & Korsch, 1986).

SiO_2 content and the K_2O/Na_2O ratio of all sediment samples analysed in this study are plotted within the arc suite (Figure 9A). A sediment origin primarily from oceanic island arc rocks was also suggested by Al_2O_3/SiO_2 versus Fe_2O_3+MgO plots as suggested by Bhatia (1983) (Figure 9B). Regarding TiO_2 versus Fe_2O_3+MgO plots, the samples fall outside of the suites suggested by Bhatia (1983) as they show lower TiO_2 contents compared to the reference rocks from an oceanic island arc settings or higher Fe_2O_3+MgO content than those typically derived from a continental arc (Figure 9C). While there is an overlap, sediment samples from the Lower Aghajari Mb older than 10 Ma tend to be closer to the continental island arc suite by their Fe_2O_3+MgO content than samples derived from the Lower Aghajari Mb younger than 10 Ma, with samples from the Lahbari Mb plotting in between. However, while

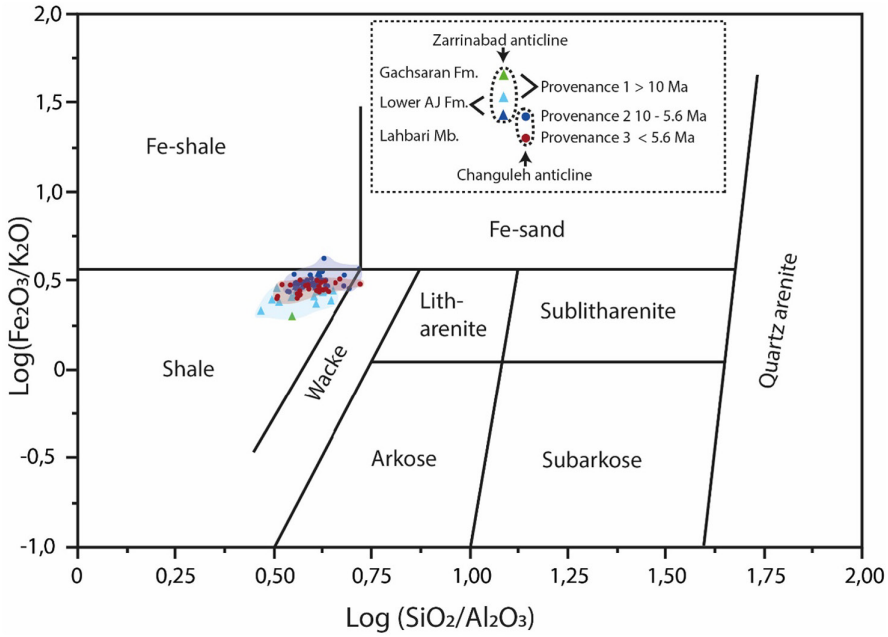

FIGURE 8 Sand Class Diagram of Samples from the Gachsaran Fm, Lower Aghajari Mb and the Lahbari Mb Classification of clastic sedimentary rocks after Herron (1988).

Fe_2O_3 + MgO is lower in the more felsic samples older than 10 Ma, TiO_2 content is higher suggesting more complex origins of TiO_2 and MgO sources than a simple derivation of calc-alkaline andesites and more felsic rocks. As all of the samples contain some detrital carbonate grains and gypsum, the total amounts of the SiO_2, TiO_2 and Fe_2O_3 + MgO, might be underestimated compared to mudstones and sandstones which do not contain any carbonate and gypsum classified by the diagrams in Figure 9. This potential problem in interpretation should not apply to element ratios. The influence of carbonate content is strongly evident in the marl-sample IZ120 from Gachsaran formation, which plots far outside of the other sample points. As the depositional environment is also highly enriched in detrital NaCl, the recalculated Na (silicate) values have a higher uncertainty.

8.2 | Trace elements as indicators for mafic and ultramafic input

The general enrichment and coherent behaviour of MgO, Ni, and Cr compared to PAAS (Figures 5–7), is suggestive of an ultramafic component in the mudstones analysed in this study (Figures 10 and 11). A mafic-ultramafic component has been derived from Mesozoic ophiolites of the Zagros foreland basin (Etemad-Saeed et al., 2020; Koshnaw et al., 2017). On a Y/Ni versus Cr/V diagram (Hiscott, 1984) ultramafic source rocks plot with low Y/Ni and high Cr/V, while felsic source rocks plot with lower Cr/V and higher Y/Ni ratios (Dinelli et al., 1999). The mudstones studied describe a nearly hyperbolic trend on such a diagram (Figure 10). Hereby a clear clustering between samples sourced from the Gachsaran Fm as well as the Lower Aghajari Mb older than 10.0 Ma and samples from the Lower Aghajari Mb deposited from 10 to 5.6 Ma is evident with a strongly enhanced input in ultramafic components towards the younger sample group. Regarding ultramafic input, the samples from the Lahbari Mb plot slightly above the samples from the Lower Aghajari Mb older than 10.0 Ma with some overlap towards the lesser enriched samples younger than 10.0 Ma.

Fine-grained shales and coarser-grained sandstones with complementary chemistries are produced by sedimentary sorting. Sorting is responsible for the systematic fractionation between relatively insoluble components such as SiO_2 (quartz) and Al_2O_3 (clays) and also between Zr (zircon) and other minor or trace elements preferentially retained in the fine-grained fraction. As igneous differentiation and sedimentary sorting trends crosscut in a ternary diagram of Zr–15Al_2O_3-300TiO_2, these diagrams have been suggested as a useful tool in understanding parent rock geochemistry as well as sedimentary sorting processes in shales and sandstones (Garcia et al., 1994). The ternary diagram originally proposed by Garcia et al. (1994) considered a typical calc-alkaline suite of granite-granodiorite-diorite-gabbro as well as peraluminous granites as parent rocks. As an ultramafic component is indicated in the studied mudstones, the ternary diagram was augmented by three metaperidotite samples from the Kermansahah ophiolite complex (Saccani et al., 2013) (Figure 11). As ultramafic rocks have generally lower total Zr, Al_2O_3 and TiO_2 contents than granites or gabbros (cf. Saccani et al., 2013; Whalen et al., 1987), an admixture of ultramafic rocks might only result in a relatively weak shift in the Zr–15Al_2O_3-300TiO_2 diagram. While there is some scatter between the sandstone and

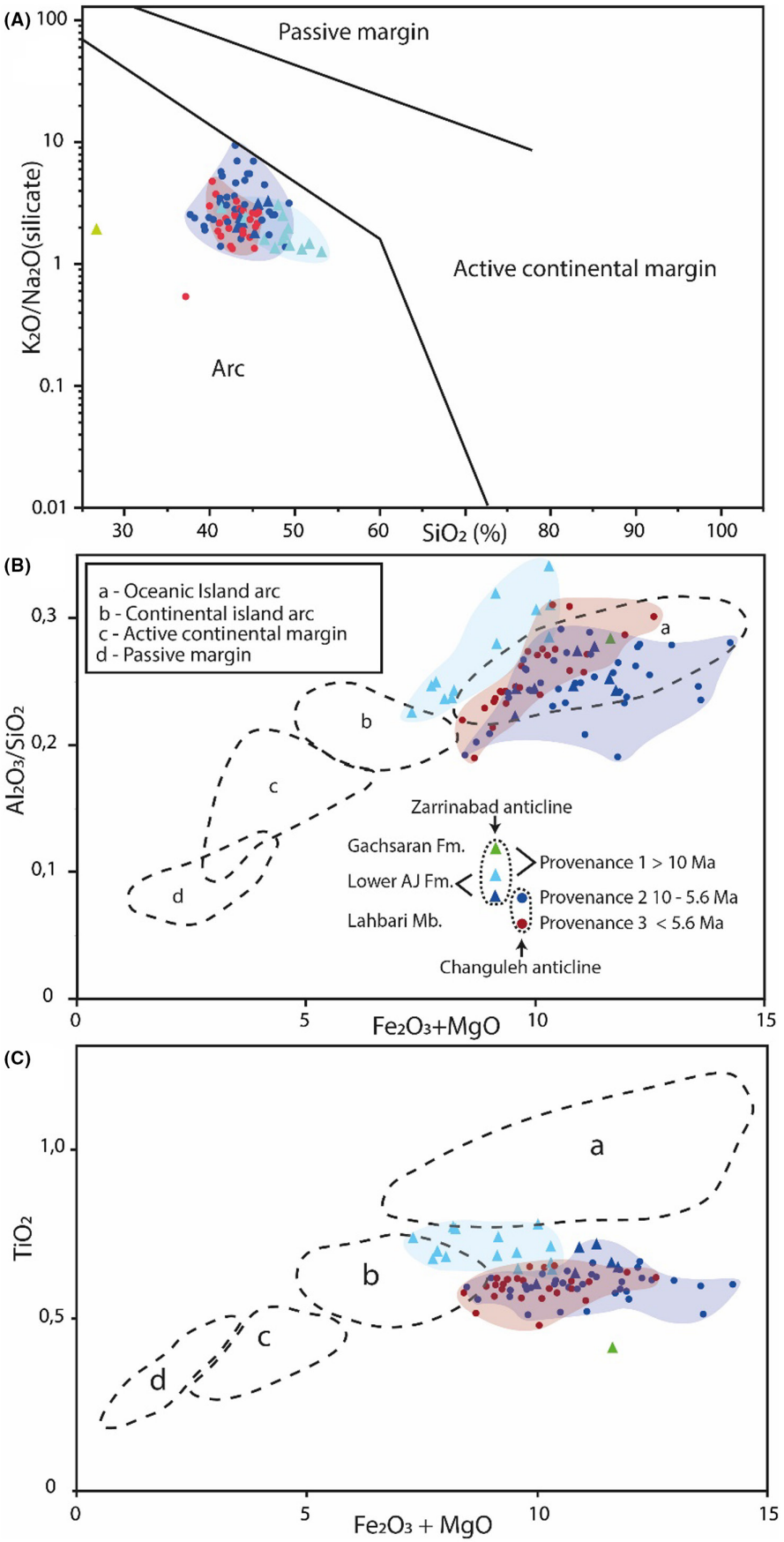

FIGURE 9 (A) Determination of tectonic provenance of sandstone-mudstone suites using SiO_2 content and K_2O/Na_2O ratio modified after Roser and Korsch (1986) for samples from Gachsaran Fm, Lower Aghajari Mb and Lahbari Mb Fields modified from Ali et al. (2017); (B) determination of tectonic provenance of sandstone-mudstone suites using Al_2O_3/SiO_2 ratio content and K_2O/Na_2O ratio modified after Bhatia (1983) for samples from the Gachsaran Fm, Lower Aghajari Mb and Lahbari Mb; (C) Determination of tectonic provenance of sandstone-mudstone suites using Al_2O_3/SiO_2 ratio content and TiO_2 content modified after Bhatia (1983) for samples from the Gachsaran Fm, the Lower Aghajari Mb and the Lahbari Mb. Sample IZ 120 (green triangle) is unreliably classified due to very high carbonate content.

shale endmembers in all sample groups, all of the mudstone samples analysed in this investigation appear to be relatively immature. Bulk geochemistry of all mudstone samples plots within an intermediate diorite composition following Garcia et al. (1994). A slight trend towards a more mafic gabbroic composition is indicated for the samples younger than 10.0 Ma (Figure 11).

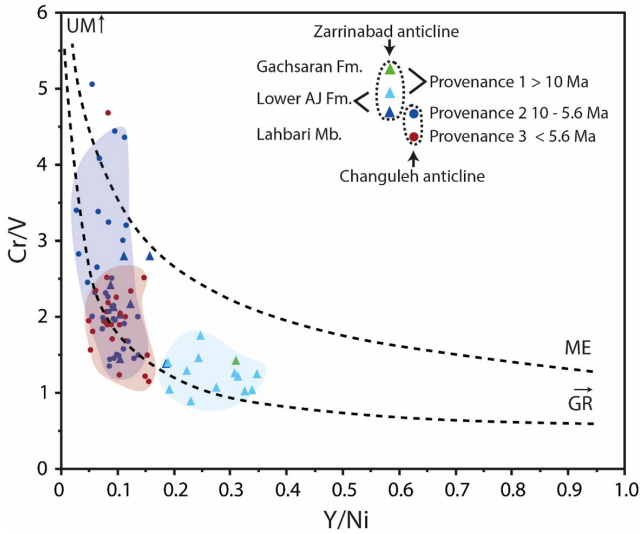

FIGURE 10 Y/Ni versus Cr/V diagram (Hiscott, 1984) as an indicator of ultramafic input for samples from the Gachsaran Fm, the Lower Aghajari Mb and the Lahbari Mb UM-ultramafic, GR-granitic, ME-metamorphic endmembers and mixing hyperboles modified from Dinelli et al. (1999).

8.3 | Multi-component analysis

A multi-component analysis of both XRF-geochemistry data and XRD data is presented in Figure 12. This analysis suggests a felsic component 1 (43.4%) and a mafic-ultramafic component 2 (18.3%). Hereby, illite shows the strongest correlation with the felsic component with smectite and chlorite also showing some correlation with the more felsic component. Palygorskite on the other hand shows a strong correlation with the mafic-ultramafic component. The samples from the Lower Aghajari Mb at 12.0–10.0 Ma cluster distinctly towards the more felsic component 1. Component 3 (11.9%) is characterized by high CaO, MnO and SrO and discriminates the dolomitized marl sample from the Gachsaran Fm Component 4 (8.16%) discriminates samples from the Lahbari Mb from the Lower Aghajari Mb. It indicates, that samples from the Lahbari Mb are distinct from the Lower Aghajari Mb by higher contents of Na_2O, Sr and Palygorskite.

8.4 | Clay mineral XRD data XRF geochemistry correlation

Illite shows a moderate positive correlation with both K_2O and Rb throughout the profile having a high correlation amongst each other (Figure 7). While there are samples with high illite content and low K_2O and Rb there are no samples with high K_2O and Rb that have high

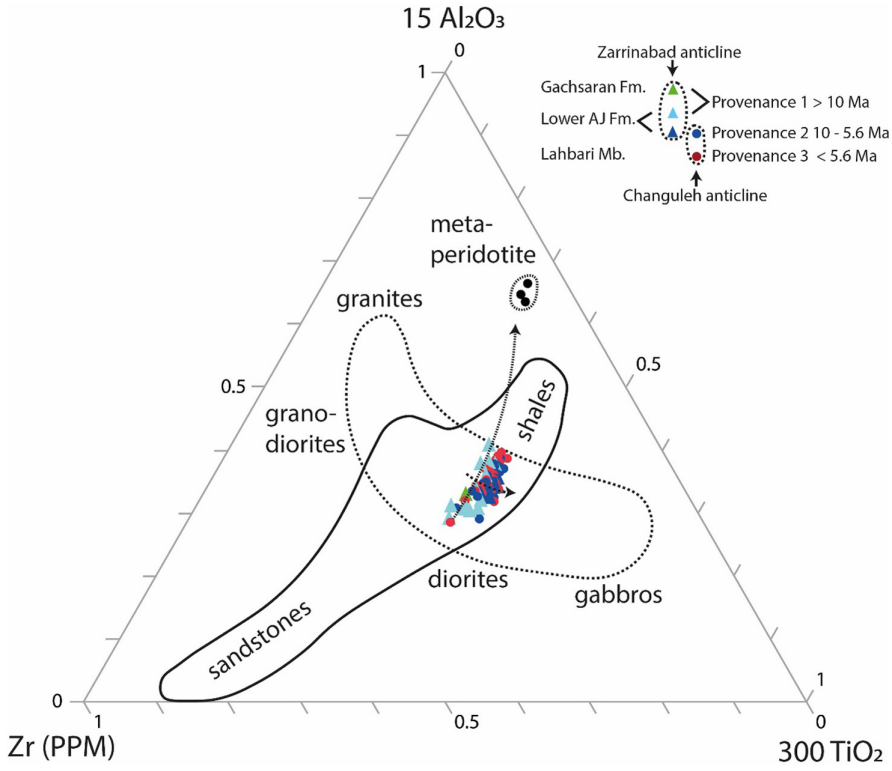

FIGURE 11 Ternary diagram of Zr–$15Al_2O_3$-$300TiO_2$ (Garcia et al., 1994), as an indicator for magmatic differentiation trends in the source area and sediment recycling processes of sandstones and associated shales for samples from the Gachsaran Fm, the Lower Aghajari Mb and the Lahbari Mb. Meta-peridotite data from the Kershmanshah ophiolite is shown as additional reference from Saccani et al. (2013) Coarse dotted arrow represents the increased input of mafic components in provencance 2 compared to provenance 1. Fine dotted arrow indicates potential mixing line of additional ultramafic material which however is limited due to low total Zr, TiO_2 and Al_2O_3 content in ultramafic rocks.

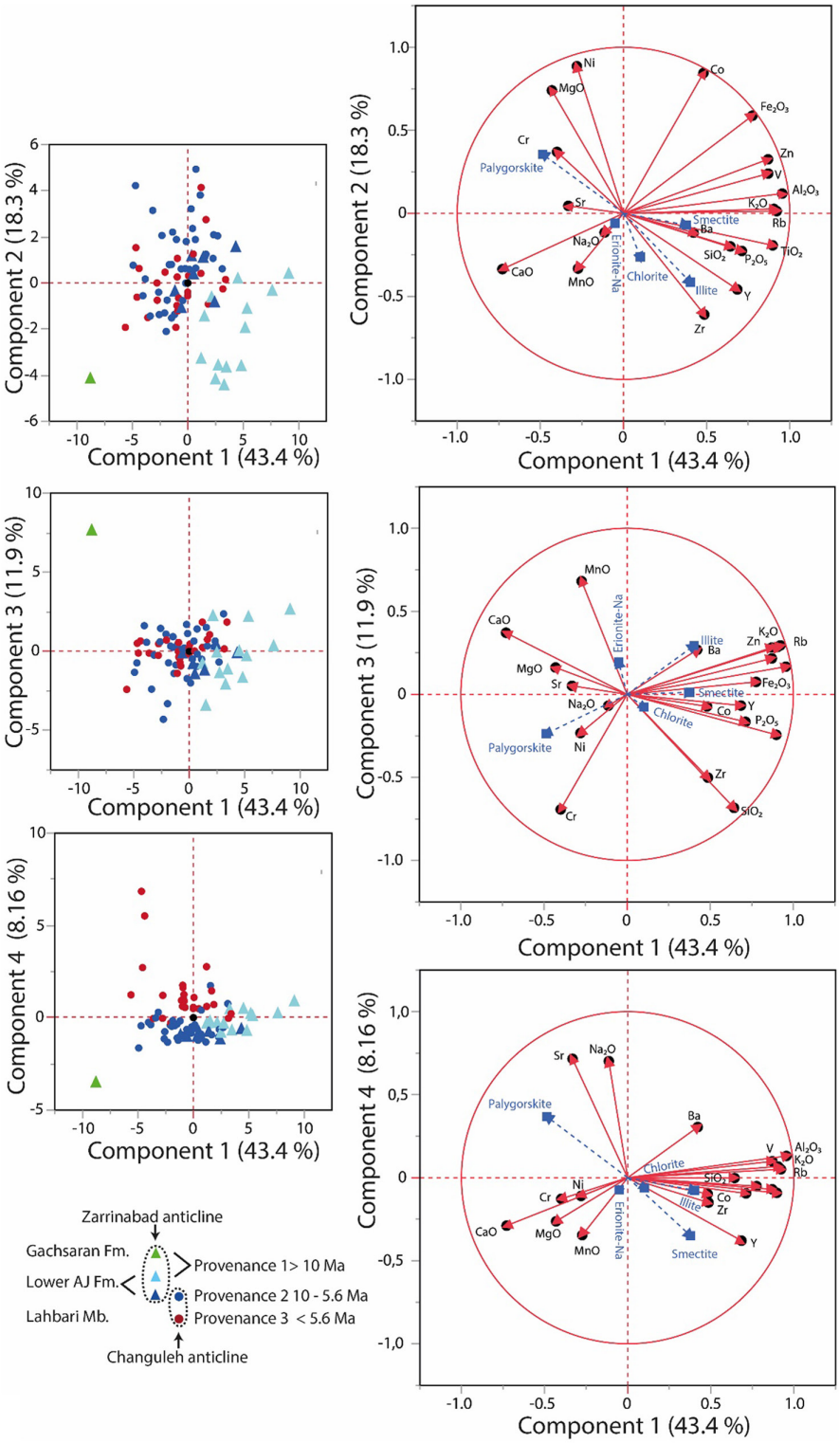

FIGURE 12 Principal component analysis using XRF data of bulk rock samples from the Gachsaran Fm, the Lower Aghajari Mb and the Lahbari Mb and XRD data of clay minerals. Major element oxides in wt% trace elements in ppm. clay minerals in % of clay fraction taken from Dietzel et al. (2023).

concentrations of illite. Smectite and chlorite do not demonstrate strong correlations with the individual elements analysed by XRF. Palygorskite in the Lower Aghajari Mb shows a strong positive correlation with MgO as well as Ni. The samples from the Lahbari Mb cluster distinctly outside of this trend with generally higher palygorskite contents but only intermediate Mg and Ni contents (Figure 7).

9 | DISCUSSION

9.1 | Shifts in sediment provenance in the lower Agha Jari Formation (Provenance 1, Provenance 2)

Whole rock geochemistry of the marls from the uppermost Gachsaran Fm and from the mudstones of the

Lower Aghajari Mb until 10.0 Ma (Provenance 1) reveal the lowest enrichment in compatible elements such as Mg, Co, Ni and Cr of all studied sample groups, with the lowest admixture from an ultramafic source. On a Zr–$15Al_2O_3$-$300TiO_2$ diagram, an overall integrated composition is geochemically similar to an intermediate diorite. Based on SiO_2 content and K_2O/Na_2O the samples are derived from an arc setting with TiO_2 versus $Fe_2O_3 + MgO$ indicating a composition in between an oceanic and continental arc. Al_2O_3/SiO_2 versus $Fe_2O_3 + MgO$ plots indicate an Al_2O_3/SiO_2 ratio slightly higher than in reference samples derived from an oceanic island arc. While erosional material derived from the Sanandaj–Sirjan domain falls within the continental arc suite on geochemical plots (Etemad-Saeed et al., 2020), clastic material from the Gaveh Rud domain (Walash-Naopurdan group of igneous rocks) gives a more mafic back arc and oceanic arc signature (Ali et al., 2017). Overall, the geochemical composition in this study of the foreland sediments between 12.6 and 10 Ma in the Lurestan arc is more mafic compared to contemporaneous sediments from the Dezful Embayment to the SE (Etemad-Saeed et al., 2020), where the mafic oceanic island arc rocks of Gave Rud domain are absent in the catchment and where its provenance likely represents a mixture of both Sanandaj–Sirjan and ultramafic ophiolite material. High Ca enrichment in this study likely indicates the reworking of carbonates from the Biotun domain. The occasional presence of Mesozoic Radiolarians furthermore indicates an admixture of eroded Kermanshah-Qulqula radiolarites (Dietzel et al, 2024). A strong contribution of metamorphic rocks as well as more felsic rocks from the Sanandaj–Sirjan domain is also supported by relatively high amounts of detrital garnet (Böhme et al., 2021) and relatively high detrital illite contents (Dietzel et al., 2023) with comparatively low detrital chlorite. A shift in provenance towards a more ultramafic-mafic source gradually starting at ca. 11 Ma culminates at ca. 10 Ma (Provenance 2) (Figure 13), where a strong increase in Ni, Cr and Mg and magnetic susceptibility can be recognized. This material is likely derived from increased tectonic obduction of ultramafic and rocks of the Cretaceous Kersmanshah-Ophiolites as indicated by helium fission-track ages (Homke et al., 2010). This increase in an ultramafic component is also complemented by an increase in the number of reworked radiolarians per sample suggesting the tectonic emplacement of the Kersmanshah-Qulqula radiolarites (Dietzel et al., 2024). Interestingly only a weak increase in a mafic component (e.g. gabbros) compared to the ultramafic component is suggested by the Zr–$15Al_2O_3$-$300TiO_2$ diagram. This shift towards an ultramafic-mafic component derived from ophiolite exhumation observed in the Zarrinabad samples is stronger and occurs about 1 Myr earlier than the shift towards a mafic-ultramafic component observed in the Dezful Embayment to SEE at ca. 9 Ma (Etemad-Saeed et al., 2020) and ca. 2 Myr later than in the Kirkuk Embayment (Koshnaw et al., 2017) in the North and might help constrain the propagation of uplift in the Imbricate Zagros from NW towards SE. This observation also highlights the importance of radial sedimentary transport from the Imbricate Zagros towards the NE even so main flow directions are indicative of an axial transport towards measured in the Lower Aghajari Mb of the Lurestan arc point towards SE parallel to the modern Tigris (Homke et al., 2004; Vergés, 2007).

9.2 | Formation of the Lahbari Member (Provenance 3)

The next major shift in sediment provenance (Provenance 3, Figure 14) is indicated by a strong increase in Sr, palygorskite, sulphate, highly soluble salts (Na_2O) and silt-sized grain fraction at the onset of the Lahbari Mb (cf. Böhme et al., 2021). Regarding major, minor and trace element distributions, sediments from the Lahbari Member cluster in between provenance 1 and 2. Similar to the Lower Aghajari Mb, apatite Fission tracks in one sample at the onset of the Lahbari Member record cooling ages congruent with input from the Sanandaj–Sirjan and Gaveh Rud domains as well as Cretaceous ophiolites (Homke et al., 2004). While the Lahbari Mb is characterized by fine-grained deposits of braided river systems in other parts of the Zagros like in the Dezful Embayment to the SE of the Lurestan arc (Jalilian, 2016), the Lahbari member at the Lurestan arc shows distinct differences and the interpretation of its sedimentology has been subject to debate. Homke et al. (2004) suggested a flat relief during the deposition of the Lahbari Mb based on the finer grain size of the Lahbari Mb contrasting to the deposition of the Lower Aghajari Mb. Modelling by Emami et al. (2010) however suggests a strong relief between the Changuleh Syncline and the adjacent Anaran anticline at 5.5 Ma along a proposed low-angle blind thrust, generating the Lurestan Arc rise around 5.5 Ma, which leads to a reworking exposed softer sediments of the Gachsaran Fm and Agha Jari Fm. Böhme et al. (2021) suggested atmospheric salt deposition and the formation of aeolian silts due to strong aeolian contribution from the western Mesopotamian plains based on grain-size end-member modelling and heavy mineral associations, during a phase of hyper-arid climate inferred from the geochemistry of highly soluble salts.

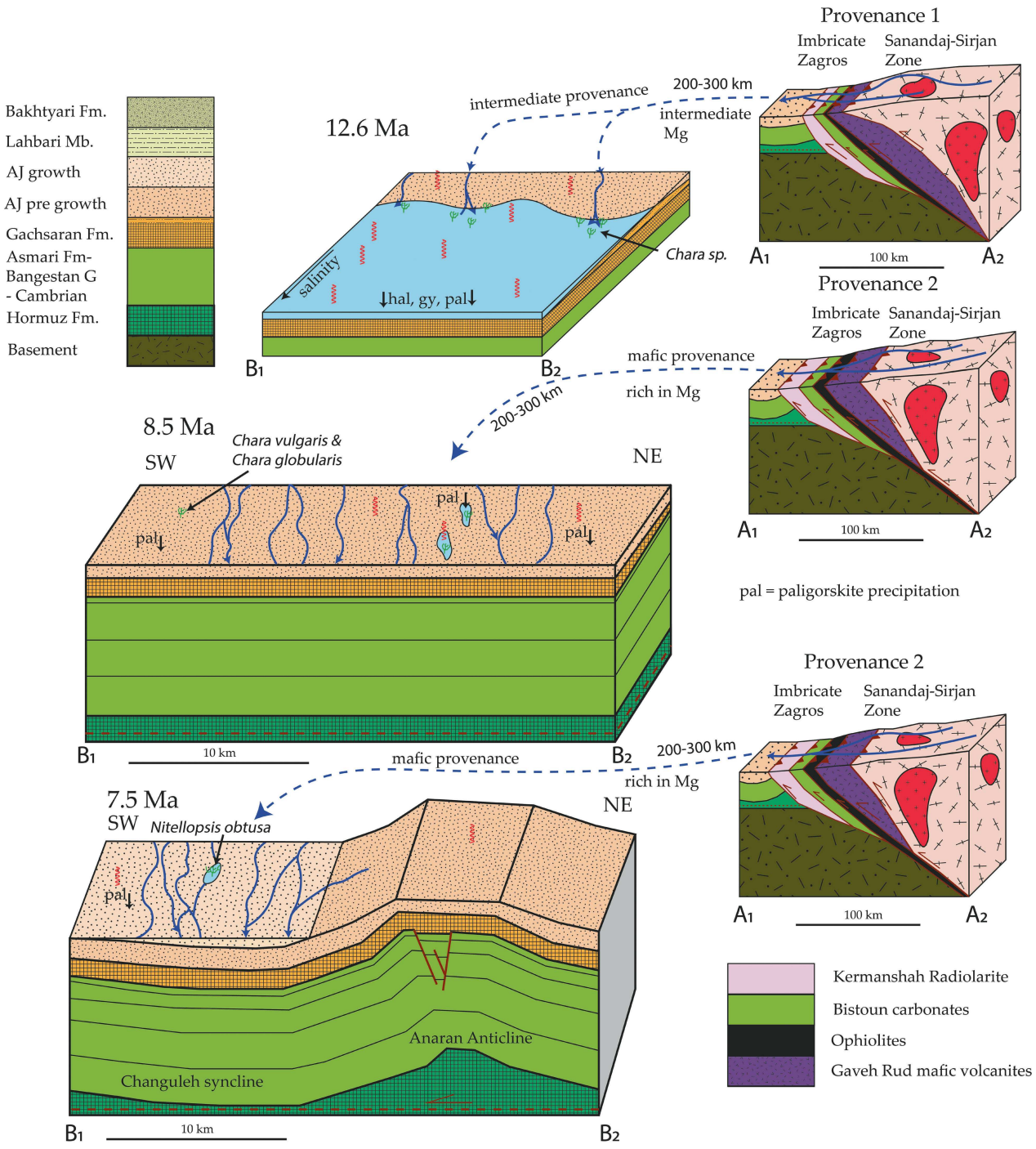

FIGURE 13 Proposed tectonic and sedimentological evolution of the central Imbricate Zagros NE of the Pusth-e-Kuh arc as source area (right) and the Changuleh-Anaran syncline anticline structure as sink area (left) during the Serravallian and Tortonian. General Changuleh-Anaran syncline-anticline structure evolution modified after Emami et al. (2010), geological cross-section of the Imbricate Zagros modified after Ali et al. (2014). Micropaleontology from Dietzel et al. (2023).

9.3 | Interaction of regional tectonic uplift and aridification in the Lahbari Member

A deposition of the Lahbari Mb by primarily fluvial processes reworking sediments of the Gachsaran evaporites and Aghajari clastics exposed at the Anaran anticline does not seem feasible as distinct channel deposits showing structures such as cross-bedding are absent and due to the preservation of very high amounts of chlorite and nitrate. A transport by alluvial fans originating at exposed Gachsaran evaporites and Aghajari deposits towards the Anran anticline located ca. 10 km to the NE represents an alternative option, which

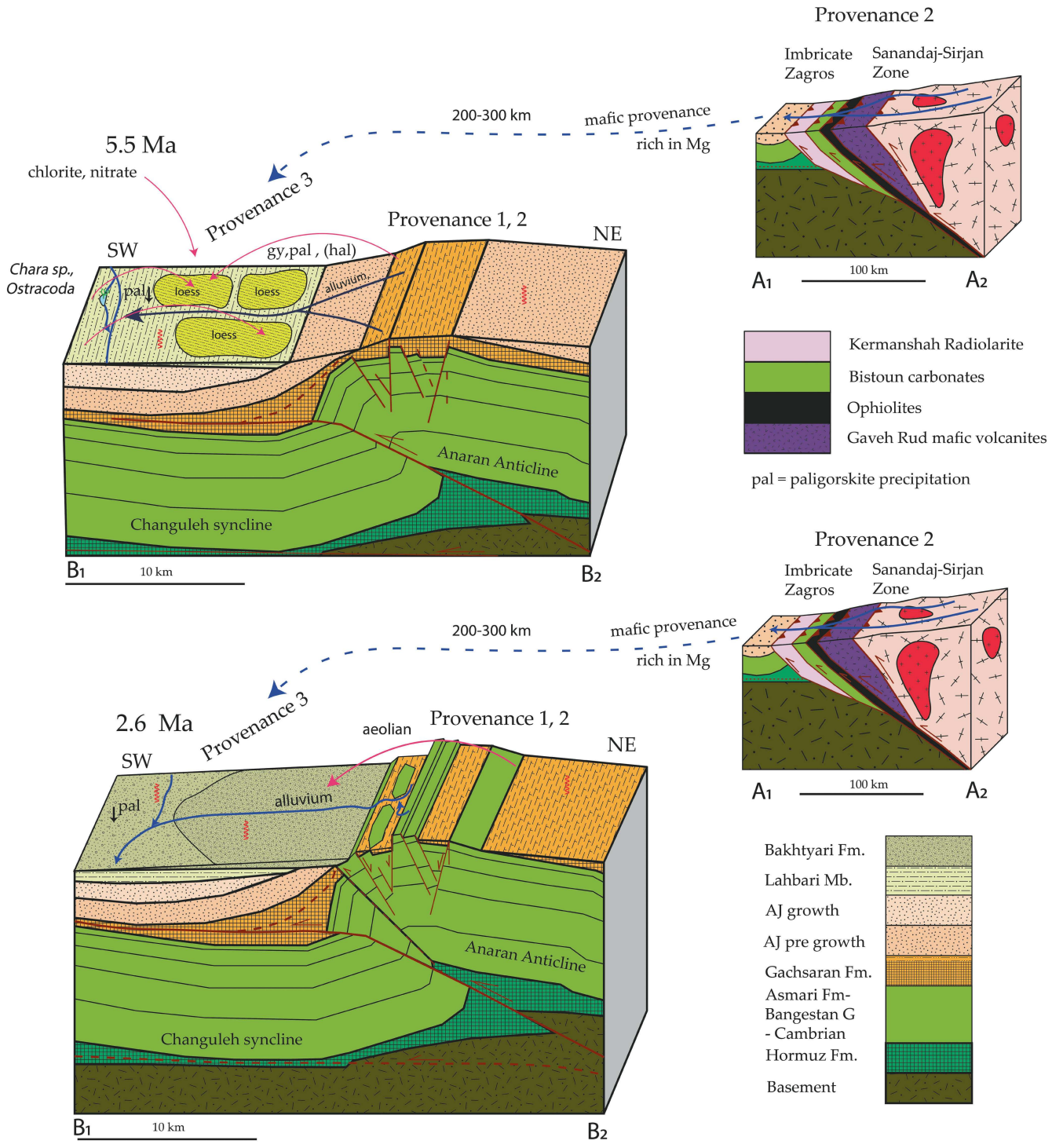

FIGURE 14 Proposed tectonic and sedimentological evolution of the central Imbricate Zagros NE of the Lurestan arc as source area (right) and the Changuleh-Anaran syncline anticline structure as sink area (left) during the Messinian and Pliocene. General Changuleh-Anaran syncline-anticline structure evolution modified after Emami et al. (2010), geological cross-section of the Imbricate Zagros modified after Ali et al. (2014). Micropaleontology from Dietzel et al. (2023).

could explain the composition and immature sorting of sediments as indicated by geochemistry. Alluvial fans have been shown to transport material derived from evaporites such as salt glaciers both as clasts as well as saturated salt brines in arid environments (Bruthans et al., 2009). They can also preserve high amounts of gypsum, chlorides and nitrates in hyper-arid environments where atmospheric and aeolian deposition can in addition lead to a further enrichment of highly soluble salts (Berger & Cooke, 1997). The deposition of vast sheeth-like sandstones with limited thicknesses and without distinct crossbedding likely represents distal alluvial fans derived from soft Aghajari and Gachsaran sediments

from the Anaran anticline deposited in the bajada environment of the mountain Front Flexure. The thick silty structureless siltstones in-between the sandstone sheaths of the Lahbari Mb are well sorted containing no larger sediment clasts probably representing peri-desert loess deposited in the piedmont of the Anaran anticline of the growing Zagros fold belt (cf. Li et al., 2020). The silt was hereby sourced locally from the above-mentioned fine-grained alluvial fans originating from the erosion of the Anaran anticline as well as from fine-grained fluvial sediments of the Mesopotamian foreland basin. A short aeolian transport distance is indicated by their geochemical composition resembling a mixture of the local Gachsaran and Aghajari sediments as well as the angular grain structure of individual quartz grains. While the heavy mineral signature at 5.5 Ma regarding garnet + tourmaline + mica – amphibol + epidote-pyroxene shows similarities to recent Euphrates signatures (Böhme et al., 2021), it is also compatible with a sediment origin from the Sanandaj–Sirjan and Gaveh Rud domains as well as Cretaceous Ophiolites as suggested by geochemical data. The presence of celestite has previously been interpreted as authigenic formation within the aeolian sediments (Böhme et al., 2021). The high amounts of strontium and celestite in the Lahbari Mb could however also point to recycled material from the Gachsaran Fm (Ehya et al., 2013). Regarding the separation of heavy minerals during aeolian transport, studies on recent dune fields in southern Iraq suggest a similar overall association of heavy minerals in these aeolian dune fields compared with local sediments of the Lower Mesopotamian Plain, acting as source of aeolian clastics sediments (Skoček & Saadallah, 1972). The high amounts of chloride can however only insufficiently be explained by the pure reworking of locally exposed Gachsaran evaporites. While a not closer defined salt extrusion at the Anaran Anticline was reported by Emami et al. (2010) the Lurestan sub-basin of the Gachsaran formation is generally lacking halite deposits (Bahroudi & Koyi, 2004), rendering the local Gachsaran deposits problematic as an exclusive source for the highly soluble salts observed in the Lahbari Mb. Furthermore, nitrate is unlikely to be derived from Gachsaran formation, as marine salt deposits are usually poor in nitrate, which is commonly derived from the atmosphere (Böhme et al., 2021). The concentration of both nitrate and chlorite suddenly increases at the onset of the Lahbari Mb at 5.6 Ma, while an increase in sulphate is only noted after a delay of ca. 0.3 Ma at 5.3 Ma. This supports the additional deposition of atmospheric nitrate and chlorite during a rapid superimposed shift from arid towards hyperarid climate conditions contemporaneous to the tectonic exhumation of the Gachsaran Fm at the onset of stage 2 of the Messinian Dessication (Böhme et al., 2021). As the top of the Gachsaran Fm comprises gypsic marls rather than halite, erosion and redeposition of gypsum should be expected to cause a moderate increase in sulphate rather than halite in the case of local sourcing. The sediments of the Lahbari Mb (provenance 3) thus likely comprise a mixture material of the Gachsaran Fm and Lower Aghahari Fm (provenances 1 and 2) reworked by a complex interplay of alluvial and aeolian processes in the piedmont of the rising MFF. Herby apart from tectonics, contemporaneous aridification likely contributed to the formation of the Lahbari Mb by the additional deposition of atmospheric chlorite and nitrate. If the aeolian silts were however mobilized by Shamal winds from the northwestern Mesopotamian Basin as suggested by the model of Böhme et al. (2021), the geochemical composition of provenance 3 indicates a widespread extend of comparable reworked Gachsaran and Aghajari Material in the Mesopotamian Basin. A short intermittent interval of primarily fluvial sediment deposition might be present between 4.5 and 4.3 Ma, where clay mineralogy and geochemistry are similar to those found in the Lower Aghajari Mb (provenance 2) and the soluble salt content is rather low. A clear transition to a depositional environment dominated by coarse-grained alluvial fans is visible at the transition towards the conglomeratic Bakhtyari Fm at 2.5 Ma. This transition is probably reflective of a steepening relief in front of the MFF and the erosion of more competent strata from a deeper stratigraphic level in the Anaran Anticline (Emami et al., 2010).

9.4 | Impact of shifting mafic input onto palygorskite genesis

Palygorskite can be formed under semi-arid or arid climate conditions and is known for its fibrous morphology (Singer, 1989). The formation of palygorskite is controlled by alkaline fluids with high Mg and Si activities (Singer, 1980, 1989) and its authigenic formation by chemical sedimentation has been reported from evaporative soils, shallow lakes and saline lagoons, but also in open oceans by hydrothermal alteration of basaltic glass or volcanogenic sediments (Al-Juboury, 2009; Callen, 1984; Chamley, 1989; Millot, 1970; Singer, 1979). In semi-arid regions, palygorskite is often associated with pedogenic carbonates (Al-Juboury, 2009). Palygorskite formation might be enhanced by the formation of pedogenic gypsum due to an increase in Mg activity by preferential uptake of Ca from solution (Hashemi et al., 2013; Khormali & Abtahi, 2003). Shallow lakes and intra-montane lagoons in the post-Neotethyan realm (Oligocene-Miocene) provided a suitable evaporative environment for extensive palygorskite formation in central and

southern Iran (Khademi & Mermut, 1998; Khormali et al., 2005) and Iraq (Al-Juboury, 2009). While a previous study by Dietzel et al. (2023) revealed large amounts of palygorskite in the Zagros foreland sediments formed under a semi-arid to hyper-arid climate, the mechanism of palygorskite formation remained elusive due to a lack of high-resolution geochemical data. XRF data now shows, that the content of palygorskite in the fluvial deposits of the Lower Aghajari Mb shows a roughly linear correlation with Mg content (Figure 7). Mg and Cr contents in the sediments are also closely correlated, which is indicative of the amount of mafic minerals such as olivine, pyroxene or amphibole from mafic volcano-clastic rocks of the Gaveh Rud domain or Cretaceous ultramafic ophiolites. The lack of palygorskite in samples older than 10.9 Ma can therefore probably be explained by insufficient magnesium for palygorskite genesis, while arid conditions were generally suitable for palygorskite formation. The increase in a mafic component was previously only suspected based on magnetic susceptibility trends (Dietzel et al., 2023). While the dolomitic marl sample of the Gachsaran Fm is very rich in Mg, interestingly no palygorskite is formed. As the sample is very low in Cr and Ni it can be inferred that the enrichment in Mg is secondary due to dolomitization in a marginal marine environment and original magnesium contents did not allow for palygorskite genesis in estuary facies that had plenty of freshwater supply by rivers. Palygorskite in older strata of the Gachsaran Fm have likely been formed in a sabkha and shallow lagoon facies further away from the coastline with higher Mg activities in the water due to evaporation (Al-Juboury, 2009). Unlike in samples of the Lower Aghajari Mb, palygorskite does not show a strong correlation with Mg content in the Lahbari Mb. Here it is probably both of authighenic origin within the gypsum-bearing sediments as well as inherited from reworked evaporative sediments of the Gachsaran Fm. It did not significantly transform to smectite in highly arid conditions with high Mg activities during reworking.

9.5 | Changes in provenance as evidenced in illite and chlorite

Whilst the oldest samples (provenance 1) are richest in illite, a steady reduction of illite compared to chlorite can be observed during the shift to provenance 2. This is congruent with a shift away from micaceous schists and calc-alkaline rocks of the Sanandaj–Sirjan zone towards the chlorite-rich volcanoclastic sediments of the Gaveh Gud domain. (cf. Ali et al., 2017).

9.6 | Correlation of K_2O and Rb in Illite

Illite shows a moderate correlation with both K_2O and Rb, which have a high correlation with each other (Figure 7). While there are samples with high illite content and low K_2O and Rb there are no samples with high K_2O and Rb that have high concentrations of illite. It is therefore likely that almost all of the K_2O and Rb measured in the samples is incorporated into illite as its concentration presents an upper boundary for K_2O and Rb. This is an opposite trend as observed for MgO and palygorskite, where the presence of palygorskite seems to be limited by the presence of MgO.

10 | CONCLUSION

10.1 | Provenance shift in the Mid Tortonian

Geochemical data indicates increased ophiolite exhumation during the Mid-Tortonian in the Imbricated Zagros by a strong increase in mafic and ultramafic elements such as Mg, Cr and Ni fluvial sediments of the Lurestan Arc at around ca. 10 Ma. This shift has previously been noted at ca. 12 Ma in the Kirkuk embayment to the North and at ca. 9 Ma in the Dezful Embayment in the south (Koshnaw et al., 2017; Etemad-Saeed et al. 2020), which helps to constrain the advance of deformation in the Imbricate Zagros from NW to SE.

10.2 | Provenance shift and changed depositional environment during the early Messinian

The Lahbari Mb in the Lurestan arc likely represents a piedmont depositional environment with alternating deposition of fine-grained alluvial sandstones and siltstones with aeolian contribution. Whole rock geochemistry is congruent with a local sourcing of sediments from both from previously deposited Gachsaran evaporites and fluvial Lower Aghajari sediments tectonically recycled by the uplifting mountain front flexure (e.g. Emami et al., 2010). The onset of the Lahbari Mb at ca. 5.6 Ma also witnesses a superimposed shift from arid towards hyper-arid climate conditions with the additional deposition of atmospheric nitrates and chlorite (e.g. Böhme et al., 2021).

10.3 | Comparison of new XRF data with previously published clay mineral data

Correlation of previously published clay mineral data (Dietzel et al., 2023) with new whole rock geochemistry showed, that in the Lower Aghajari Mb, palygorskite is only formed where sufficient Mg from the weathering of mafic minerals derived from the obduction and erosion of ultramafic and mafic rocks is present. This correlation of palygorskite and detrital mafic minerals in the Lower Aghajari Mb stands in contrast to the Lahbari Mb, where palygorskite is both derived from authigenic formation from wethered mafic minerals and detrital reworking of older palygorskite from evaporites from the older Gachsaran Fm. The results of this study indicate that clay mineral associations can be a useful additional proxy in deciphering the provenance of sediments as they can show the intermediate deposition of sediments in the evaporative environment of the Gachsaran Fm which would not be deducible by proxies such as apatite fission track chronology or whole rock geochemistry alone.

ACKNOWLEDGEMENTS

We would like to thank Jaume Vergés and the one anonymous reviewer, whose comments greatly helped to improve the manuscript. Open Access funding enabled and organized by Projekt DEAL.

FUNDING INFORMATION

Open Access charges were covered by the DFG DEAL agreement.

CONFLICT OF INTEREST STATEMENT

The authors report no conflict of interest.

DATA AVAILABILITY STATEMENT

The data that supports the findings of this study are available in the supplementary material of this article.

ORCID

Christian A. F. Dietzel https://orcid.org/0000-0002-0140-1952
Uwe Kirscher https://orcid.org/0000-0003-4203-1430

REFERENCES

Alavi, M. (1994). Tectonics of the Zagros orogenic belt of Iran: New data and interpretations. *Tectonophysics*, *229*(3–4), 211–238, 234.

Alavi, M. (2004). Regional stratigraphy of the Zagros fold-thrust belt of Iran and its proforeland evolution. *American Journal of Science*, *304*(1), 1–20.

Alavi, M. (2007). Structures of the Zagros fold-thrust belt in Iran. *American Journal of Science*, *307*(9), 1064–1095.

Ali, S. A., Mohajjel, M., Aswad, K., Ismail, S., Buckman, S., & Jones, B. (2014). *Tectono-stratigraphy and structure of the northwestern Zagros collision zone across the Iraq–Iran border*. Faculty of Science, Medicine and Health – Papers: Part A 2058.

Ali, S. A., Sleabi, R. S., Talabani, M. J., & Jones, B. G. (2017). Provenance of the Walash-Naopurdan back-arc–arc clastic sequences in the Iraqi Zagros suture zone. *Journal of African Earth Sciences*, *125*, 73–87.

Al-Juboury, A. I. (2009). Palygorskite in Miocene rocks of northern Iraq: Environmental and geochemical indicators. *Acta Geologica Polonica*, *59*(2), 269–282.

Baharifar, A., Moinevaziri, H., Bellon, H., & Piqué, A. (2004). The crystalline complexes of Hamadan (Sanandaj–Sirjan zone, western Iran): Metasedimentary Mesozoic sequences affected by late cretaceous tectono-metamorphic and plutonic events. *Comptes Rendus Geoscience*, *336*(16), 1443–1452.

Bahroudi, A., & Koyi, H. A. (2004). Tectono-sedimentary framework of the Gachsaran formation in the Zagros foreland basin. *Marine and Petroleum Geology*, *21*(10), 1295–1310.

Berberian, F., Muir, I., Pankhurst, R., & Berberian, M. (1982). Late cretaceous and early Miocene Andean-type plutonic activity in northern Makran and Central Iran. *Journal of the Geological Society*, *139*(5), 605–614.

Berberian, M. (1995). Master "blind" thrust faults hidden under the Zagros folds: Active basement tectonics and surface morphotectonics. *Tectonophysics*, *241*(3–4), 193–224, 200.

Berberian, M., & King, G. (1981). Towards a paleogeography and tectonic evolution of Iran. *Canadian Journal of Earth Sciences*, *18*(2), 210–265.

Berger, I., & Cooke, R. (1997). The origin and distribution of salts on alluvial fans in the Atacama Desert, Northern Chile: Earth surface processes and landforms. *The Journal of the British Geomorphological Group*, *22*(6), 581–600.

Bhatia, M. R. (1983). Plate tectonics and geochemical composition of sandstones. *The Journal of Geology*, *91*(6), 611–627.

Blanc, E.-P., Allen, M. B., Inger, S., & Hassani, H. (2003). Structural styles in the Zagros simple folded zone, Iran. *Journal of the Geological Society*, *160*(3), 401–412.

Böhme, M., Spassov, N., Majidifard, M. R., Gärtner, A., Kirscher, U., Marks, M., Dietzel, C., Uhlig, G., El Atfy, H., & Begun, D. R. (2021). Neogene hyperaridity in Arabia drove the directions of mammalian dispersal between Africa and Eurasia. *Communications Earth & Environment*, *2*(1), 1–13.

Bruthans, J., Filippi, M., Asadi, N., Zare, M., Šlechta, S., & Churáčková, Z. (2009). Surficial deposits on salt diapirs (Zagros Mountains and Persian gulf platform, Iran): Characterization, evolution, erosion and the influence on landscape morphology. *Geomorphology*, *107*(3–4), 195–209.

Callen, R. A. (1984). *Clays of the palygorskite-sepiolite group: Depositional environment, age and distribution, developments in sedimentology* (Vol. *37*, pp. 1–37). Elsevier.

Chamley, H. (1989). *Clay sedimentology* (p. 623). Springer.

Dietzel, C., El Atfy, H., Berthold, C., Majidifard, M., & Böhme, M. (2024). Reworked Mesozoic radiolarians in Miocene-Pliocene foreland sediments in the Zagros Belt, Iran. *Rivista Italiana di Paleontologia e Stratigrafia*, *130*(1), 35–46.

Dietzel, C. A., Berthold, C., Kirscher, U., Majidifard, M. R., & Böhme, M. (2023). Using clay mineralogy and

micropalaeontological observations to unravel Neogene climate variations in Northern Arabia. *Arabian Journal of Geosciences*, *16*(5), 343.

Dinelli, E., Lucchini, F., Mordenti, A., & Paganelli, L. (1999). Geochemistry of Oligocene–Miocene sandstones of the northern Apennines (Italy) and evolution of chemical features in relation to provenance changes. *Sedimentary Geology*, *127*(3–4), 193–207.

Ehya, F., Shakouri, B., & Rafi, M. (2013). Geology, mineralogy, and isotope (Sr, S) geochemistry of the Likak celestite deposit, SW Iran. *Carbonates and Evaporites*, *28*, 419–431.

Emami, H., Vergés, J., Nalpas, T., Gillespie, P., Sharp, I., Karpuz, R., Blanc, E., & Goodarzi, M. (2010). Structure of the mountain front flexure along the Anaran anticline in the Pusht-e Kuh arc (NW Zagros, Iran): Insights from sand box models. *Geological Society, London, Special Publications*, *330*(1), 155–178, 173.

Etemad-Saeed, N., Najafi, M., & Vergés, J. (2020). Provenance evolution of Oligocene–Pliocene foreland deposits in the Dezful embayment to constrain central Zagros exhumation history. *Journal of the Geological Society*, *177*(4), 799–817.

Garcia, D., Fonteilles, M., & Moutte, J. (1994). Sedimentary fractionations between Al, Ti, and Zr and the genesis of strongly peraluminous granites. *The Journal of Geology*, *102*(4), 411–422.

Hashemi, S., Baghernejad, M., & Najafi, G. M. (2013). Clay mineralogy of gypsiferous soils under different soil moisture regimes in Fars Province, Iran. *Journal of Agricultural Science and Technology*, *15*, 1053–1068.

Herron, M. M. (1988). Geochemical classification of terrigenous sands and shales from core or log data. *Journal of Sedimentary Research*, *58*(5), 820–829.

Hiscott, R. N. (1984). Ophiolitic source rocks for Taconic-age flysch: Trace-element evidence. *Geological Society of America Bulletin*, *95*(11), 1261–1267.

Homke, S., Vergés, J., Garcés, M., Emami, H., & Karpuz, R. (2004). Magnetostratigraphy of Miocene? Pliocene Zagros foreland deposits in the front of the push-e Kush arc (Lurestan Province, Iran). *Earth and Planetary Science Letters*, *225*(3–4), 397–410.

Homke, S., Vergés, J., Serra-Kiel, J., Bernaola, G., Sharp, I., Garcés, M., Montero-Verdú, I., Karpuz, R., & Goodarzi, M. H. (2009). Late cretaceous–Paleocene formation of the proto–Zagros foreland basin, Lurestan Province, SW Iran. *Geological Society of America Bulletin*, *121*(7–8), 963–978.

Homke, S., Vergés, J., Van Der Beek, P., Fernandez, M., Saura, E., Barbero, L., Badics, B., & Labrin, E. (2010). Insights in the exhumation history of the NW Zagros from bedrock and detrital apatite fission-track analysis: Evidence for a long-lived orogeny. *Basin Research*, *22*(5), 659–680, 660.

Honarmand, M., Omran, N. R., Corfu, F., Emami, M. H., & Nabatian, G. (2013). Geochronology and magmatic history of a calc-alkaline plutonic complex in the Urumieh-Dokhtar Magmatic Belt, Central Iran. *Zircon Ages as Evidence for Two Major Plutonic Episodes: Neues Jahrbuch für Mineralogie-Abhandlungen*, *190*(1), 67–77.

Jalilian, A. H. (2016). The Neogene molasse deposits of the Zagros Mountains in central Dezful embayment: Facies, sedimentary environments and controls. *Journal of Stratigraphy and Sedimentology Researches*, *32*(1), 81–98.

Khademi, H., & Mermut, A. (1998). Source of palygorskite in gypsiferous Aridisols and associated sediments from central Iran. *Clay Minerals*, *33*(4), 561–578.

Khormali, F., & Abtahi, A. (2003). Origin and distribution of clay minerals in calcareous arid and semi-arid soils of Fars Province, southern Iran. *Clay Minerals*, *38*(4), 511–527.

Khormali, F., Abtahi, A., & Owliaie, H. (2005). Late Mesozoic—Cenozoic clay mineral successions of southern Iran and their palaeoclimatic implications. *Clay Minerals*, *40*(2), 191–203.

Koshnaw, R. I., Horton, B. K., Stockli, D. F., Barber, D. E., & Tamar-Agha, M. Y. (2020). Sediment routing in the Zagros foreland basin: Drainage reorganization and a shift from axial to transverse sediment dispersal in the Kurdistan region of Iraq. *Basin Research*, *32*(4), 688–715, 709.

Koshnaw, R. I., Horton, B. K., Stockli, D. F., Barber, D. E., Tamar-Agha, M. Y., & Kendall, J. J. (2017). Neogene shortening and exhumation of the Zagros fold-thrust belt and foreland basin in the Kurdistan region of northern Iraq. *Tectonophysics*, *694*, 332–355.

Lawa, F., Koyi, H., & Ibrahim, A. (2013). Tectono-stratigraphic evolution of the NW segment OF the Zagros fold-thrust belt, Kurdistan, NE Iraq. *Journal of Petroleum Geology*, *36*(1), 75–96.

Le Garzic, E., Vergés, J., Sapin, F., Saura, E., Meresse, F., & Ringenbach, J. (2019). Evolution of the NW Zagros fold-and-Thrust Belt in Kurdistan region of Iraq from balanced and restored crustal-scale sections and forward modeling. *Journal of Structural Geology*, *124*, 51–69.

Li, Y., Song, Y., Fitzsimmons, K. E., Chen, X., Prud'homme, C., & Zong, X. (2020). Origin of loess deposits in the North Tian Shan piedmont, Central Asia. *Palaeogeography, Palaeoclimatology, Palaeoecology*, *559*, 109972.

McLennan, S. M. (2001). Relationships between the trace element composition of sedimentary rocks and upper continental crust. *Geochemistry, Geophysics, Geosystems*, *2*, 1021. https://agupubs.onlinelibrary.wiley.com/action/showCitFormats?doi=10.1029%2F2000GC000109&mobileUi=0

McQuarrie, N. (2004). Crustal scale geometry of the Zagros fold–thrust belt, Iran. *Journal of Structural Geology*, *26*(3), 519–535.

Millot, G. (1970). *Geology of clays: Weatering, sedimentology, geochemistry*. Springer-Verlag.

Mohajjel, M., & Fergusson, C. (2013). Jurassic to Cenozoic tectonics of the Zagros Orogen in northwestern Iran. *International Geology Review*, *56*(3), 263–287.

Mohajjel, M., & Fergusson, C. L. (2000). Dextral transpression in Late Cretaceous continental collision, Sanandaj–Sirjan zone, western Iran. *Journal of Structural Geology*, *22*(8), 1125–1139.

Molinaro, M., Guezou, J.-C., Leturmy, P., Eshraghi, S., & de Lamotte, D. F. (2004). The origin of changes in structural style across the Bandar Abbas syntaxis, SE Zagros (Iran). *Marine and Petroleum Geology*, *21*(6), 735–752.

Mouthereau, F., Tensi, J., Bellahsen, N., Lacombe, O., De Boisgrollier, T., & Kargar, S. (2007). Tertiary sequence of deformation in a thin-skinned/thick-skinned collision belt: The Zagros Folded Belt (Fars, Iran). *Tectonics*, *26*(5), 1–28.

Najafi, M., Beamud, E., Ruh, J., Mouthereau, F., Tahmasbi, A., Bernaola, G., Yassaghi, A., Motamedi, H., Sherkati, S., Goodarzi, M. G. H., & Verges, J. (2021). Pliocene growth of the Dowlatabad syncline in frontal Fars arc: Folding propagation across the Zagros Fold Belt, Iran. *Bulletin*, *133*(7–8), 1381–1403.

Pettijohn, F. J., Potter, P. E., & Siever, R. (1972). *Sand and sandstone*. Springer Science & Business Media.

Raffi, I., Wade, B. S., Pälike, H., Beu, A. G., Cooper, R., Crundwell, M. P., Krijgsman, W., Moore, T., Raine, I., Sardella, R., & Vernyhorova, Y. V. (2020). Chapter 29 – The neogene period. In F. M. Gradstein, J. G. Ogg, M. D. Schmitz, & G. M. Ogg (Eds.), *Geologic Time Scale, 2020* (pp. 1141–1215). Elsevier.

Roser, B., & Korsch, R. (1986). Determination of tectonic setting of sandstone-mudstone suites using SiO_2 content and K_2O/Na_2O ratio. *The Journal of Geology*, *94*(5), 635–650.

Saccani, E., Allahyari, K., Beccaluva, L., & Bianchini, G. (2013). Geochemistry and petrology of the Kermanshah ophiolites (Iran): Implication for the interaction between passive rifting, oceanic accretion, and OIB-type components in the southern neo-Tethys Ocean. *Gondwana Research*, *24*(1), 392–411.

Saura, E., Garcia-Castellanos, D., Casciello, E., Parravano, V., Urruela, A., & Vergés, J. (2015). Modeling the flexural evolution of the Amiran and Mesopotamian foreland basins of NW Zagros (Iran–Iraq). *Tectonics*, *34*(3), 377–395.

Sepehr, M., Cosgrove, J., & Moieni, M. (2006). The impact of cover rock rheology on the style of folding in the Zagros fold-thrust belt. *Tectonophysics*, *427*(1–4), 265–281.

Sherkati, S., & Letouzey, J. (2004). Variation of structural style and basin evolution in the central Zagros (Izeh zone and Dezful embayment), Iran. *Marine and Petroleum Geology*, *21*(5), 535–554.

Singer, A. (1979). Palygorskite in sediments: Detrital, diagenetic or neoformed—A critical review. *Geologische Rundschau*, *68*(3), 996–1008.

Singer, A. (1980). The paleoclimatic interpretation of clay minerals in soils and weathering profiles. *Earth-Science Reviews*, *15*(4), 303–326.

Singer, A. (1989). Palygorskite and sepiolite group minerals. *Minerals in Soil Environments*, *1*, 829–872.

Skoček, V., & Saadallah, A. (1972). Grain-size distribution, carbonate content and heavy minerals in eolian sands, southern desert, Iraq. *Sedimentary Geology*, *8*(1), 29–46.

Stoecklin, J. (1968). Structural history and tectonics of Iran: A review. *AAPG Bulletin*, *52*(7), 1229–1258, 1230.

Un-Escwa, B. (2013). *United Nations economic and social commission for western Asia; Bundesanstalt für Geowissenschaften und Rohstoffe*. Inventory of Shared Water Resources in Western Asia.

Vergés, J. (2007). Drainage responses to oblique and lateral thrust ramps: A review. In G. Nichols, E. Williams, & C. Paola (Eds.), *Sedimentary processes, environments and basins: A tribute to Peter friend* (pp. 29–47). https://onlinelibrary.wiley.com/doi/book/10.1002/9781444304411

Vergés, J., Emami, H., Garcés, M., Beamud, E., Homke, S., & Skott, P. (2019). Zagros foreland fold belt timing across Lurestan to constrain Arabia–Iran collision. *Developments in Structural Geology and Tectonics*, *3*, 29–52.

Vergés, J., Goodarzi, M., Emami, H., Karpuz, R., Efstathiou, J., & Gillespie, P. (2011). Multiple detachment folding in Pusht-e Kuh arc, Zagros: Role of mechanical stratigraphy. In K. McClay, J. Shaw, & J. Suppe (Eds.), *Thrust fault-related folding* (pp. 69–94). AAPG Memoir.

Vergés, J., Sandra, E., Casciello, E., Fernandez, M., Villaseñor, A., Jimenez-Munt, I., & García-Castellanos, D. (2011). Crustal-scale cross-sections across the NW Zagros belt: Implications for the Arabian margin reconstruction. *Geological Magazine*, *148*(5–6), 739–761.

Whalen, J. B., Currie, K. L., & Chappell, B. W. (1987). A-type granites: Geochemical characteristics, discrimination and petrogenesis. *Contributions to Mineralogy and Petrology*, *95*, 407–419.

Wrobel-Daveau, J.-C., Ringenbach, J.-C., Tavakoli, S., Ruiz, G. M., Masse, P., & De Lamotte, D. F. (2010). Evidence for mantle exhumation along the Arabian margin in the Zagros (Kermanshah area, Iran). *Arabian Journal of Geosciences*, *3*(4), 499–513.

SUPPORTING INFORMATION

Additional supporting information can be found online in the Supporting Information section at the end of this article.

How to cite this article: Dietzel, C. A. F., Kirscher, U., Berthold, C., Majidifard, M. R., & Böhme, M. (2024). A revised model for Neogene Zagros foreland sedimentation in the Lurestan arc based on new geochemical data. *Basin Research*, *36*, e12861. https://doi.org/10.1111/bre.12861